ATSR Reprocessing for Climate Lake Surface Water Temperature: ARC-Lake

Algorithm Theoretical Basis Document

Title: ATSR Reprocessing for Climate Lake Surface Water Temperature: ARC-Lake: Algorithm Theoretical Basis Document

Document Number: ARC-Lake-ATBD-v1.4

Issue: 1

Revision: 1.4

Date: 23 October 2013

Signature Table

	Name	Function	Company	Signature	Date
Prepared	S MacCallum C Merchant	Researcher PI/Professor	University of Edinburgh University of Reading		23 October 2013
Approved					
Released					

Document Change Record

Version	Date	Author	Description
1.0	8 Oct 2010	SM, CM	
1.1	1 Nov 2011	SM, CM	Updated to reflect changes in methodology and terminology between v1.0 and v1.1 data products
1.2	22 Nov 2011	SM, CM	Updated to reflect changes in methodology: addition of ATSR1, 2010, and changes to estimation of prior LSWT
1.3	23 Oct 2013	SM, CM	Updated to reflect addition of AATSR, 2011 for v2.0 data products.
1.4	23 Oct 2013	SM, CM	Updated to reflect changes in methodology between v2 and v3 data products: extended target list and new water masks derived from ATSR water detection.

Table of Contents

List of Figures

1 INTRODUCTION

1.1 Acronyms and Abbreviations

AATSR	*Advanced ATSR*
ARC	*ATSR Reprocessing for Climate*
ATBD	*Algorithm Theoretical Basis Document*
ATSR	*Along-Track Scanning Radiometer*
BT	*Brightness Temperature*
DINEOF	*Data Interpolating Empirical Orthogonal Functions*
DISORT	*Discrete Ordinates Radiative Transfer Program for a Multi-Layered Plane-Parallel Medium*
GLWD	*Global Lakes and Wetlands Database*
LIC	*Lake Ice Concentration*
LSWT	*Lake Surface Water Temperature*
LUT	*Look-Up Table*
MAP	*Maximum Aposteriori Probability*
MODIS	*Moderate Resolution Imaging Spectroradiometer*
NEΔT	*Noise Equivalent Differential Temperature*
NIR	*Near Infra-Red*
NWP	*Numerical Weather Prediction*
OE	*Optimal Estimation*
PDF	*Probability Density Function*
RFM	*Reference Forward Model*
RMSD	*Root-Mean-Square Deviation*
RT	*Radiative Transfer*
RTM	*Radiative Transfer Model*

RTTOV	*Radiative Transfer for TOVs (a fast RTM)*
SD	*Standard Deviation*
SST	*Sea Surface Temperature*
TCWV	*Total Column Water Vapour*
TIR	*Thermal Infra-Red*
ToA	*Top of Atmosphere*

1.2 Purpose and Scope

This document is an Algorithm Theoretical Basis Document for the generation of Lake Surface Temperature (LSWT) and Lake Ice Concentration (LIC) products from Along-Track Scanning Radiometer (ATSR) imagery.

Such products have not been adequately delivered by previous systems developed for either sea surface temperature or land surface temperature determination. However, there is a need for LSWT and LIC for many applications: numerical weather prediction is the most pressing application, since increasing spatial resolution and sophistication of surface-atmosphere interactions in weather simulations no longer permits that lakes are neglected or very crudely represented; other applications include climate monitoring, limnological research, and climate prediction for commercial and societal institutions.

In terms of scope, this ATBD covers ATSR-1, ATSR-2 and Advanced ATSR (AATSR) processing.

1.3 Algorithm Identification

The ATBD provides the theoretical basis for the following algorithms:

- identification of image pixel locations covering required “target lakes” (which are defined)
- determination of lake-specific inputs required for radiative transfer modelling (the radiative transfer models are not part of the ATBD, since the algorithms are independent of these)
- discrimination of cloudy and non-cloudy pixels, and of water and ice clear-sky pixels (“classification”)
- estimation of LSWT, uncertainty in LSWT for clear-sky pixels
- conversion of pixel observations to a gridded product

2 ALGORITHM OVERVIEWS

2.1 Identification of lakes

2.1.1 Phase-1 and phase-2

The algorithms were designed to support production of LSWT and LIC for large lakes in phases 1 and 2 (v1 and v2 data products). Large lakes are commonly defined as natural inland water bodies of >500 km^2 in surface area (Herdendorf (1982), Beeton (2002). In addition, the target lakes for the first two phases of the ARC-Lake project include some inland waters that are less than 500 km^2 in area (because ARC-Lake users have requested these, or because there are useful validation data available).

The lake identification algorithm determines, on the basis of the longitude and latitude of a pixel in the ATSR level 1b imagery, whether that pixel is geolocated over a target lake, and, if so, which lake is in view. This is done on the basis of a hierarchical temporally fixed lake mask. Being temporally fixed, ephemeral lakes are not included in the target lake list, and lakes undergoing dramatic hydrological changes are not properly accounted for in this version of the algorithm.

2.2 Phase-3

In phase-3 of ARC-Lake (v3 data products) the set of target lakes is extended to include smaller lakes (down to surface areas of order 50 km^2), reservoirs, ephemeral lakes and other lakes with significant temporal variations in surface area. The inclusion of water bodies with variable surface area is possible due to the introduction of a water detection algorithm both within the retrieval scheme and as a pre-processing step used to define the maximum target area over the ATSR-2/AATSR time period and to estimate the minimum target area on an annual basis (§3.3).

As in the earlier phases, the target identification algorithm determines which target the pixel is over through the lookup of a temporally fixed lake mask (maximum area mask) with the ATSR level 1b pixel longitude and latitude. To enable inclusion of targets with variable surface area, this fixed-mask is combined with the application of the water detection algorithm for day-time observations and with the binary masks of annual minimum area for night-time observations.

2.3 Lake-specific inputs to radiative transfer modelling (simulation)

The classification and retrieval algorithms discussed in §6 and §8 are based on radiative transfer modelling. The algorithms are generic with respect to what choice of radiative transfer model (RTM) is applied, so long as appropriate simulations of brightness temperature (BT) and visible reflectance, can be made. In addition, the jacobian (derivative of

BT) is required with respect to prior surface temperature (x^b) and prior total column water vapour (w^b); any radiative transfer model that simulates BT can provide the jacobians by perturbation if it does not directly output them. Thus, discussion of the RTMs as such is properly outside the scope of this ATBD. Likewise, the algorithms are generic with respect to the origin of the profiles of atmospheric temperature and water vapour that are required to run the RTM: the sourcing of such numerical weather prediction (NWP) fields for a given location and observation is a generic process for which any implementer of ARC-Lake algorithms will have a preferred local solution.

However, the sourcing of the prior surface temperature, x^b, and the lake surface emissivity, ε, are also required, and we have found that NWP-based values for these are not (at present) sufficiently accurate for use in ARC-Lake. Therefore, they need to be specified by an algorithm, presented here. The x^b algorithm is simple: it involves looking up pre-calculated data giving a spatially complete field of prior surface temperature for the period 1991 to 2012. This ATBD is therefore focussed on documenting the basis for those look-up data. The emissivity algorithm involves interpolation of fresh and saline water emissivity according to the nature of any given lake.

2.4 Classification

Valid LSWT can be estimated only for pixels that are effectively clear-sky (free of cloud). The algorithm for assigning a probability of clear-sky to each pixel is based on Bayes' theorem (Merchant *et al*, 2005), and exploits the BT and visible simulations.

The LIC value for a cell is based on the fraction of clear-sky pixels in a cell that also triggers an ice detection algorithm.

2.5 Lake Surface Water Temperature retrieval

The LSWT is estimated for each clear-sky water pixel using joint optimal estimation (OE) of x^b and w^b given the simulations and observations. The form of optimal estimation used is to return the *maximum aposteriori probability* (MAP) assuming Gaussian error characteristics.

OE also gives an uncertainty estimate for each retrieval.

2.6 Gridding

The lake products are required on a 0.05° latitude-longitude grid, and thus a gridding algorithm is specified, to take the observations from the imagery resolution to the product resolution.

3 IDENTIFICATION OF LAKES

3.1 Overview

A key component of the ARC-Lake processing system is the land/water mask, used to define the locations of lakes, and therefore locations where Lake Surface Water Temperature (LSWT) and Lake Ice Cover (LIC) should be derived. As we wish to treat each lake as a single entity, the land/water mask must also allow (A)ATSR observations to be attributed to a particular lake. Different approaches, with some shared methodology and goals, have been used for lake identification in the first two phases and in the third phase of ARC-Lake. The methodology of each approach is outlined in the following sections.

3.2 Versions 1 and 2 ARC Lake dataset

This section describes the development and implementation of the target identification methods used in v1 and v2 ARC-Lake data products.

3.2.1 Algorithm and justification

Following assessment of existing land water masks, a new land/water mask was developed specifically for the lakes defined in Phase one of ARC-Lake (MacCallum and Merchant, 2010). Details of this development process follow.

The Envisat ATSR land/water mask (used operationally) was compared with the NAVOCEANO mask (GHRSST, 2006). A summary of these two masks is given in Table 1. Although it does not provide full latitudinal coverage, the NAVOCEANO mask was preferred to the Envisat mask as it suffered fewer problems with missing or mis-located lakes. It also has the benefit of being at a higher resolution, allowing better representation of shorelines, and the potential advantage of containing information about the distance of each cell from the shore. Although not currently utilised, this information could be used to aid screening of land contaminated cells.

Mask	Resolution (degrees)	Latitude Coverage	Mask type	Number of lakes with no water cells
Envisat	0.01	[-90,90]	Binary	10
NAVOCEANO	0.00833	~[-80,80]	Distance from shore	3

Table 1. Summary of land/water masks assessed in ARC-Lake.

A problem shared by both the NAVOCEANO and Envisat ATSR masks is the lack of means by which to attribute water cells *to a particular lake*. Due to the irregular shapes of lakes and the close proximity of other water bodies (e.g. other lakes, rivers, and oceans), it is not possible to do this by simply selecting a regular-shaped area surrounding the location of the lake centre . It is also not possible to define the cells for a given lake as the group of

connecting water cells overlying the location of the lake centre, as areas of some lakes (e.g. Lake Astray) are smaller than the resolution of the mask, and therefore the lakes (although fully connected in reality) may consist of groupings of non-connecting cells. This problem of correctly attributing water cells in the mask to specific lakes was tackled by incorporating a polygon definition of each lake.

The Global Lakes and Wetlands Database, GLWD (Lehner and Döll, 2004), describes each lake as a polygon. These polygons consist of an array of longitude/latitude coordinates defining the main shoreline of the lake and the shorelines of islands within the lake. Lehner and Döll (2004) derive these polygons from the Digital Chart of the World (DCW) of ESRI (1993), with manual adjustments made to define boundaries between the lakes and other water bodies. A new land/water mask (GLWD mask) at the NAVOCEANO resolution was generated from these polygons, with cells being flagged as water only if they were completely land free (i.e. entirely enclosed by the lake shoreline polygon and not intersected/contaminated by any island polygons). Unlike the Envisat and NAVOCEANO masks that only distinguish between land and water, the new GLWD mask distinguishes between individual lakes by flagging water cells with a unique lake identifier number.

As a conservative approach, the NAVOCEANO and GLWD masks were combined to create the ARC-Lake land/water mask. Only cells flagged as water in both masks were defined as water in the new mask, giving a conservative representation of the water cells comprising each lake. In the special cases where the NAVOCEANO mask contained no water cells for the lake (e.g. Lake Hazen), the GLWD mask was used. The result of this process is a global (including the high latitudes) land/water mask at a grid resolution of 0.00833°, where each of the Phase one lakes is represented by a unique number.

3.2.2 Practical considerations

The lakes covered Phase one of ARC-Lake, and indeed all lakes, only cover a small fraction of the Earth's surface. Therefore compression techniques are applied to reduce the memory storage requirements of the mask. The mask is stored in a hierarchical data structure, with three levels of increasing resolution as detailed in Table 2. By storing only the full resolution mask for 0.1° resolution cells that contain lakes, the hierarchical data structure greatly reduces the storage requirements for this mask. The land/water mask is available in NetCDF format from an online data repository (MacCallum and Merchant, 2011c).

Level	Resolution	Dimensions	Details
1	1.0° x 1.0°	[360, 180]	0 - No lake data > 0 - Index (n) of 2nd dimension of Level 2 (indexing starts at 1, i.e. F90 standard) Number of non-zero elements = N = size of 2nd

			dimension of Level 2
2	0.1° x 0.1°	[100, N]	0 - No lake data > 0 - Index (m) of 2nd dimension of Level 3 (indexing starts at 1, i.e. F90 standard) Number of non-zero elements = M = size of 2nd dimension of Level 3
3	0.01° x 0.01°	[100, M]	0 - No lake data > 0 - ARC-Lake index number for lake

Table 2. Structure of hierarchical land/water mask developed for ARC-Lake v1 and v2 data.

3.2.3 Assumptions and limitations

The new land/water mask outlined in §3.2 is generated only for the lakes defined in v1 and v2 of the ARC-Lake dataset (MacCallum and Merchant, 2010). This set of target lakes contains water bodies broadly described as permanent, natural water bodies with surface area > 500 km^2, with a number of exclusions and additions (MacCallum and Merchant, 2010). One such exclusion is lakes with highly variable surface area (> 25%). Such lakes are not included to avoid the issue of LSWT retrievals being performed over land when the lakes recede. There are however still lakes where lesser (or undocumented) variations in surface area occur. Therefore it should be noted that land contamination may still be an issue around lake edges.

There are also two lakes (the Aral Sea and Kara-Bogaz-Gol) where significant changes to the surface area have occurred over the lifetime of the ATSR missions, rather than seasonally. In these cases, the land/water mask represents the lake extent at a snap-shot in time, so therefore does not accurately represent the lake area throughout the ATSR mission lifetime. Consequently, LSWT products for these lakes should be used with caution.

The problem of variations in lake surface area is one that must be addressed in future. A water detection algorithm based on visible reflectance channel observations is proposed, and will be trialled in Phase 3 of the ARC-Lake project (months 27 to 36) in the context of extending the range target lakes within the project to smaller inland water bodies.

3.3 Version 3 ARC Lake dataset

This section describes the development and implementation of the target identification methods used in v3 ARC-Lake data products.

3.3.1 Algorithm and justification

As discussed in §3.2.3, the lake identification methods employed in creating v1 and v2 datasets of ARC-Lake limit targets to those with invariant surface areas, with land

contamination a potential issue to LSWT retrievals if targets with variable surface area are included. To allow such targets to be included in the v3 dataset while minimizing the risk of land contaminated LSWT retrievals, a water detection algorithm has been introduced. This has been implemented in two stages: (a) as a pre-processing step using all available ATSR observations to determine masks of maximum target area and of annual minimum area, and (b) as an addition to the LSWT processing scheme for day-time observations.

3.3.1.1 Water detection - Pre-processsing

The water detection scheme implemented in ARC-Lake v3 utilises the visible (VIS), near-IR (NIR), and short-wave-IR (SWIR) channels of the ATSR2 and AATSR instruments, through a combination of simple threshold tests. Two tests are based on normalized difference indices, with further threshold tests performed on individual channel reflectances and brightness temperatures. Thresholds used are defined in **Table** 3.

The two normalised difference indices used are presented in equations 3.1 and 3.2. They are: the Modified Normalised Difference Water Index (MNDWI), described by Xu, 2006, and the Normalised Difference Vegetation Index (NDVI) (Townshend and Justice, 1986).

Eq. 3.1 $$MNDWI = \frac{R_{0.55} - R_{1.6}}{R_{0.55} + R_{1.6}}$$

Eq. 3.2 $$NDVI = \frac{R_{0.87} - R_{0.67}}{R_{0.87} + R_{0.67}}$$

Channel / Normalised difference	Threshold
MNDWI	> 0.1
NDVI	< 0.0
0.55 µm	< 15 %
0.87 µm	< 10 %
1.6 µm	< 10 %
10.8 µm	> 260 K
MNDWI-NDVI	> 0.4

Table 3. Threshold tests for water detection.

This water detection scheme was applied to ATSR level 1b imagery pixels for the full ATSR2/AATSR time period, recording counts of positive water detection (Ncounts) on a 1/120° grid (as used in phases 1 and 2). Using the GLWD polygons as a basis for target location, but not a limit, GLWD IDs were assigned to each region identified as water.

Subsequent filtering based on Ncounts values was applied on a target-by-target basis to reduce potential land contamination from mixed land/water pixels. This filtering assumes the distribution of Ncounts across cells in each target is Gaussian, and excludes cells with Ncounts less than the lower limit of the Gaussian fit to the Ncounts distribution. The resulting water mask provides an estimate of the maximum extent of each target over the ATSR2/AATSR time period.

Annual masks of minimum target extent are estimated from annual accumulations of water counts ($Ncounts_y$) on the 1/120° grid, using a similar $Ncounts_y$ filtering method as applied to minimize potential land contamination in the maximum extent mask.

3.3.1.2 Water detection – LSWT-processing

The water detection scheme and water masks described in §3.3.1.1 are implemented within the LSWT processing scheme as follows. For day-time observations, the water detection threshold tests (Table 3) are applied to all level-1b imagery pixels flagged as water within the maximum area mask determined in the pre-processing water detection step (§3.3.1.1). This allows day-time observations to capture the full range of water surface area exhibited by each target.

A different approach is required for night-time observations, as the VIS, NIR, and SWIR channels used in the water detection algorithm are not available at night. The annual minimum area masks are used for night-time observations. These do not allow the full range of water surface area to be captured but instead provide a conservative estimate of target surface area, appropriate to that year. While a higher temporal frequency for minimum area detection would be better suited to seasonally varying lakes in particular, the sampling rate from the narrow-swath ATSRs is insufficient to support better than annual determination. (Potentially, an approach combining multiple sensors could yield seasonal discrimination.)

3.3.2 Practical considerations

Although there is a six-fold increase in the number of targets between phase-2 and phase-3, the fraction of the Earth's surface covered remains small. Therefore compression techniques are again required to reduce the memory storage requirements of the mask. Rather than using the hierarchical data structure used in the earlier phases (described in §3.2.2), phase-3 water masks are stored using the in-built NetCDF-4 compression.

To further minimise storage requirements, the target-ID of each grid cell is only stored in the maximum area mask. Annual minimum area masks contain only a binary (land/water) mask and must be used in conjunction with the maximum area mask to assign observations to the appropriate target-ID.

3.3.3 Advantages, assumptions and limitations

The new phase-3 water masks and water detection scheme offer considerable advantages over the static water mask used in the earlier phases of ARC-Lake. As the phase-3 scheme allows changes in surface area to be captured, it is no longer necessary to exclude targets known to have highly variable surface area. This allows a new category of, potentially high interest, target to be included in the dataset.

Applying the water detection scheme rather than the combination of GLWD polygons and NAVOCEANO mask (§3.2.1) can also provide a better representation of target surface area for targets with static area. The GLWD polygons do not provide an accurate representation of the target shape for all cases. For example, a number of reservoirs with complex shape are defined as perfect circles in the GLWD.

The potential problem of land contamination around lake edges in the earlier phases (§3.2.3) should also be reduced using the new water detection methods. This is particularly important as smaller targets are considered in phase-3, as any land contaminated LSWT retrievals will have a more significant impact on lake-mean LSWTs for smaller lakes.

Although the water detection method offers clear advantages over the static water mask, it is not without limitations. Perhaps the most significant is that it is not possible for ATSR-1, as the VIS and NIR channels are not available. Consequently, ARC-Lake v3 data products only cover ATSR-2 and AATSR.

In addition to excluding mixed land/water cells, part of the rationale behind filtering using Ncounts in the definition of the maximum area mask was to exclude false positive water detections. These can arise due to effects such as cloud shadow or land surfaces with spectral signature similar to water in the available ATSR channels (e.g. lava fields). For lakes with significant variation in surface area, it is possible that some false positive water detections may occur in dry pixels. However, it is expected that the number of such cases will be relatively small and may be subsequently flagged as not-clear in the later cloud detection tests.

As the annual minimum area water masks used for night-time observations are fixed for all observations within a given year, it is clearly not possible to capture seasonal variations in lake area at night. The night-time observations therefore may not return LSWT for all cells for which LSWT is retrieved during the day. This is true not just for targets with highly variable surface area. For some stable targets and some years, the night-time minimum area mask may under-estimate the lake area, with the loss of water cells typically around the lake shoreline, as a result of the annual Ncounts filtering.

4 LAKE-SPECIFIC PRIOR SURFACE TEMPERATURE

The prior surface temperature is a key component of the optimal estimation (OE) LSWT retrieval scheme implemented in ARC-Lake. NWP-based values, as used in sea surface temperature (SST) retrievals, are not (at present) adequate for use in ARC-Lake. The reasons for this are two-fold: the NWP-based values are not accurate enough and their spatial resolution too coarse to provide information of spatial thermal structures on lake-scales. This is particularly apparent for smaller or less well monitored lakes. It is therefore necessary to specify the prior surface temperature by other means. These means take the form of an iterative scheme, using the ARC-Lake LSWT product to generate a spatially and temporally complete field of surface temperatures by means of principal component reconstruction, that are then used as the input field for the next run of the ARC-Lake processor.

4.1 Initialization with MODIS Climatology

In many instances (e.g., for ECMWF and Met Office), NWP surface temperature over lakes is provided by prescribing a monthly climatology value, for example, based on nearby sea surface temperatures (Saunders and Basalmo, personal communications). As NWP-based values are therefore insufficiently accurate and at a resolution too coarse for ARC-Lake LSWT retrievals over many lakes an alternative initial prior temperature field was sought. This was necessary in order to limit the number of potentially valid observations flagged as cloud because of very large differences between the prior and the retrieval. SST and land surface temperature (LandST) retrievals from the Moderate Resolution Imaging Spectroradiometer (MODIS) were deemed to be a potentially suitable alternative to NWP, as they have been applied with some success to lakes from 2000 to present (Oesch *et al*, 2005, Reinart and Reinhold, 2008, and Wan *et al*, 2008) and are available at a finer resolution than NWP data (~$^{1}/_{20}$° compared to ~1.0°).

Although monthly temporal resolution may result in the loss of information about short-lived thermal fronts, it was both feasible to achieve this and was deemed adequate for the creation of prior LSWT fields for the first iteration. Monthly climatology from MODIS SST products (which operate over all identified water bodies) were used, with MODIS LandST products being used for lakes where SST products were unavailable (because the MODIS SST algorithm had not been applied), in order to maximise the coverage of the target lakes.

Terra MODIS SST (11 µm day-time and night time) monthly climatology products, at $^{1}/_{24}$° longitude/latitude resolution, were obtained from http:/oceancolor.gsfc.nasa.gov (MODIS, 2010). Equivalent climatology products were not available for MODIS LandST, so these were generated from monthly average files (MOD11C3) downloaded from https://lpdaac.usgs.gov (Wan, 2007). MODIS LandST products are on $^{1}/_{20}$° longitude/latitude resolution.

A global MODIS Lake Surface Water Temperature (LSWT) climatology at $^1/_8°$ resolution was created, as a composite of the SST and LandST products, using the ARC-Lake land/water mask (MacCallum and Merchant, 2010) to define lake cells. Data were not available in all temperature products (SST/LandST, day/night) for all lake cells and in some cases data was unavailable in all products. Where available, MODIS day-time SST was used. If these data were not present, the MODIS night time SST product was used. If no SST data were present for a given lake, a lake-area-average LandST value was used, with preference to the day-time product if available. As fine resolution spatial features such as thermal fronts may persist for shorter timescales than this climatology, there is some redundancy in using the MODIS products at their full resolution at this stage. Therefore, the MODIS products were spatially averaged to a $^1/_8°$ resolution grid to further maximise spatial coverage and reduce processing time.

Interpolation from surrounding LSWTs is used to fill lake cells or lakes that have missing data. This interpolation stage is performed in the ARC-Lake processing code to provide a spatially complete input field. Linear interpolation between monthly time steps is used to determine the prior LSWT field for a given day of the year.

4.2 Iterative Scheme for Generating Prior Surface Temperature for ARC-Lake

The climatology for each lake developed from MODIS is useful for providing a reasonable prior for some of the smaller lakes, but does not provide the temporal and spatial resolution necessary to correctly represent the how lake temperatures vary in time and in space across a given lake. Nor does it capture any inter-annual variability, of course. It was therefore adequate for an initial run of the ARC-Lake processor, but is not capable of giving best results. A better prior (with adequate temporal and spatial resolution, and with inter-annual variability present where possible) was therefore developed by an iterative approach as described in this section.

The climatology derived from MODIS was used as input to the ARC-Lake processor, and some valid observations of LSWT were obtained. A prior LSWT field of the spatial and temporal resolution necessary for an improved result was then achieved by applying data-interpolating principal component techniques (Alvera-Azcárate, 2005) to these satellite observations of LSWT. This allows gaps in the LSWT data, arising from cloud cover and incomplete lake coverage in the instrument swath, to be filled in space, thereby providing complete spatial coverage on each day of observation. These fields were then linearly interpolated in time to yield a spatially complete LSWT time series for every day of the year during the ATSR2 and AATSR missions (in most cases – see below). Since the interpolation process creates fields with errors that are uncorrelated or very weakly correlated to LSWT retrieval errors, the complete time series may be fed back into the retrieval scheme as a prior LSWT, and the process repeated, with improved results, particularly in terms of cloud

detection. Figure 1 illustrates this iterative process, the components of which are described in the following sections.

There are three key components to this iterative processing scheme: the ARC-Lake processor for LSWT, software for reconstructing a spatially complete LSWT field from the ARC-Lake output using empirical orthogonal function (EOF)-based techniques, and a lake model. The ARC-Lake processor is described in this document and the references herein. The EOF decomposition based reconstructions of the spatially incomplete output from the ARC-Lake processor are generated using the software package, DINEOF (Data Interpolating Empirical Orthogonal Functions). This software, described in detail by Alvera-Azcárate (2005), allows missing data points (e.g. clouds and areas not under the instrument swath) in the ARC-Lake LSWT product to be calculated from an optimal number of EOFs determined using a cross-validation technique. Finally, output from the lake model, FLake (Mironov, 2005) is used for cases where the number of valid observations from ARC-Lake is extremely low and/or the EOF reconstruction is poor. It is also used to enhance the representation of frozen periods, which may suffer from problems of extensive cloud cover and of surface ice being flagged as cloud by the ARC-Lake processor. The simplified online version of FLake is used (http://www.flake.igb-berlin.de/) which provides an approximation to a climatic mean temperature cycle. It is beyond the scope of this document to explain the workings of DINEOF or Flake in further detail and the user is directed to the references given. The iterative processing scheme for generating and using the prior LSWT field is outlined in Figure 1 and described below.

Per-lake output products (as described in MacCallum and Merchant, 2011a) from the ARC-Lake processor are the starting point for the process that ultimately creates a global prior LSWT fields at daily resolution that are then used as input to the ARC-Lake processor in the next iteration (except for the first pass, where the climatology based on MODIS observations was used). Cloud cover and orbit tracks prevent the ARC-Lake LSWT product providing spatially complete observations over each lake at every opportunity. Alvera-Azcárate (2005) demonstrate that these data gaps can be filled using EOF-based reconstructions. Before running DINEOF a number of preprocessing steps are required to remove erroneous observations that may adversely affect the reconstructions, and to ensure that there are adequate observations to perform the reconstruction.

Erroneous outliers in the input LSWT field (e.g. from land contamination) can result in unrealistic features being propagated through the reconstruction. To eradicate this problem, the input LSWT data are filtered by their χ^2 value (the OE retrieval cost), with all points with $\chi^2 > 100$ flagged as missing data.

During periods where temperatures are approach freezing or are frozen, long periods with no valid LSWT observations or detected ice cover occur over some lakes. To avoid unrealistic temperatures over these periods, missing data points are replaced by FLake simulations in the

reconstructed/interpolated time series. As the FLake simulations approximate to a climatic mean over the entire lake, they do not capture seasonal or spatial variations in ice cover. Consequently, a more conservative estimate of the frozen period is taken to avoid unrealistic switches between frozen and unfrozen conditions across the lake and in the reconstructed time series. The conservative estimate of the frozen period adopted is the central 60% of the frozen period simulated in FLake. All potential (but cloud or ice covered) observations during this period are replaced with the value 273.15 K.

The methodology above is updated for the prior LSWT for v2.0. Following the updates made to the ice detection algorithm in v1.1 (to reduce the possibility of thin cirrus being flagged as ice) the LIC product is integrated into prior LSWT field for v2.0. All cells containing ice observations but no valid LSWT observations are replaced with the value 273.15 K prior to the substitution of FLake simulations. This provides improved representation of ice cover and LSWT during freeze/thaw periods and reduces the influence of FLake simulations on the prior LSWT field. Note that ice detection is only performed during the day (§7), as it uses visible channel observations. To avoid losing the benefits of the ice observations in the night-time reconstructions, day-time ice observations are substituted into the night-time LSWT observations (as above), only days where there is both a day and night-time observation.

Alvera-Azcárate (2005) demonstrate that EOF-based reconstructions perform best when each temporal slice of data (each day) has valid data for at least 5% of the potential points. A filter is applied to the data based on this criterion. Following this, a check is made on the number of remaining time-steps of data relative to the total number of potential observation days. If more than 15% of the time-steps have valid observations the algorithm proceeds with this data. However, if there are fewer time steps than this, a daily climatology for an average year is constructed from all the available data, and this single year time series used as input to DINEOF. It should be noted that days where FLake simulations have been substituted in are excluded from this filtering stage.

A spatially complete time series (covering observation days only) is then generated using DINEOF (Alvera-Azcárate, 2005). This is used to further filter the original input LSWT field to remove remaining outliers. Observation-reconstruction differences are calculated for all valid observations. Where this difference is greater than 2.5 times the standard deviation over all differences, the LSWT observation is replaced with the reconstructed temperature.

Following the second stage of filtering a second reconstruction is generated using DINEOF. This reconstruction is then linearly interpolated in time to provide a spatially and temporally complete time series of LSWT for each lake. Lake cells with no valid observations result in missing data in the reconstruction. Such cells are replaced by the median of the surrounding cells, where the size of the median filter applied is variable, to ensure a minimum of 5 cells are used. Occasional unrealistic spatial and temporal variations in temperature may still be

present in the reconstructions. These are removed by applying median filters in space (as above) and in time (with a width of 15 to ensure ~5 observations are used).

Manual checks are performed at this stage: comparing the time series of lake-mean reconstructed LSWTs with the lake-mean observation. The purpose of these checks is to determine whether the reconstruction is realistic or whether the FLake simulation is a more suitable prior. FLake simulations are used as a last resort for cases where the reconstructions are in poor agreement with observations, typically cases where the observations are extremely sparse. Where DINEOF reconstructions are of good quality, day and night time reconstructions are averaged to provide a single time series for each instrument. Only a single reconstruction is used if only one of the day/night pair is of suitable quality,

Reconstructions for all the Phase one lakes are then merged to create daily files with global coverage at a resolution of $^{1}/_{20}°$. An estimate of the error in the prior LSWT field is also required. For lakes where FLake is used as the prior, the error (SD) is assigned to 2.0 K. For lakes where the DINEOF reconstruction is used, the error estimate is taken from the comparison of the prior from the previous iteration with *in situ* observations in the MD (MacCallum and Merchant, 2010). These daily global files of reconstructed and modelled LSWTs with associated error estimates are then used as the prior LSWT field in the next run of the ARC-Lake processor and the process, as outlined above and in Figure 1, repeats iteratively. As illustrated in Figure 1 the full time series of observations for each instrument is used as input to the iterative scheme.

A modified approach is used for ATSR-1 and additional AATSR observations (e.g. 2010 and 2011). For efficiency, we use the ATSR-2/AATSR climatology from v1.1 products (rather than MODIS climatology) as the initial prior LSWT, with a fixed error estimate of 2 K. Following this initialisation run, one further iteration of the processing scheme (Figure 1) is performed to generate the v2.0 data products for ATSR-1 and 2010-2011 (AATSR). Two further modifications are made to the ATSR-1 processing. Firstly, no visible channels are available on ATSR-1 and therefore no ice cover observations (§7) are possible during the day or night. To reduce dependence on FLake simulations, we substitute in frozen periods based on ATSR-2/AATSR climatology before generating the reconstructions. This is done by replacing potential but missing observations with value 273.15 for cells/dates where the ATSR-2/AATSR climatology is < 273.4 K (the additional 0.25 K is to accommodate deviations from frozen that can occur in the reconstructions). Secondly, for lakes where a lack of ATSR-1 observations prevents the generation of a full time-series reconstruction the ATSR-2/AATSR climatology is used, as this generally provides a more realistic representation of the seasonal cycle.

A further modification to the approach is implemented in creating the v3 ARC Lake dataset, to accommodate the inclusion of ~1000 smaller water bodies in the target list and to account for differences in the land/water masks for targets included in both v2 and v3. For new

targets, where no prior LSWT data is available from ARC-Lake, a climatological seasonal LSWT cycle from Flake simulations is used as the first-pass prior LSWT, as before. For existing targets, ARC-Lake v2 reconstructions are used. As the land/water masks differ between phases 2 and 3, an intermediate step was required to convert the reconstructions to the new land/water mask. Cells were flagged as water in both masks use the v2 LSWT reconstruction, cells flagged as water only in the phase-2 mask are omitted from the phase-3 prior, and cells flagged as water only in the phase-3 mask are filled using a weighted mean of the three nearest neighbouring cells with valid LSWT in the v2 reconstruction. As with earlier iterations of the processing scheme the ARC-Lake LSWT output from this first-pass phase-3 processing were used to determine the prior LSWT for a second-pass of the processing scheme, as described earlier and as illustrated in Figure 1.

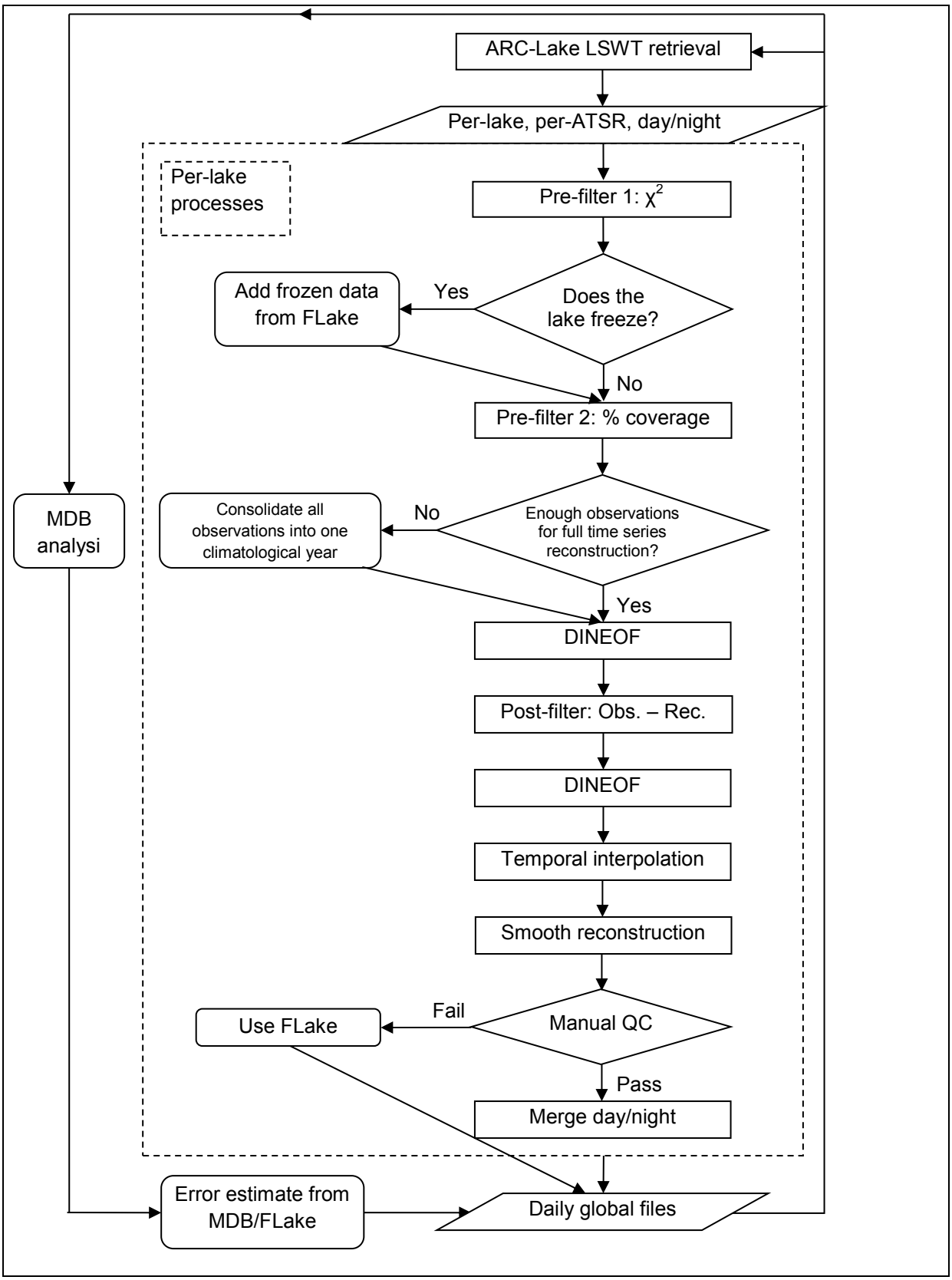

Figure 1. Flow-chart describing iterative processed used to generate high resolution prior LSWT field.

4.3 Sources of prior and availability of reconstructed time series

As outlined in §4.2, the final time series of LSWT used as input in the ARC-Lake processor come from one of three possible sources (in order from most to least preferred): DINOEF reconstructions of the full instrument time series, DINEOF reconstructions of daily climatology, or FLake simulations. With each iteration it is found that the number of lakes where the prior comes from the more preferred sources increases. In generating the version 1.0 release of ARC-Lake, two iterations were undertaken. A third iteration was performed in generating the version 1.1 release of ARC-Lake products. A fourth iteration was performed to generate v2.0 ARC-Lake data products. The expansion of the target list in phase-3 required a further two iterations, the first for initialisation of the new target using FLake priors and a second using output from the first phase-3 pass as priors.

A summary of the sources of prior LSWT for each release of ARC-Lake products is given in Table 4, while a detailed breakdown of the version 3.0 data in Table 4 is given in Table 7 in §13.2 (a detailed breakdown for v2.0 data is given in Table 6 in §13.1). Note that v3.1 data products do not exist. The sources of prior LSWT for v3.1 data are included in Table 4. Sources of data for prior LSWT field used to generate different versions of the ARC-Lake dataset. Note that v3.1 data does not exist and that these values are included for illustrative purposes only.Table 4 to illustrate that the source of prior LSWT improves with each iteration.

Version	Instrument	Reconstructed time series	Reconstructed climatology	Mix of reconstructions	FLake
1.0	**ATSR2**	81	135	22	25
	AATSR	112	112	17	22
1.1	**ATSR2**	126	97	28	12
	AATSR	160	73	16	14
2.0	**ATSR1**	112	113	34	4
	ATSR2	174	27	57	5
	AATSR	183	16	60	4
3.0	**ATSR1**	N/A	N/A	N/A	N/A
	ATSR2	138	976	134	380
	AATSR	427	818	160	223

3.1	**ATSR1**	N/A	N/A	N/A	N/A
	ATSR2	266	828	132	402
	AATSR	551	686	173	218

Table 4. Sources of data for prior LSWT field used to generate different versions of the ARC-Lake dataset. Note that v3.1 data does not exist and that these values are included for illustrative purposes only.

4.4 Implementation of high resolution prior surface temperature field

The OE retrieval scheme requires the input of prior meteorological fields and forward modelling based on these fields. As atmospheric fields are smooth compared to the spatial scales of LSWT variation, it is not necessary to perform the forward modelling at every satellite pixel or grid cell of a high resolution prior. Instead, forward modelling is carried out at ATSR tie-points (resolution ~ 0.225°), using the distance weighted average of the four nearest neighbours from the high resolution LSWT prior. Due to computational limitations this transform to ATSR tie-points is performed on a reduced resolution (0.1°) version of the prior (generated from the 0.05° reconstruction). The full resolution (0.05°) prior is later combined with the forward model output at tie-points to estimate the prior BTs at the higher resolution. This is achieved by bilinear interpolation of the quantity

$$\mathbf{F}(x_a) + \frac{\partial y}{\partial x}(x_{hi-res} - x_a)$$

which is then used as the forward model value for pixels corresponding to $x_{hi\text{-}res}$ rather than $\mathbf{F}(\mathbf{x}_a)$. Here: x_a is the prior LSWT on tie-points, x_{hi-res} x_{hi-res} is the high resolution LSWT prior, $\frac{\partial y}{\partial x}$ is the tangent linear of BTs with respect to surface temperature, and $\mathbf{F}(x_a)$ represents the forward modelled BTs for the state vector at the tie-points.

5 LAKE-SPECIFIC EMISSIVITY

Values of the infrared emissivity of water surfaces are another important component of the forward model, and require a spectral emissivity model to calculate them. Such a model must account for the emissivity variations associated with wavelength, view angle, wind speed, water temperature and, for the case of lake surfaces, salinity. A suitable emissivity model for ocean surfaces (neglecting salinity variations) is described by Embury et al. (2010), and is the basis of the lake-specific emissivity model used in ARC-Lake.

Embury et al. (2010) model the emissivity at any view angle using the following methods. They assume the water surface consisting of plane facets with a wind speed dependent slope distribution, calculate Fresnel reflection coefficients for each facet, and obtain the sum of their contributions (Masuda et al, 1988 and Masuda, 2006). In addition to the direct emission, Embury et al. (2010) also include a contribution from emitted radiation that has been reflected by the surface into the view angle (Watts et al. 1996, Wu and Smith 1997).

The isotropic Gaussian version of the clean surface slope distribution measured/modelled by Cox and Munk (1954) provides an appropriate description of the sea slope distribution (i.e., wind azimuth angle need not be considered). This distribution also provides an estimate of the background mean squared slope due to swell.

In order to avoid significant errors in simulated BTs the emissivity model must account for the temperature dependence of emissivity (Newman et al. 2005). This may be achieved through the use of temperature dependent values of refractive indices of water (pure and sea water). The refractive indices of Newman et al (2005) are recommended for the frequency range 760-1230 cm^{-1}, and those of Downing et al (1975) elsewhere. Suitable treatment of the temperature dependence of the refractive indices is given by Newman et al (2005) for the range 760-1230 cm^{-1}, and by Pinkley et al (1977) for other spectral regions. Temperature and salinity dependences may be assumed independent, and may be combined to calculate refractive indices for sea water (using a fixed standard value of 35 PSU) at different temperatures.

Embury et al.'s results are available at Filipiak (2008)

For the lake-specific emissivity model, refractive indices are also calculated for pure water and double sea water salinity (70 PSU) using the treatments of salinity dependence given by Pinkley and Williams (1976).

It is not necessary for the emissivity model to include the effect of surface foam, which will affect the emissivity at higher wind speeds. The effect of foam on the emissivity is likely to be smaller than the maximum effect proposed in Watts et al (1996), demonstrated by Salisbury et al (1993) who show emissivity is unaffected by foam in the 8-14 μm region. In

addition, the temperature of the foam may not match the skin temperature (Marmorino, 2005).

In the ARC-Lake processor, a salinity is associated with each lake ID. The forward model simulations then use an emissivity appropriate to that salinity obtained by linear interpolation of the emissivity for salinities of 0, 35, 70 PSU. This dependence upon salinity was introduced in ARC-Lake v1.1 data products (v1.0 products used a fixed salinity of 35 PSU for all lakes).

In phase-3 of ARC-Lake, over 1000 new targets were added. Information on the salinity of water bodies is not readily available on this global scale. Therefore only a small fraction of these additional water bodies have been determined to be either saline or fresh water, and an even smaller number have been assigned a salinity value. All targets with undefined salinity have been assumed to be fresh water.

Limitations of this approach are as follows:

- The facet slope distribution with respect to wind speed used for emissivity calculations is appropriate to open ocean, and may not represent well situations of short fetch from lake shores.
- The relationship between NWP wind speed and local winds over a lake is likely to be less accurate than for the open ocean (because of topographical effects).
- A few lakes have salinity that varies spatially or in time to a significant degree, these variations not being represented by the single value used in the ARC-Lake processor.
- Salinity information is not readily available for individual water bodies on a global scale.

6 BAYESIAN CLEAR-SKY PROBABILITY

The following sections describe the general principles of Bayesian probability theory and their application to cloud detection. It should be noted that all predefined probability density function look-up tables describing the distributions of cloudy radiances used in the ARC-Lake processing at present have been developed for SST observations rather than LSWT observations. To the degree that cloudy radiance distributions vary between land and sea, this gives scope for further improvement. Equivalent look-up tables based on ARC-Lake LSWT observations may be developed in the future, but this is not reckoned to be a priority, since cloud regimes vary significantly over the ocean in any case.

6.1 Bayesian Probability Theory

The problem being addressed is:

> *To deduce the likelihood of an image pixel being cloud-free given the radiance values from various thermal and reflectance channels for the pixel (and perhaps for other pixels in the image).*

The radiance information can be supplemented with prior (background) knowledge. From the time and geographical location of the observations, climatological and/or NWP forecast values of surface temperature and atmospheric state can be specified. The addition of background information allows Bayesian statistics to be used to solve the problem posed.

Bayes' theorem for the probability of clear sky, c, given the observations, $\mathbf{y}^o$, and the background knowledge, $\mathbf{x}^b$, amounts to:

Eq. 6.1
$$P\left(c \mid \mathbf{y}^o, \mathbf{x}^b\right) = \frac{P\left(\mathbf{y}^o \mid \mathbf{x}^b, c\right) P\left(\mathbf{x}^b \mid c\right) P(c)}{P\left(\mathbf{y}^o \mid \mathbf{x}^b\right) P\left(\mathbf{x}^b\right)}$$

where each P represents a probability or probability density function as specified in its argument; c is the state of clear-sky clear-ocean; $\mathbf{y}$ is the observation vector; $\mathbf{x}$ is the state vector; superscript o indicates *observed* and superscript b indicates *background* (i.e., prior knowledge). The definition of the elements of the observation vector and background state will vary according to the sensor and forward model respectively.

For imagers used in meteorology, the clear-sky probability varies on length scales down to the pixel dimensions (~1 km). This is much finer than the length scales of variation in the atmospheric terms (other than cloudiness) in the background state (~100 km). To a good approximation on pixel-to-pixel scales, the background state is independent of clear-sky probability, that is $P\left(\mathbf{x}^b \mid c\right) = P\left(\mathbf{x}^b\right)$, simplifying Eq. 6.1 to

Eq. 6.2
$$P\left(c \mid \mathbf{y}^o, \mathbf{x}^b\right) = \frac{P\left(\mathbf{y}^o \mid \mathbf{x}^b, c\right) P(c)}{P\left(\mathbf{y}^o \mid \mathbf{x}^b\right)}$$

The term $P(\mathbf{y}^o \mid \mathbf{x}^b)$ describes the probability density function of the observations given the background state. We may decompose this probability density function into the contribution from clear and cloudy conditions, i.e.

Eq. 6.3 $$P(\mathbf{y}^o \mid \mathbf{x}^b) = P(c)P(\mathbf{y}^o \mid \mathbf{x}^b, c) + P(\bar{c})P(\mathbf{y}^o \mid \mathbf{x}^b, \bar{c})$$

where an over-bar signifies the logical *not* condition, and $P(\bar{c}) = 1 - P(c)$ by definition. Substituting into Eq. 6.2 and rearranging gives the final form used to estimate the clear-sky probability:

Eq. 6.4 $$P(c \mid \mathbf{y}^o, \mathbf{x}^b) = \left[1 + \frac{P(\bar{c})P(\mathbf{y}^o \mid \mathbf{x}^b, \bar{c})}{P(c)P(\mathbf{y}^o \mid \mathbf{x}^b, c)}\right]^{-1}$$

Given a prior estimate of $P(c)$, evaluating the clear-sky probability in the light of the observations amounts to finding the probability density for the observations given the background state for both clear and cloudy conditions, and then using these values to evaluate Eq. 6.4

6.2 Probability density functions – clear-sky

6.2.1 Definitions

$P(\mathbf{y}^o \mid \mathbf{x}^b, c)$ is the probability of the observations given the background fields and assuming clear-sky. The observation vector, $\mathbf{y^o}$, consists of spectral and textural components. These are the channel brightness temperatures (or reflectances) and the local standard deviations of these, denoted by $\mathbf{y}_s^o$ and $\mathbf{y}_t^o$ respectively. It will be assumed that the local standard deviation PDFs are independent of the brightness temperatures (and reflectances), therefore for the clear probability:

Eq. 6.1 $$P(\mathbf{y}^o \mid \mathbf{x}^b, c) = P(\mathbf{y}_s^o \mid \mathbf{x}^b, c) \times P(\mathbf{y}_t^o \mid \mathbf{x}^b, c)$$

Using night-time AATSR retrievals as an example, the spectral component, $\mathbf{y}_s^o$, is composed of the brightness temperatures at 3.7 μm, 11 μm, and 12 μm, denoted by y_1, y_2, and y_3. For the textural component, only the local standard deviation of the 11 μm brightness temperature is used, denoted by y_4. Eq. 6.1 can therefore be written as:

Eq. 6.2 $$P(\mathbf{y}^o \mid \mathbf{x}^b, c) = P\left(\begin{bmatrix} y_1 \\ y_2 \\ y_3 \end{bmatrix} \mid \mathbf{x}^b, c\right) \times P([y_4] \mid \mathbf{x}^b, c)$$

For day-time AATSR retrievals, the 3.7 μm channel is replaced with the 1.6 μm channel, to avoid problems with solar contamination.

6.2.2 Definitions

If it is assumed that the errors in the observed and background brightness temperatures have a Gaussian distribution, then the joint probability density function is given by:

Eq. 6.3 $$P\left(\mathbf{y}_s^o \mid \mathbf{x}^b, c\right) = \frac{\exp\left\{-\frac{1}{2}\Delta\mathbf{y}^{\mathrm{T}}\left(\mathbf{K}\mathbf{S}_a\mathbf{K}^T + \mathbf{S}_\varepsilon\right)^{-1}\Delta\mathbf{y}\right\}}{2\pi \mid \mathbf{K}\mathbf{S}_a\mathbf{K}^T + \mathbf{S}_\varepsilon \mid^{\frac{1}{2}}}$$

which for the AATSR example can be written as:

Eq. 6.4 $$P\left(\begin{bmatrix} y_1 \\ y_2 \\ y_3 \end{bmatrix} \mid \mathbf{x}^b, c\right) = \frac{\exp\left\{-\frac{1}{2}\Delta\mathbf{y}^{\mathrm{T}}\left(\mathbf{K}\mathbf{S}_a\mathbf{K}^T + \mathbf{S}_\varepsilon\right)^{-1}\Delta\mathbf{y}\right\}}{2\pi \mid \mathbf{K}\mathbf{S}_a\mathbf{K}^T + \mathbf{S}_\varepsilon \mid^{\frac{1}{2}}}$$

If the clear-sky probability density evaluates to less than 10^{-15} K^{-2}, it is set to 10^{-15} K^{-2}. In conjunction with a minimum of 10^{-10} K^{-2} imposed on the cloudy probability density function, this means that any outlying/aberrant BTs are flagged as not clear, while avoiding dividing by zero.

The vector and matrix terms in Eq. 6.3 are defined as follows:

(i) $\Delta\mathbf{y}$ is the difference vector for the observed and background brightness temperatures, defined for the *i*th element as $y_i^b = F_i\left(\mathbf{x}^b\right)$.

(ii) $\mathbf{K}\mathbf{S}_a\mathbf{K}^T$ is the error covariance in the background observation vector resulting from the propagation of the background variable errors through the FFM.

$\mathbf{K}$ is the tangent linear of the forward model defined as:

$$\mathbf{K} = \frac{\partial \mathbf{y}_s^{\mathbf{b}}}{\partial \mathbf{x}^{\mathbf{b}}}$$

For the example of AATSR, $\mathbf{K}$ can be written as:

$$\mathbf{K} = \begin{bmatrix} \frac{\partial T_{3.9}}{\partial SST}^b & \frac{\partial T_{3.9}}{\partial TCWV}^b \\ \frac{\partial T_{11}}{\partial SST}^b & \frac{\partial T_{11}}{\partial TCWV}^b \\ \frac{\partial T_{12}}{\partial SST}^b & \frac{\partial T_{12}}{\partial TCWV}^b \end{bmatrix}$$

$\mathbf{S}_a$ is the background covariance matrix defined as

$$\mathbf{S}_a = \begin{bmatrix} \left(\varepsilon^{b}_{SST}\right)^2 & 0 \\ 0 & \left(\varepsilon^{b}_{TCWV}\right)^2 \end{bmatrix}$$

where ε^{b}_{SST} and ε^{b}_{TCWV} are the errors in the background state variables.

(iii) $\mathbf{S}_\varepsilon$ is the total covariance in the difference between the background and actual observation vectors in the absence of background variable error. This is the sum of the RTM model covariance and the covariance in the observed values. The examples below illustrate the three-channel case (e.g. AATSR night-time retrievals, where i = 3.7 µm, j = 11 µm, and k = 12 µm), and are readily generalized to other configurations.

$$\mathbf{S}_r = \begin{bmatrix} \left(\varepsilon^{m}_{i}\right)^2 & r^2\left(\varepsilon^{m}_{i}\right)\left(\varepsilon^{m}_{j}\right) & r^2\left(\varepsilon^{m}_{i}\right)\left(\varepsilon^{m}_{k}\right) \\ r^2\left(\varepsilon^{m}_{j}\right)\left(\varepsilon^{m}_{i}\right) & \left(\varepsilon^{m}_{j}\right)^2 & r^2\left(\varepsilon^{m}_{j}\right)\left(\varepsilon^{m}_{k}\right) \\ r^2\left(\varepsilon^{m}_{k}\right)\left(\varepsilon^{m}_{i}\right) & r^2\left(\varepsilon^{m}_{k}\right)\left(\varepsilon^{m}_{j}\right) & \left(\varepsilon^{m}_{k}\right)^2 \end{bmatrix}$$

where r is the correlation coefficient of RTM error between the two channels. By default, the errors in the modelled brightness temperatures are assumed to be uncorrelated, i.e., $r^2 = 0$ (which needs further assessment).

The other variance component for the observed brightness temperatures is due to radiometric noise, which is assumed to be uncorrelated between TIR channels, therefore the covariance matrix for the observed parameters is:

$$\mathbf{S}_o = \begin{bmatrix} \left(\varepsilon^{o}_{i}\right)^2 & 0 & 0 \\ 0 & \left(\varepsilon^{o}_{j}\right)^2 & 0 \\ 0 & 0 & \left(\varepsilon^{o}_{k}\right)^2 \end{bmatrix}$$

The sum of the covariances in the RTM model and observed values gives the total covariance matrix:

Eq. 6.5
$$\mathbf{S}_\varepsilon = \mathbf{S}_r + \mathbf{S}_o = \begin{bmatrix} \left(\varepsilon^{m}_{i}\right)^2 + \left(\varepsilon^{o}_{i}\right)^2 & r^2\left(\varepsilon^{m}_{i}\right)\left(\varepsilon^{m}_{j}\right) & r^2\left(\varepsilon^{m}_{i}\right)\left(\varepsilon^{m}_{k}\right) \\ r^2\left(\varepsilon^{m}_{j}\right)\left(\varepsilon^{m}_{i}\right) & \left(\varepsilon^{m}_{j}\right)^2 + \left(\varepsilon^{o}_{j}\right)^2 & r^2\left(\varepsilon^{m}_{j}\right)\left(\varepsilon^{m}_{k}\right) \\ r^2\left(\varepsilon^{m}_{k}\right)\left(\varepsilon^{m}_{i}\right) & r^2\left(\varepsilon^{m}_{k}\right)\left(\varepsilon^{m}_{j}\right) & \left(\varepsilon^{m}_{k}\right)^2 + \left(\varepsilon^{o}_{k}\right)^2 \end{bmatrix}$$

NOTE: The example for AATSR night-time pixels can be easily modified to perform cloud screening for day-time pixels. For the day-time case, the 3.7 µm channel is replaced by the near-infrared channel, giving i = 1.6 µm in Eq. 6.5. Again, $r^2 = 0$ is appropriate, since the forward models are independent.

6.2.3 LSD Distributions

The texture measure used in ARC-Lake is local standard deviation (LSD) and has a non-Gaussian distribution, for both clear and cloudy scenes. A satisfactory analytical solution has not been found, and PDFs for the textural component are derived empirically from pre-screened observations over oceans. Since the spatial distribution of thermal features and gradients in lakes can be different over lakes (typically, less uniformity than the ocean), creation of a PDF specific to inland waters will be considered in future. The distribution of local standard deviation for clear-sky cases also depends on radiometric noise. Lower channel noise requires a higher bin resolution to accurately represent the peak in the PDF. The low-noise (NEDT ~0.04 K) 1 km resolution ATSR2/AATSR are used to create the pdfs empirically. A 1-D textural PDF for the 11 μm channel is used for ATSR-2 and AATSR night-time (Figure 2) and day-time retrievals.

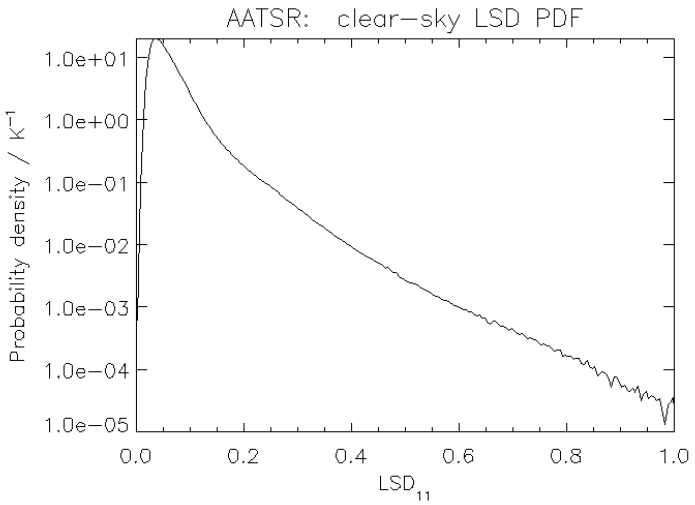

Figure 2. Clear-sky 11 μm textural PDF for night-time AATSR.

6.3 Probability density functions – cloudy-sky

6.3.1 Definitions

$P\left(\mathbf{y}^{o} \mid \mathbf{x}^{b}, \bar{c}\right)$ is the probability of the observations given the background fields and assuming cloudy-sky (the condition '*not clear-sky*' is more correct as this condition could also result from extreme aerosol loading or clear-sky over ice). As with the clear-sky probabilities, it will be assumed that the local standard deviation PDFs are independent of the brightness temperatures (and reflectances), therefore for the cloudy probability

Eq. 6.6. $$P\left(\mathbf{y}^{o} \mid \mathbf{x}^{b}, \bar{c}\right) = P\left(\mathbf{y}_{s}^{o} \mid \mathbf{x}^{b}, \bar{c}\right) \times P\left(\mathbf{y}_{t}^{o} \mid \mathbf{x}^{b}, \bar{c}\right)$$

For the AATSR example (as introduced in §6.2.1), Eq. 6.6 can be written as:

Eq. 6.7 $$P(\mathbf{y}^o \mid \mathbf{x}^b, \bar{c}) = P\left(\begin{bmatrix} y_1 \\ y_2 \\ y_3 \end{bmatrix} \mid \mathbf{x}^b, \bar{c}\right) \times P([y_4] \mid \mathbf{x}^b, \bar{c})$$

6.3.2 Joint BT Distributions

The joint probability density function $P(\mathbf{y}_s^o \mid \mathbf{x}^b, \bar{c})$ will have no analytic form and must be inferred from empirical observations or numerical modelling and then tabulated.

The approach taken in the ARC-Lake processor is to define $P(\mathbf{y}_s^o \mid \mathbf{x}^b, \bar{c})$ as a function of only one variable in the background state, $\mathbf{x}^b$, namely, the prior surface temperature. The tabulations have been defined within the ARC SST project for cloud radiances associated with different bands of prior SST, and are assumed to apply similarly for different LSWTs.

The global joint probability density function (hereafter, '*P-cloud*'), derived empirically from satellite imagery or numerical modelling, is represented by an *N*-dimensional look-up table (LUT), where *N* is the number of channels used (and must match the number of channels used to define the clear scene PDF, §6.2). Appropriate bin widths must be chosen so as to give as smooth a representation of the PDF as possible given the number of data points. The PDFs must also be correctly normalized so that their units match the analytical PDF for $P(\mathbf{y}_s^o \mid \mathbf{x}^b, c)$. It is also necessary to define a minimum allowed value for elements of all PDFs, with any values less than this reset to the minimum. In ARC-Lake, the LUTs for '*P-cloud*' derived from the ARC SST project is used.

For the AATSR example (§6.2.1), *P-cloud* is taken from cloud-screened ocean imagery of AATSR. The *P-cloud* is defined as the fraction of known cloudy-pixel BTs occurring in each bin of size **2** K along the dimension T_{11}-SST and of size $(0.2\ K)^2$ in the area defined by axes $\{T_{11}-T_{12}, T_{3.7}-T_{11}\}$. The occurrences counted are those flagged cloudy in the ARC SST mask from all AATSR night-time images from all latitudes and seasons, giving a huge number of observations from which to deduce a smooth LUT. *P-cloud* was determined for nadir and forward views separately and as a function of prior SST. As a method of compression, the *P-cloud* LUTs are stored in terms of temperature differences (e,g, 3.7 µm - 11 µm, 11 µm - 12 µm, and 11 µm – SST for the AATSR night-time example).

Slices of the *P-cloud* LUT for the AATSR example are shown in Figure 3 for the nadir view and a prior SST or LSWT of 280.0-282.5 K. The full night-time LUT is an array of dimensions [2,14,80,50,15] corresponding to dimensions of: satellite zenith angle, prior SST, 3.7 µm - 11 µm, 11 µm - 12 µm, and 11 µm – SST. Bin sizes for these dimensions are: 30°, 2.5 K, 0.2, K, 0.2 K, and 2 K. Ranges vary for dimensions representing temperature differences, while the SST dimension covers from 270.0 K to 305.0 K. The minimum is not zero, but is set to 10^{-10} K^2. This is to avoid geophysically implausible values of BT being given zero probability of there being cloud: the minimum of the clear-sky probability density

function is set to 10^{-15} K^2, and so BT outliers will be flagged as '*not clear*', as one would wish.

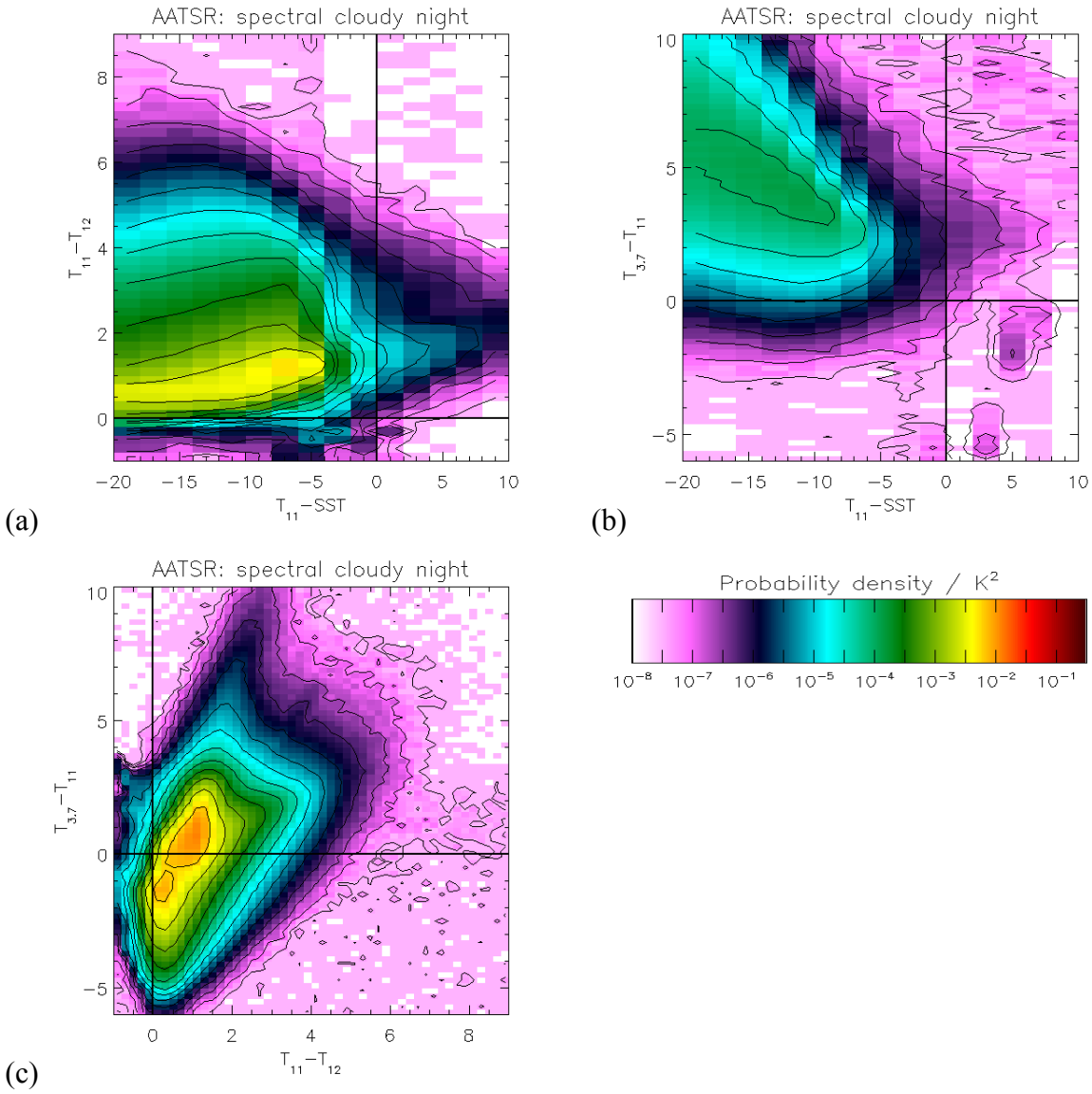

Figure 3. Examples of slices of the night-time cloudy-sky spectral PDF LUT for AATSR. All figures illustrate the LUT used for the nadir view for a prior LSWT range of 280.0 K to 282.5 K. (a) 11 µm - SST vs 11 µm – 12 µm for 3.7 µm – 11 µm differences of 2.0 K to 2.2 K. (b) 11 µm - SST vs 3.7 µm – 11 µm for 11 µm – 12 µm differences of 4.0 K to 4.2 K. . (c) 11 µm – 12 µm vs 3.7 µm – 11 µm for 11 µm – SST differences of -6.0 K to -4.0 K.

For the day-time AATSR example, *P-cloud* is determined for the dual-view configuration rather than for each view separately as in the night-time case. This dual-view method is only possible for day-time retrievals as the reduced TIR channel set enables a manageable-sized LUT to be defined. As for night-time retrievals, *P-cloud* is determined as a function of prior SST and the LUTs are stored in terms of temperature differences. The full day-time LUT is

an array of dimensions [14, 15, 20, 20, 20] corresponding to: prior SST, 11 µm nadir – SST, 11 µm nadir - 12 µm nadir, 11 µm forward - 12 µm forward, 11 µm nadir – 11 µm forward. Bin sizes for these dimensions are: 2.5 K, 2.0 K, 0.4 K, 0.4, K, and 0.4 K. *P-cloud* for the AATSR day –time example is shown in Figure 4 for a prior SST of 280.0 K to 282.5 K.

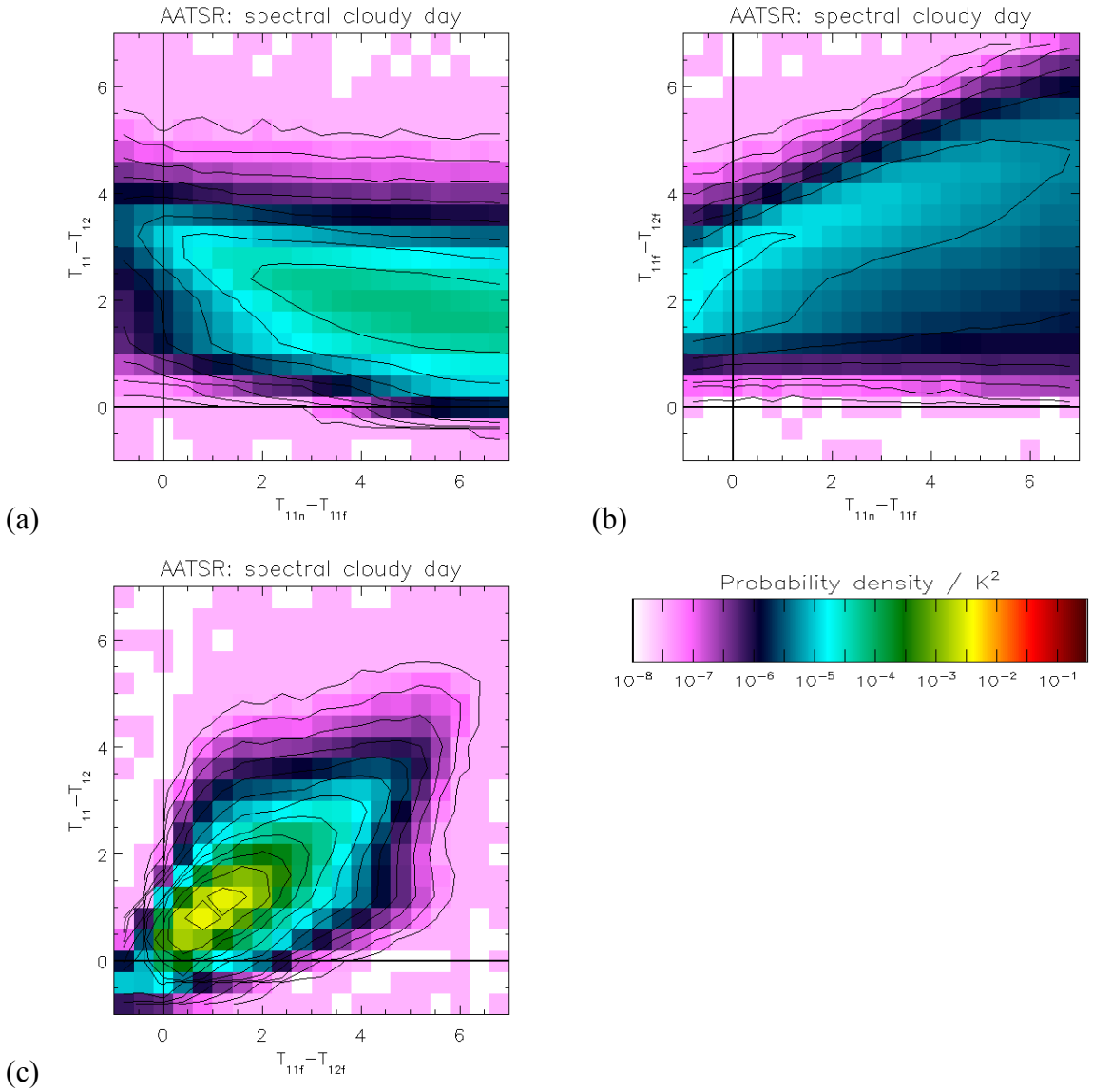

Figure 4. Examples of slices of the day-time cloudy-sky spectral PDF LUT for AATSR. All figures are illustrative for a prior SST range of 280.0 K to 282.5 K and 11 µm – SST differences of -6.0 K to -4.0 K. (a) 11 µm nadir – 11 µm forward vs 11 µm nadir – 12 µm nadir for 11 µm forward – 12 µm forward differences of 3.0 K to 3.4 K. (b) 11 µm nadir – 11 µm forward vs 11 µm forward – 12 µm forward for 11 µm nadir – 12 µm nadir differences of 3.0 K to 3.4 K. (c) 11 µm forward – 12 µm forward vs 11 µm nadir – 12 µm nadir for 11 µm nadir – 11 µm forward differences of 3.0 K to 3.4 K.

It is assumed that the near infra-red (NIR) reflectance (1.6 μm) is uncorrelated with the TIR BTs (11 μm and 12 μm for AATSR), therefore for the day-time pixels the general form of the globally cloudy PDF is given by:

Eq. 6.8 $$P\left(\mathbf{y}_s^o \mid \bar{c}\right) = P\left(y_{NIR} \mid \bar{c}\right) \times P\left(y_{TIR} \mid \bar{c}\right)$$

For the AATSR example this is:

Eq. 6.9 $$P\left(\begin{bmatrix} y_{NIR} \\ y_2 \\ y_3 \end{bmatrix} \mid \bar{c}\right) = P\left(y_{NIR} \mid \bar{c}\right) \times P\left(\begin{bmatrix} y_2 \\ y_3 \end{bmatrix} \mid \bar{c}\right)$$

where *P-cloud* for the NIR reflectance is determined for the dual-view configuration in a similar manner to that outlined above. The full day-time LUT for the NIR reflectance is an array of dimensions [28, 100, 100] corresponding to: solar zenith angle, 1.6 μm nadir, and – 1.6 μm forward. Bin sizes for these dimensions are: 2.5°, 0.01, and 0.01. *P-cloud* for the AATSR day –time reflectance channel is shown in Figure 5 for a solar zenith angle range of 55° to 57.5°.

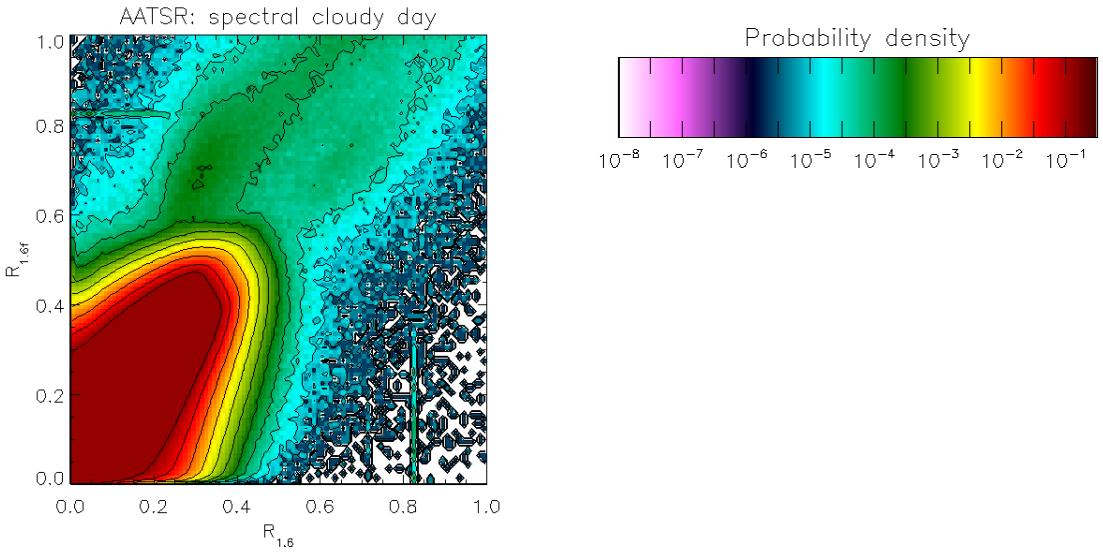

Figure 5. Example slice of cloudy-sky spectral PDF LUT for 1.6 μm day-time for solar zenith angles in the range 55° to 57.5°.

6.3.3 LSD Distributions

The joint probability distribution $P\left(\mathbf{y}_t^o \mid \mathbf{x}^b, \bar{c}\right)$ of LSD for TIR channels can be determined empirically from pre-screened observations (the cloudy scene is too complex to be represented analytically). Textural measures are only useful for screening over water surfaces where the length of scale of variability can be assumed to be much larger than the pixel scale. For SST retrievals this is generally true, except in regions of ocean fronts. For LSWT

retrievals however, the length of scale of variability may be shorter and this assumption may no longer be adequate. Therefore further assessment of LSD distributions for lakes is required.

For the AATSR example, $P(\mathbf{y}_t^o \mid \mathbf{x}^b, \bar{c})$ of LSD for 11 μm was found empirically from cloudy pixels in the full set of AATSR imagery. The probability function estimated is shown in Figure 6.

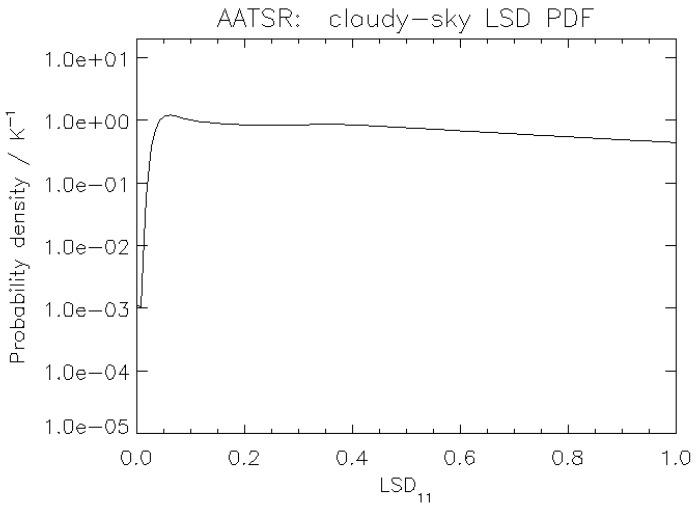

Figure 6. Cloudy-sky 11 μm textural PDF for night-time AATSR.

6.4 Clear-sky Probability

6.4.1 Unconditional clear-sky probability - $P(c)$

The unconditional clear-sky probability is currently set to a globally constant value of 10%, i.e.

Eq. 6.10 $$P(c) = 0.10$$

Using an existing database of imagery for a given satellite sensor this PDF could be improved to allow for the spatial and seasonal variability in clear-sky conditions. From a longer time series it will also be possible to allow for climatic patterns such as the El Nino southern oscillation (ENSO) and the North Atlantic oscillation (NAO) which both significantly affect cloud distributions. However, the influence of this parameter is not dominant, and these refinements are not a priority.

6.4.2 Conditional clear-sky probability - $P(c \mid \mathbf{y}^o, \mathbf{x}^b)$

The conditional clear-sky probability is a measure of the likelihood of a given pixel being cloud-free, and is the value returned as part of the SST product. It is calculated using the equation:

Eq. 6.11 $$P\left(c \mid \mathbf{y}^{o}, \mathbf{x}^{b}\right) = \left[1 + \frac{P(\bar{c})P\left(\mathbf{y}^{o} \mid \mathbf{x}^{b}, \bar{c}\right)}{P(c)P\left(\mathbf{y}^{o} \mid \mathbf{x}^{b}, c\right)}\right]^{-1}$$

where $P(\bar{c}) = 1 - P(c)$

$P\left(\mathbf{y}^{o} \mid \mathbf{x}^{b}, c\right)$ is defined in §6.2

$P\left(\mathbf{y}^{o} \mid \mathbf{x}^{b}, \bar{c}\right)$ is defined in §6.3

6.5 Practical considerations

The LUTs for all PDFs are stored across two files per instrument: one for clear-sky probabilities and the other for cloudy-sky probabilities. These files are in NetCDF format. Each file contains the various LUTs along with data defining the dimensions of each LUT. Selection of LUTs from these files and the look-up of the LUTs is handled by the ARC-Lake processing code, and is dependent on the following factors: channels available, solar zenith angle, satellite zenith angle, prior LSWT, and the channel BTs and reflectances.

7 ICE IN PIXEL TEST

The ARC-Lake project also provides observations of lake ice concentration (LIC). This is based on the Normalized Difference Snow Index (NDSI) of Hall et al (1995) and is limited to daytime observations (as it uses visible reflectance channels). The NDSI is calculated using

Eq. 7.1 $$NDSI = \frac{R_{0.8} - R_{1.6}}{R_{0.8} + R_{1.6}}$$

Where $R_{0.8}$ and $R_{1.6}$ are the reflectance observations in the 0.87 µm and 1.6 µm channels respectively. Image pixels where NDSI > 0.5 are flagged as ice.

The NDSI test is only performed on pixels that pass a prior threshold test, based on reflectances in the 0.67 µm, 0.87 µm and 1.6 µm channels:

$$2 \times R_{0.8} - R_{0.6} - R_{1.6} > 0.003$$

This threshold test is included to prevent excessive flagging of open-water pixels as ice, and is derived empirically from AATSR imagery over oceans. In some cases this test results in ice pixels being flagged as open-water (MacCallum and Merchant, 2011b) and therefore an underestimation of ice cover in some scenes.

Coarse cloud screening, performed in advance of this ice test in the retrieval scheme, results in some ice pixels being flagged as cloud rather than ice, if the ice is very cold (around -10^{o}C or colder, depending on the atmospheric conditions). This resulted in an underestimation of ice cover in some scenes in v1.0. To reduce the impact of this effect, the ice test is performed in advance of the coarse cloud screening in v1.1 onwards. The ice test is also prone to occasional false positive flagging ice-clouds as surface ice, with some cloud pixels being flagged as ice. In v1.1 onwards the impact of this effect is again reduced, through an additional threshold test: observations are only flagged as ice for cases where the prior LSWT < 278 K. For ATSR-2 there may also be occasional times when this ice test cannot be performed due to erroneous or unpredictable switching from the 1.6 µm to 3.7 µm channel (Mutlow *et al*, 1999). This can happen when reflectances are particularly low (e.g. when the surface is in shadow). The more general effect of shading on reflectances and any subsequent impact on NDSI is a relevant issue for lakes, due to potential shading effects of topography and cloud cover. (For ATSR-1, there is no 0.87 µm channel, and LIC is not generated.)

The LIC field in the ARC-Lake products then reports the fraction of clear-sky (i.e., not flagged as cloudy) lake pixels in the cell in which surface ice was flagged as above.

The limitations are thus suspected low hit rate for surface ice (when classed as cloud instead) and suspected significant false alarm rate (when ice cloud is classed as surface ice). These statements cannot be quantified at time of writing. Future work should involve assessing the

(mis)classification rate, synthesizing feedback from users regarding the LIC product, reviewing the literature for improvements/additions to the scheme and devising or implementing such improvements.

8 LAKE SURFACE WATER TEMPERATURE RETRIEVAL WITH UNCERTAINTY

Using standard ATSR SST retrieval coefficients for LSWT retrievals is prone, for some lakes, to retrieval biases of 0.5 K (Marsham, 2003). (By retrieval bias, we mean the systematic offset between satellite and true LSWT that arises from imperfection in the retrieval algorithm. Occasional "biases" from failures in cloud detection can be larger.) This contrasts with a level of SST retrieval bias for ATSR that is generally <0.2 K. The relatively larger potential for bias arises because of the range of lake altitudes, emissivity and the continentality of air masses; all these factors change the relationships between BTs and surface temperature. One solution could be to specify lake-specific retrieval coefficients. But this is not really a scalable solution as we look forward to later phases of the project, where more lakes will be tackled.

The LSWT retrieval is therefore done by optimal estimation (OE). We use a simplified formulation of the inverse problem originally developed for SST observations from the Advanced Very High Resolution Radiometer (AVHRR) (Merchant *et al*, 2008) . This formulation includes only LSWT and total column water vapour as retrieved (state) variables (all though full profile forward modelling is of course used). No radiance bias correction is yet derived for ATSR BTs, so the RTTOV8.7-simulated BTs are used "as is"

8.1 Optimal Estimation (OE) Retrievals

Optimal Estimation (OE) techniques combine prior information on the expected state of the atmosphere and the lake surface with observations to provide an optimal solution of the state and an associated uncertainty estimate.

Prior information, referred to as the prior state vector and denoted $\mathbf{x}_a$, where the "a" subscript denotes *a priori*, consists of: NWP forecast fields, reconstructed lake temperatures derived from ARC-Lake observations (§4), and a modelled estimate of emissivity (§5). This *a priori* information is input into a forward model to simulate observations for the prior state, $\mathbf{y}_a = \mathbf{F}(\mathbf{x}_a)$. The forward model used in ARC-Lake is RTTOV8.7 (Brunel *et al*, 2005), which provides simulated BTs corresponding to the ATSR channels. Partial derivatives of these simulated BTs with respect to state variables are also calculated. These provide an estimate of the sensitivity of the prior observations to the state. This sensitivity information is combined with the differences between satellite observations, $\mathbf{y}_o$, and prior observations, $\mathbf{y}_a$, to estimate the actual state.

The process is optimal in the sense that it will give an unbiased, minimum SD estimate provided the prior information, forward model and error covariance estimates are unbiased (Merchant *et al*, 2008). Two additional assumptions are also made: the retrieval is assumed to be linear within the range of BT corresponding to errors in NWP fields and that only the

leading two terms controlling BT need be considered. The second of these assumptions leads to a reduced state vector, $\mathbf{z}(\mathbf{x}) = \begin{bmatrix} x \\ w \end{bmatrix}$, in the retrieval, where x and w are the LSWT and total column water vapour respectively. However, the full prior state vector, $\mathbf{x}_a$, is used in the forward model.

The optimal solution is a weighted combination of the prior LSWT and TCWV, $\mathbf{z}(\mathbf{x}_a)$, and the difference between the observations, $\mathbf{y}_o$, and the BTs simulated for the prior field, $\mathbf{y}_a = \mathbf{F}(\mathbf{x}_a)$. Following the methods of Rodgers (1990) and Rodgers (2000), the equation for this solution is:

Eq. 8.1 $$\hat{\mathbf{z}} = \mathbf{z}(\mathbf{x}_a) + \left(\mathbf{K}^T \mathbf{S}_\varepsilon^{-1} \mathbf{K} + \mathbf{S}_a^{-1}\right)^{-1} \mathbf{K}^T \mathbf{S}_\varepsilon^{-1} (\mathbf{y}_o - \mathbf{F}(\mathbf{x}_a))$$

where $\hat{\mathbf{z}}$ consists of the retrieved LSWT and TCWV, $\mathbf{K}$ is the matrix of partial derivatives of observations with respect to the state, $\mathbf{S}_\varepsilon$ is the combined covariance matrix of prior and satellite observations, and $\mathbf{S}_a$ is the prior covariance matrix of the reduced state vector.

For day-time ARC-Lake LSWT retrievals these matrices are defined as follows (in Eq. 8.2 to Eq. 8.4). For night-time retrievals , the retrieval methodology outlined below is expanded to include the 3.7 µm channel.

Eq. 8.2 $$\mathbf{K} = \begin{bmatrix} \dfrac{\partial \mathbf{F}(\mathbf{x}_a)}{\partial \mathbf{z}} \end{bmatrix} = \begin{bmatrix} \partial y_{11}/\partial x & \partial y_{11}/\partial w \\ \partial y_{12}/\partial x & \partial y_{12}/\partial w \end{bmatrix}$$

where y_{11} and y_{12} represent the simulated BTs for the 11 µm and 12 µm channels, for the prior state, $\mathbf{x}_a$. The tangent linear outputs of the forward model, RTTOV, are used to represent $\mathbf{K}$.

Eq. 8.3 $$\mathbf{S}_\varepsilon = \begin{bmatrix} e_{11}^2 & 0 \\ 0 & e_{12}^2 \end{bmatrix}$$

where it is assumed that both radiometric noise in the satellite BTs and forward modelling errors are uncorrelated between channels (indicated by zero-value off-diagonal terms). Radiometric noise is calculated as a function on BT, based on channel NEΔT values at calibration black-body temperatures.

Eq. 8.4 $$\mathbf{S}_a = \begin{bmatrix} e_{x_a}^2 & 0 \\ 0 & e_{w_a}^2 \end{bmatrix}$$

where the zero-value off-diagonal terms indicate that errors in the prior LSWT and TCWV are assumed to be independent. The prior uncertainty in LSWT is determined from comparisons of retrieved LSWT with *in situ* observations (§4), while the prior uncertainty in TCWV is calculated as a function of TCWV, using coefficients derived from analysis on the ARC SST match-up database.

The expected total random uncertainty in $\hat{\mathbf{z}}$ is represented by the error covariance matrix:

Eq. 8.5 $$\hat{\mathbf{S}} = \left(\mathbf{K}^T \mathbf{S}_\varepsilon^{-1} \mathbf{K} + \mathbf{S}_a^{-1}\right)^{-1}$$

which includes the effects of instrumental noise, random forward model error, and errors in the prior state. Here, the leading element of $\hat{\mathbf{S}}$ provides an estimate of the random Gaussian variance in the retrieved LSWT from the sources above. Full details of the treatment of uncertainties in the LSWT retrieval is given in §8.2.

8.2 Treatment of Uncertainties

8.2.1 Introduction

All LSWT retrievals have an associated uncertainty estimate. Appropriate consideration and incorporation of uncertainties from all possible sources is important for any LSWT retrieval scheme. Uncertainties are typically split into two broad categories: systematic and random. Systematic uncertainties are described in terms of bias and give a measure of the accuracy of the retrieval. This is normally estimated by the mean difference between retrieved values and "truth" data (e.g. *in situ* buoy measurements). Random uncertainties are described in terms of scatter and provide an estimate of the precision of the retrieval. The standard deviation (SD) of the differences between retrieved and "truth" data are commonly used to estimate (or give an upper bound on) this uncertainty. Although these basic categorisations may be used to provide an overall picture of the errors in a retrieval scheme, error characteristics are in reality more complex, as discussed below.

It should be noted that in ARC-Lake v2.0 products, the uncertainty estimate provided, "Err_LSWT" (MacCallum and Merchant, 2011a), is simply an estimate of the variance of LSWT observations within each 0.05°x0.05° grid cell. The treatment of errors as discussed in the following sections will be implemented in later versions of ARC-Lake products.

8.2.2 Systematic Errors

General comment

Uncertainty distributions for systematic errors are not included in the uncertainty estimates associated with LSWTs in the ARC-Lake products. The reason is that systematic errors (biases) are subject to characterisation and reduction by, for example, improved retrieval algorithms. Information about biases is given by validation against independent

measurements. The sections below, however, discuss some forms of systematic errors relevant to ARC-Lake, for information.

Forward modelling errors

Systematic errors are introduced to the retrieval through the forward model, specified in §8.1, that is used to simulate radiances, $\mathbf{y}$, where:

Eq. 8.6 $$\mathbf{y} = \mathbf{F}(\mathbf{x}, \mathbf{b}) + \varepsilon_F$$

Here, **F** represents the function of the RTM, and ε_F the radiative transfer model error. The surface and atmospheric state are described by **x**, while **b** incorporates other model parameters such as spectroscopic data and sensor characterisation. The RTM error, ε_F, represents the departure of the simulation from what would really be observed by a sensor observing the situation described by **x** and **b**, but it does not account for errors due to systematic differences between state vectors and reality or errors in the model parameters. Including these errors, the full forward model error can described as:

Eq. 8.7 $$\varepsilon_y = \varepsilon_F + \frac{\partial F}{\partial \mathbf{x}}\varepsilon_x + \frac{\partial F}{\partial \mathbf{b}}\varepsilon_b$$

where the subscripts of ε define the parameter in error. As discussed by Merchant and Le Borgne (2004), any or all of the terms in Eq. 8.7 can be significant in the context of SST (and therefore LSWT) retrievals.

The forward model error, ε_y, propagates through into the LSWT retrieval error. Contributions to the error from forward model parameters can be isolated by performing identical radiative transfer simulations, except for perturbed values of the parameters of interest. Defining $\mathbf{y}_p$ as the BTs simulated after a perturbation, Δb, of parameter, b, of the forward model, the resulting error in BT from a parameter error of size Δb can be defined as:

Eq. 8.8 $$\mathbf{e}_b = \mathbf{y}_a - \mathbf{y}_p \cong \frac{\partial F}{\partial b}\Delta b$$

The associated error in LSWT can be determined from the forward model parameter error covariance matrix, defined by Rodgers (2000) as:

Eq. 8.9 $$\mathbf{S}_f = \mathbf{G}_y \mathbf{K}_b \mathbf{S}_b \mathbf{K}_b^T \mathbf{G}_y^T$$

where $\mathbf{G}_y = \left(\mathbf{K}^T \mathbf{S}_\varepsilon^{-1} \mathbf{K} + \mathbf{S}_a^{-1}\right)^{-1} \mathbf{K}^T \mathbf{S}_\varepsilon^{-1}$, is the sensitivity of the retrieval to measurement, $\mathbf{K}_b = \frac{\partial \mathbf{F}}{\partial \mathbf{b}}$, is the sensitivity of the forward model to the forward model parameters, and $\mathbf{S}_b = \left\langle (\mathbf{b} - \hat{\mathbf{b}})(\mathbf{b} - \hat{\mathbf{b}})^T \right\rangle$, is the error covariance matrix of $\mathbf{b}$.

The model parameters for which error propagation should be evaluated and an example of their impact on ATSR-2 coefficient-based SST retrievals are given in Table 5.

Model Parameter	Example Perturbation	ΔSST retrieval	
		Bias (K)	ΔSD (%)
Sea surface emissivity	Increase by 0.001 (approximate uncertainty estimate for emissivity)	-0.05	0.4
Trace gas profiles	Change in concentrations from 1999 to 1991 levels.	-0.03	0.03
Water vapour continuum parameterization	Different parameterizations, e.g. CKD 2.2.2 and MT_CKD (see http://www.rtweb.aer.com/), as appropriate at time of implementation	0.01	0.08
Humidity profile	Reduce upper-tropospheric humidity by 15% (systematic error in UTH of this magnitude in NWP profiles is conceivable)	-0.04	6.8
Instrument SRF	Random changes of to the normalized SRF within the SRF uncertainty	-0.12	4.4

Table 5. Model parameters (and example perturbations) for which Eq. 8.9 should be evaluated. Example perturbations and resulting errors are taken from Merchant and Le Borgne (2004) for SST retreivals.

Other systematic errors

There is also a contribution to the overall systematic error from the satellite calibration. The contribution from satellite calibration errors must be assessed by propagating calibration uncertainties through the OE retrieval scheme.

Additional errors caused by stratospheric volcanic aerosol may also need to be considered for the case of ATSR1. Such errors can be considered as systematic, asymmetric errors. Stratospheric volcanic aerosols have life-times longer than synoptic time scales and affect regions on up to hemispheric space scales.

8.2.3 Random Errors (Uncertainty Estimate)

Symmetric (Gaussian) uncertainties

The total uncertainty (Eq 8.5) represents the distribution of three components of error, all of which are assumed to be symmetric and Gaussian. These are: instrumental noise, forward model "noise" and prior error. This is an accurate description of error propagation for a single pixel. However, different components within that total uncertainty differ in their degree of correlation between nearby pixels, and therefore differ in how they should be combined when forming cell-average LSWT. Briefly, the radiometric component is uncorrelated, and the uncertainty reduces with "1/√n", whereas the other components are highly correlated, and the best approximation is to assume no average with respect to the number of pixels within the cell. These comments are expanded below.

Radiometric (instrumental) noise

The radiometric noise in the sensors depends on the scene radiance (or BT) and the temperature of the detector. Radiometric noise expressed as a noise equivalent differential temperature is available to the LSWT retrieval within the processing chain.

The radiometric noise propagates through the LSWT retrieval via the covariance matrix, $\mathbf{S}_\varepsilon$, defined in Eq, 6.5, where the contribution from radiometric noise is denoted, $\mathbf{S}_o$. An overall estimate of the radiometric noise in the retrieval can be obtained using

Eq. 8.10a $$\mathbf{S}_m = \left(\mathbf{K}^T\mathbf{S}_\varepsilon^{-1}\mathbf{K} + \mathbf{S}_a^{-1}\right)^{-1}\mathbf{K}^T\mathbf{S}_o^{-1}\mathbf{K}\left(\mathbf{K}^T\mathbf{S}_\varepsilon^{-1}\mathbf{K} + \mathbf{S}_a^{-1}\right)^{-1}$$

The radiometric uncertainty in LSWT, ε_{rad}, is then the square root of the error variance for LSWT, which is the leading term of $\mathbf{S}_m$

Pseudo-random uncertainty

The forward model may have systematic errors, as discussed earlier, but even after correction of these, a distribution of forward modelling errors would remain. We treat these as random to reflect our ignorance, although, of course, for a given NWP profile, the forward model error is (on a given computer) fixed (although unknown). This means that the forward model component of error is highly correlated between nearby pixels in an image, since the same simulations on the NWP profiles have been interpolated to the pixel. In this sense, the forward model uncertainty is pseudo-random rather than truly random.

In addition the prior error is also highly correlated for nearby pixels within a cell, again because the prior information is defined either at tie points or for 0.05° cells – i.e., varies slowly between adjacent pixels.

Thus, the total "pseudo-random" uncertainty is defined by the error covariance matrix:

Eq. 8.10b $$\mathbf{S}_{PR-sym} = \left(\mathbf{K}^T\mathbf{S}_\varepsilon^{-1}\mathbf{K} + \mathbf{S}_a^{-1}\right)^{-1}\left(\mathbf{K}^T\mathbf{S}_r^{-1}\mathbf{K} + \mathbf{S}_a^{-1}\right)\left(\mathbf{K}^T\mathbf{S}_\varepsilon^{-1}\mathbf{K} + \mathbf{S}_a^{-1}\right)^{-1}$$

The pseudo-random uncertainty in LSWT, $\varepsilon_{PR\text{-}sym}$, is then the square root of the error variance for LSWT, which is the leading term of $\mathbf{S}_{PR\text{-}sym}$.

Pseudo-random – asymmetric

Another source of pseudo-random error in the LSWT retrievals takes the form of cloud (and perhaps aerosol) contamination in the channel brightness temperatures. This contamination may be a result of either residual cloud in view or reflections from clouds (in the along-track view). The contribution to the overall retrieval error from this source may be determined empirically through comparisons of retrieved LSWTs ($LSWT_{ret}$) with in-situ observations ($LSWT_{buoy}$) for different levels of cloud cover in neighbouring pixels. Comparison of the root-mean-square deviation (RMSD) of the LSWT difference ($\Delta LSWT = LSWT_{ret} - LSWT_{buoy}$), between clear-sky conditions and cases with differing numbers of adjacent cloudy pixels, yields an estimate of the error contribution as a function of cloud cover in adjacent pixels. The asymmetric component of the pseudo-random uncertainty is termed, $\varepsilon_{PR-asym}$.

The form of the contribution is cloud-detection and retrieval dependent, and can only be obtained empirically using validation matches. This form of uncertainty is likely to be modified when cloud detection and/or retrieval algorithm are changed. Thus, although it has been assessed for AATSR SST, use of SST-based parameters is therefore not ideal, and this should be re-appraised for lakes using the OE retrieval scheme. A practical difficulty will be that there are greatly fewer matches to validation data for lakes than for SSTs.

Please note, for the reasons above this source of error is described for information purposes only and is **not** accounted for in ARC-Lake v2.0 products. It is not presently clear how and when this uncertainty component will be included.

Thus, for ARC-Lake v2.0, the assumption is "perfect cloud detection", and $\varepsilon_{PR-asym} = 0$.

Combining random errors

Ideally, the (pseudo) random errors discussed in §8.2.3 are combined to provide an overall estimate of the retrieval error using (treating the asymmetric error as if it were zero mean, which is a conservative assumption):

Eq. 8.11 $$\varepsilon_{total-random} = \sqrt{\varepsilon_{rad}^2 + \varepsilon_{PR-sym}^2 + \varepsilon_{PR-asym}^2}$$

This is the pixel level uncertainty estimate associated with LSWT for each pixel at full resolution. It is consistent with Eq 8.5. The propagation of pixel level uncertainty into the uncertainty associated with a cell average is described in Section 9.

In the ARC-Lake v2.0 products, these errors are not accounted for in the returned error estimate. Radiometric noise and the symmetric component of the pseudo-random uncertainty (ε_{rad} and ε_{PR-sym}) will be introduced by ARC-Lake v3.0.

8.2.4 Other Errors

Other sources of error could also be considered. Incorrect cloud screening (as opposed to undetectable residual cloud contamination characterized as pseudo-random asymmetric error) is one example of such errors. Such errors are occasional and erratic, and cannot be naturally included in the uncertainty estimates. The limitations of the cloud screening method used and the potential errors therefore should be appreciated by users, who can implement quality control or other measures appropriate to their application. Sampling errors may arise from valid clear-sky scenes being flagged as cloudy. This is more likely to eliminate cold than warm features in LSWT. In doing so, warm sampling biases may be introduced into averaged LSWT products.

Another source of sampling error arises from the nature of the ERS/Envisat orbit and swath. As a sun-synchronous polar orbiting satellite, observations are made at a fixed local time on each overpass. Consequently diurnal variations in LSWT cannot be fully captured and diurnal variations in cloud cover may result in consistently low LSWT coverage for some regions. However, this class of "errors" is of a different type to the error estimated with Eq. 8.11, which is an appropriate uncertainty estimate for the LSWT taken for what it is: an observation of LSWT at a particular location and instant.

Sampling errors within areas must be considered when creating and analysing spatially and temporally averaged LSWT products, as in the following section 9.

8.2.5 Confidence Indicators

In addition to the uncertainty information described in §8.2 a further diagnostic on the retrieval is provided in the form of the χ^2 statistic. This provides quantitative measure of the consistency of the retrieval with the satellite observations. The forward model is evaluated for the retrieved state ($\hat{\boldsymbol{z}} = \begin{bmatrix} \hat{x} \\ \hat{\omega} \end{bmatrix}$) and these simulated BTs compared with the satellite BTs for consistency. The expression used to quantify this is given by Rodgers (2000) as:

Eq. 8.12 $$\hat{\chi}^2 = (\mathbf{K}\hat{\mathbf{z}}' - \mathbf{y}')^T \left(\mathbf{S}_\varepsilon \left(\mathbf{K}\mathbf{S}_a\mathbf{K}^T + \mathbf{S}_\varepsilon \right)^{-1} \mathbf{S}_\varepsilon \right)^{-1} (\mathbf{K}\hat{\mathbf{z}}' - \mathbf{y}')$$

where $\mathbf{y}' = \mathbf{y} - \mathbf{F}(\mathbf{x}_a)$ and $\hat{\mathbf{z}}' = \hat{\mathbf{z}} - \mathbf{z}_a$. Eq. 8.12 returns a single number as a statistic for each pixel. Provided the OE retrieval is unbiased and errors in the priors and observations are Gaussian and correctly represented in the covariance matrices, the distribution of $\hat{\chi}^2$ should be a $\hat{\chi}^2$ distribution with *n* degrees of freedom (where *n* corresponds to the number of channels used in the retrieval). A demonstration of the practical usefulness of the $\hat{\chi}^2$ statistic for a twin-channel retrieval is given by Merchant *et al* (2008). Thus, the $\hat{\chi}^2$ statistic could be interpreted by users as a basis for a confidence indicator akin to the concept used in the SST community (Group for High Resolution SST, GDS 2.0, 2010). At present, the statistic is present, but conversion to a confidence indicator is not provided in ARC-Lake products. If user demand is established for a GHRSST-style indicator (e.g., in order to convert products to GHRSST GDS2.0 format), this could be considered in future work.

9 GRIDDING

Spatially and temporally averaged LSWT products are generated for each LSWT retrieval type independently. Averaging is performed using the retrieved LSWT values on the ATSR footprint scale (rather than calculating LSWTs from averaged channel BTs). Only pixels with valid LSWT retrievals for the specific retrieval type are used to produce the averaged LSWT product for that retrieval type, using Eq. 9.1

Eq. 9.1 $$Lake\_ST_{i,j} = \frac{\sum G_{k,l}\left(Lake\_ST_{k,l}\right)}{\sum G_{k,l}}$$

Here i,j represent the coordinates of the cell in the averaged product, k,l represent the pixel coordinates within the cell of dimension N. $G_{k,l}$ is a cloud-screening operator that takes a value of

0 when the pixel, k,l is cloudy in any of the views used for the current retrieval type

1 when the pixel is cloud-free.

Eq. 9.1 is be used to calculate averaged LSWT products for each retrieval scheme independently. Single-view LSWTs for a given cell may be based on a different sample from any dual-view LSWT for that cell, if the cloud mask for the along-track view differs from the across-track view (which in general it does).

The error estimate associated with $LSWT_{i,j}$ needs to take into account the distinction between random and pseudo-random error, and uncertainty from sub-sampling within the grid cell. It is assumed that radiometric errors are completely uncorrelated between pixels in the cell (true except for cosmetic fill pixels), while PR errors are assumed correlated across the cell (and therefore not reduced by averaging over pixels). The appropriate error estimate is therefore

Eq. 9.2

$$\varepsilon_{i,j} = \sqrt{\frac{\sum G_{k,l}\left(\varepsilon_{rad,k,l}{}^{2}+\right)}{\left(\sum G_{k,l}\right)^{2}} + \frac{\sum G_{k,l}\left(\varepsilon_{PR-sym,k,l}{}^{2}+\varepsilon_{PR-asym,k,l}{}^{2}\right)}{\left(\sum G_{k,l}\right)} + \frac{\left(N-\sum G_{k,l}\right)\widehat{V}_{Lake\_ST,i,j}}{N-1}}$$

$$\widehat{V}_{Lake\_ST,i,j} = \frac{1}{\left(\sum G_{k,l}\right)-1}\sum\left(G_{k,l}x_{k,l} - \frac{\sum\left(G_{k,l}x_{k,l}\right)}{\sum G_{k,l}}\right);\ \widehat{V}_{Lake\_ST,i,j} \geq V_{\min} \text{ if } \sum G_{k,l} < f_{\min}N$$

where the first two terms on the right follow directly by analogy with Eq. 9.1 under the assumptions about correlations of errors with the cells. The final term represents the uncertainty in the cell average from sub-sampling, i.e., from the fact that LSWTs under cloud pixels are not included, and the unknown LSWTs for these pixels are therefore excluded from the cell average. It has the form of an estimate (indicated by the hat symbol) of the true

variance of LSWT in the cell, $V_{LSWT,i,j}$, scaled by a fraction related to the proportion of the N pixels within the cell boundary that are included in the cell LSWT average. The justification for this model of sampling error is straight-forward: if only one pixel contributes to the cell average LSWT, the uncertainty from this sampling effect is the full variance of LSWT in the cell (as perceived at the ATSR spatial resolution); if all pixels are clear, the sampling uncertainty is zero. The problem is then to find an estimate of $V_{LSWT,i,j}$. The options are (i) try to estimate it from the observed data, or (ii) define an external reference (from a climatology of variability at an appropriate resolution for the grid-cells required). Where the grid cell is relatively completely observed, (i) is clearly preferable; however, if relatively few or one pixels are clear within the cell, such an estimate of $V_{LSWT,i,j}$ becomes highly uncertain or undefined. The second option is complex to define, being a function of observation resolution, grid cell size, location and seasonality. In the equation above, the option (i) is therefore assumed and the expression for the variance estimate is given. However, for the case where the number of clear pixels is 1 (variance undefined) or less than a fraction $f_{\min}$ of the cell (for which the variance estimate is particularly unreliable in the face of spatial correlations within the cell area), a minimum value, V_{min} is imposed $V_{min} = 0.1^2$ K^2 and $f_{\min} = 0.2$). These parameters are based on judgment (not formally optimized) and are subject to refinement.

As discussed in §8, ARC-Lake v2.0 products provide only an estimate of the variance of LSWT across the cell, and therefore do not implement Eq. 9.2 for the error estimate. Eq. 9.2 will hold for subsequent versions of ARC-Lake products, with $\varepsilon_{PR-asym} = 0$, as discussed in §8.23. It should also be noted that the methods described above to account for uncertainty in the cell average from sub-sampling are not implemented in ARC-Lake v2.0 products, but will again be implemented in subsequent versions.

10 ATSR-1 Modifications

A number of modifications to the processing scheme are implemented for ATSR-1 to account for instrument differences and the effect of aerosols from the Pinatubo eruption in 1991. Some of these have already been described in earlier sections but are summarized here, along with more in depth detail of further ATSR-1 specific modifications.

The lack of visible observing channels results in no ice detection (§7) being performed for ATSR-1. As a consequence, modifications are made to the v2.0 methods used for generating the prior LSWT field (§4.2): ice climatology from ATSR-2/AATSR is substituted into ATSR-1 observations prior to generation of the prior LSWT for the next iteration, and ATSR-2/AATSR climatology is used in preference to FLake simulations and ATSR-1 climatology-based reconstructions.

In addition to modifications already described, two further ATSR-1 specific modifications are implemented: one to correct for variations in the 12µm detector temperature and another to account for volcanic aerosol from the Pinatubo eruption in 1991.

Problems with the ATSR-1 cooler resulted in the detector temperature being allowed to rise gradually over the ATSR-1 lifetime. This warming affects all detectors with the 12 µm channel most significantly affected (Mutlow et al, 1999). The detector warming impacts on the 12 µm channel in two ways: the radiance to BT conversion is biased due to using the wrong calibration, and the 12 µm channel response is shifted, modifying the long-wave filter cut-off, and subsequently affecting retrieved LSWTs. The first of these effects is small (<0.01 K) and is corrected for by adjusting the 12 µm BT using a quadratic fit with dependence on detector temperature. The second of these effects is accounted for through adjustment of the modeled 12 µm BT. RTTOV 12 µm BTs are calculated using RTTOV coefficients representing three detector temperatures (85 K, 97.5 K, and 110 K), and the modeled 12 µm BT for the detector temperature at time of observation derived through linear interpolation of these values.

The eruption of Pinatubo in 1991 resulted in a period of increased aerosol loading in the atmosphere, affecting ATSR-1 BTs. Provided the effects of aerosol are accounted for in the forward model, the performance of the OE retrieval scheme and Bayesian cloud screening are expected to be maintained. Modelled BTs are adjusted by a time, latitude, and satellite zenith angle dependent factor determined from line-by-line model simulations and SST observations from the ARC project over the ATSR-1 lifetime. A latitude and time dependent look-up-table of aerosol index (a measure of the aerosol loading) is estimated from the difference between aerosol robust dual-view and nadir-view SST retrievals. A satellite zenith angle dependent look-up-table of aerosol mode (the change in BT due to the aerosol) is estimated from line-by-line simulations RFM (http://www.atm.ox.ac.uk/RFM/) / DISORT (Stamnes et al, 1988) and is combined with the time/latitude varying look-up-table for aerosol index to provide an adjustment factor for the RTTOV modeled BTs.

11 Other Sources of Information

This document describes the theoretical basis for the practical implementation of the ARC-Lake processor for generating Lake Surface Water Temperature (LSWT) and Lake Ice Concentration (LIC) products from Along-Track Scanning Radiometer (ATSR) imagery. Details of other sources of information associated with the generation and validation of these products are given in this section.

An outline of the selection process used to identify the target lakes for ARC-Lake v3.0 products is given in the ARC-Lake Technical Note on target selection strategy for v3 data products (MacCallum and Merchant, 2013a). The selection process used to identify the target lakes for v1 and v2 ARC-Lake products is given in the ARC-Lake Technical Note on lake definition (MacCallum and Merchant, 2010).

The results of validation studies for the v1.2 LSWT and LIC products are given in the ARC-Lake Validation Report (MacCallum and Merchant 2011b).

The ARC-Lake v3.0 product file format is described in MacCallum and Merchant, (2013b). This document and the v3.0 data files are available for download from the ARC-Lake project website, http://www.geos.ed.ac.uk/arclake. Basic data analysis tools are also available on this site. Earlier product (v1 and v2) file formats are described in MacCallum and Merchant, (2011a). Earlier v1.1 data files and associated documentation are available from http://hdl.handle.net/10283/88.

Further details of the Generalised Bayesian Cloud Screening (GBCS) methods on which are available from the GBCS website, http://www.geos.ed.ac.uk/gbcs. Bayesian cloud screening is also described in detail in Merchant *et al* (2005).

Useful information on the series of ATSR instruments is available from the following websites:

- http://earth.esa.int/ers/atsr
- http://www.atsr.rl.ac.uk

The radiative transfer model, RTTOV, is described in Brunel et al (2005). Additional information on RTTOV is available from:
http://research.metoffice.gov.uk/research/interproj/nwpsaf/rtm/

The lake model, FLake, (Mironov, 2005) is available online at:
http://www.flake.igb-berlin.de/

DINEOF, the software used to generate reconstructed temperature time series using principal component techniques, is described in Alvera-Azcárate (2005). Additional information is

available from the DINEOF website:
http://modb.oce.ulg.ac.be/mediawiki/index.php/DINEOF

12 References

Alvera-Azcárate, A., Barth, A., Rixen, M., & Beckers, J. (2005). Reconstruction of incomplete oceanographic data sets using empirical orthogonal functions: application to the Adriatic Sea surface temperature. *Ocean Modelling*, *9*(4), 325-346. doi: 10.1016/j.ocemod.2004.08.001.

Beeton, A. M. (2002). Large freshwater lakes: present state, trends, and future. *Environmental Conservation*, *29*(01), 21-38. doi: 10.1017/S0376892902000036.

Brunel, P., English, S., Bauer, P., Keeffe, U. O., & Francis, P. (2005). RTTOV8 - Science and Validation Report, NWP SAF, EUMETSAT

Cox, .C. and Munk, W. (1954), Measurement of the roughness of the sea surface from photographs of the Sun's glitter, *J. Opt., Soc., Am*., 44, 838-850.

Downing, H.D. and Williams, D. (1975), Optical constants of water in the infrared. *Journal of Geophysical Research*, 80, 1656–1661.

ESRI: Environmental Systems Research Institute, (1993). Digital Chart of the World 1:1 Mio. Redlands, CA.

Embury, O., Filipiak, M.J., & Merchant, C.J. (2010), A Reprocessing for Climate of Sea Surface Temperature from the Along-Track Scanning Radiometers: Basis in Radiative Transfer, submitted to *Remote Sensing of Environment*.

Filipiak, M. (2008). Refractive indices (500-3500 cm-) and emissivity (600-3350 cm-1) of pure water and seawater, http://hdl.handle.net/10283/17

GHRSST, (2006), http://ghrsst.org/GHRSST-PP-NAVO-Land-and-sea-Mask.html

Herdendorf, C. E. (1982). Large Lakes of the World. *Journal of Great Lakes Research*, *8*(3), 379-412. doi: 10.1016/S0380-1330(82)71982-3.

Lehner, B., & Döll, P. (2004). Development and validation of a global database of lakes, reservoirs and wetlands. *Journal of Hydrology*, *296*(1-4), 1-22. doi: 10.1016/j.jhydrol.2004.03.028.

MacCallum, S. N. and C. J. Merchant (submitted 2011), Surface Water Temperature Observations of Large Lakes by Optimal Estimation, *Can J Remote Sensing*.

MacCallum, S. N., and Merchant, C. J. (2011a), ARC-Lake Data Product Description – v1.1.2, School of GeoSciences, The University of Edinburgh, http://hdl.handle.net/10283/88.

MacCallum, S. N., and Merchant, C. J. (2011b), ARC-Lake Validation Report – v1.2, School of GeoSciences, The University of Edinburgh.

MacCallum, S. N., and Merchant, C. J. (2011c), ARC-Lake v1.1, 1995-2009 [Dataset], The University of Edinburgh, School of GeoSciences / European Space Agency, http://hdl.handle.net/10283/88.

MacCallum, S. N., and Merchant, C. J. (2010), ARC-Lake Technical Note 1 - Lake Definition and Validation Strategy, School of GeoSciences, The University of Edinburgh.

MacCallum, S. N., and Merchant, C. J. (2013a), ARC-Lake Technical Note 2 - Target Selection Strategy for v3 Data Products, School of GeoSciences, The University of Edinburgh.

MacCallum, S. N., and Merchant, C. J. (2013b), ARC-Lake Data Product Description – v3.0, School of GeoSciences, The University of Edinburgh.

Marmorino, G.O. and Smith, G.B. (2005), Bright and dark ocean whitecaps observed in the infrared. *Geophysical Research Letters*, 32, L11604, doi:10.1029/2005GL023176.

Marsham, J. H. (2003), Lake temperatures - thermal remote sensing and assimilation into a lake model, *PhD thesis*, The University of Edinburgh.

Masuda, K., Takashima, T. and Takayama, Y.(1988), Emissivity of pure and sea waters for the model sea surface in the infrared window region. *Remote Sensing of Environment*, 24, 313–329.

Masuda, K. (2006), Infrared sea surface emissivity including multiple reflection effect for isotropic Gaussian slope distribution model. *Remote Sensing of Environment*, 103, 488–496, .

Merchant, C. J., Harris, a. R., Maturi, E., & Maccallum, S. (2005). Probabilistic physically based cloud screening of satellite infrared imagery for operational sea surface temperature retrieval. *Quarterly Journal of the Royal Meteorological Society*, *131*(611), 2735-2755. doi: 10.1256/qj.05.15.

Merchant, C., Leborgne, P., Marsouin, a., & Roquet, H. (2008). Optimal estimation of sea surface temperature from split-window observations. *Remote Sensing of Environment*, *112*, 2469 - 2484. doi: 10.1016/j.rse.2007.11.011.

Mironov, D., Golosov, S., Heise, E., Kourzeneva, E., Ritter, B., Schneider, N., et al. (2005). FLake – A Lake Model for Environmental Applications. In *9th European Workshop on Physical Processes in Natural Waters* (pp. 2005-2005).

MODIS (2010), Ocean Level-3 Standard Mapped Image Products, http://oceancolor.gsfc.nasa.gov/DOCS/Ocean_Level-3_SMI_Products.pdf

Mutlow, C., Bailey, P., Birks, A., & Smith, D. (1999). ATSR-1 / 2 User Guide.

Newman, S.M., Smith, J.A., Glew, M.D., Rogers, S.M., and Taylor, J.P. (2005), Temperature and salinity dependence of sea surface emissivity, *Quarterly Journal of the Royal Meteorological Society*, 131, 2539-2557.

Oesch, D. C., Jaquet, J., Hauser, a., & Wunderle, S. (2005). Lake surface water temperature retrieval using advanced very high resolution radiometer and Moderate Resolution Imaging Spectroradiometer data: Validation and feasibility study. *Journal of Geophysical Research*, *110*(C12), 1-17. doi: 10.1029/2004JC002857.

Pinkley, L. W., & Williams, D. (1976). Optical properties of sea water in the infrared. Journal of the Optical Society of America, 66(6), 554. doi: 10.1364/JOSA.66.000554.

Pinkley, L.W., Sethna, P.P. and Williams, D. (1977), Optical constants of water in the infrared: Influence of temperature. *J. Opt. Soc. Am.*, 67, 494–499.

Reinhart, A., & Reinhold, M. (2008). Mapping surface temperature in large lakes with MODIS data. *Remote Sensing of Environment*, *112*(2), 603-611. Elsevier. doi: 10.1016/j.rse.2007.05.015.

Rodgers, C. D. (1990). Characterization and Error Analysis of Profiles Retrieved From Remote Sounding Measurements. *Journal of Geophysical Research*, *95*(D5), 5587-5595. doi: 10.1029/JD095iD05p05587.

Rodgers, C. D. (2000). *Inverse Methods for Atmospheric Sounding: Theory and Practice*. (F. W. Taylor). World Scientific.

Salisbury, J.W. and D'Aria, D.M. (1993), Thermal infrared remote sensing of crude oil slicks. *Remote Sensing of Environment*, 45, 225–231.

Stamnes, K., Tsay, S.C., Wiscombe, W., and Jayaweera, K. (1988), Numerically stable algorithm for discrete-ordinate-method radiative transfer in multiple scattering and emitting layered media, *Applied. Optics.* 27 (12), 2502–2509.

Townshend, J. R. G. and Justice, C. O. 1986. Analysis of the Dynamics of African Vegetation Using the Normalized Difference Vegetation Index. *Int. J. Remote Sensing*, **7**, 1435-1446.

Wan, Z. (2007). MODIS Land Surface Temperature Products Users' Guide, ICESS, University of California, Santa Barbara

Wan, Z. (2008). New refinements and validation of the MODIS Land-Surface Temperature/Emissivity products. *Remote Sensing of Environment*, *112*(1), 59-74. doi: 10.1016/j.rse.2006.06.026.

Watts, P.D., Allen, M.R., and Nightingale, T.J. (1996), Wind effects on the sea surface emission and reflection for the Along Track Scanning Radiometer, *J. Atmos. And Oceanic Technology*, 13, 126-141.

Wu, X.Q. and Smith, W.L.(1997), Emissivity of rough sea surface for 8-13 µm:modelling and verification, *Applied Optics*, 36, 2609-2619.

Xu, H. 2006. Modification of normalised difference water index (NDWI) to enhance open water features in remotely sensed imagery. *Int. J. Remote Sensing*, **27**, 14.

13 Appendix

13.1 Sources of data for prior LSWT field for v1 and v2 dataset

ID	Name	Lon.	Lat.	ATSR-1				ATSR-2				AATSR			
				T	C	M	F	T	C	M	F	T	C	M	F
166	ABAYA	37.83	6.30			Y				Y				Y	
527	ABE	41.79	11.17	Y				Y				Y			
152	ABERDEEN	-98.59	64.55		Y					Y				Y	
418	ABY	-3.23	5.23		Y					Y		Y			
58	ALAKOL	81.75	46.11			Y		Y				Y			
30	ALBERT	30.91	1.67	Y				Y				Y			
210	ALEXANDRINA	139.09	-35.52	Y				Y				Y			
1748	ALMANOR	-121.19	40.26		Y			Y						Y	
56	AMADJUAK	-71.13	64.99		Y					Y				Y	
354	ANG-LA JEN	83.09	31.53		Y					Y		Y			
324	ANGIKUNI	-100.04	62.27		Y				Y				Y		
4	ARAL	60.08	45.13		Y				Y				Y		
117	ARGENTINO	-73.03	-50.33	Y				Y				Y			
334	ARTILLERY	-107.82	63.17		Y					Y				Y	
345	ASHUANIPI	-66.14	52.69		Y					Y				Y	
115	ASTRAY	-66.32	54.38		Y				Y				Y		
23	ATHABASCA	-109.96	59.10	Y				Y				Y			
311	ATLIN	-133.75	59.57		Y			Y						Y	
312	AYAKKUM	89.35	37.55	Y				Y				Y			
226	AYLMER	-108.46	64.15		Y					Y				Y	
181	BAGHRASH	87.07	41.98			Y		Y				Y			
8	BAIKAL	108.14	53.63	Y				Y				Y			
97	BAKER	-95.28	64.13		Y					Y				Y	
310	BALATON	17.83	46.88	Y				Y				Y			
17	BALKHASH	73.95	45.91	Y				Y				Y			
536	BANGONG	79.71	33.61		Y			Y				Y			
229	BARUN-TOREY	115.81	50.07	Y				Y				Y			
205	BAY	121.26	14.36	Y				Y				Y			
145	BECHAROF	-156.40	57.85	Y				Y				Y			
160	BELOYE	37.64	60.18	Y				Y				Y			
267	BEYSEHIR	31.52	37.78	Y				Y				Y			
155	BIENVILLE	-72.98	55.05		Y				Y					Y	
280	BIG TROUT	-90.02	53.77		Y			Y				Y			
268	BIWA	136.08	35.25			Y		Y				Y			
333	BLACK	-105.73	59.05		Y			Y				Y			
191	BRAS D'OR	-60.83	45.95			Y		Y				Y			
94	BUENOS AIRES	-72.50	-46.66	Y				Y				Y			
299	BUFFALO	-115.49	60.22			Y		Y				Y			
291	BUYR	117.69	47.81	Y				Y				Y			
257	CARATASCA	-83.85	15.35	Y				Y				Y			
1	CASPIAN	50.36	41.85	Y				Y				Y			
265	CAXUANA	-51.50	-2.04			Y		Y						Y	
57	CEDAR	-100.14	53.33	Y				Y				Y			
165	CHAMPLAIN	-73.27	44.45		Y					Y		Y			
233	CHAO	117.57	31.57	Y				Y				Y			
153	CHAPALA	-103.05	20.21	Y				Y				Y			
204	CHILKA	85.38	19.69	Y				Y				Y			

256	CHILWA	35.71	-15.32	Y				Y				Y			
84	CHIQUITA	-62.61	-30.74	Y				Y				Y			
119	CHISHI	29.72	-8.71	Y				Y				Y			
323	CHURCHILL	-108.29	55.96			Y		Y				Y			
125	CLAIRE	-112.08	58.59	Y				Y				Y			
1188	CLEAR	-122.77	39.02			Y		Y				Y			
275	CLINTON COLDEN	-107.45	63.94		Y			Y				Y			
277	COARI	-63.37	-4.25		Y			Y				Y			
219	COLHUE HUAPI	-68.76	-45.47	Y						Y		Y			
352	CONSTANCE	9.28	47.65			Y		Y				Y			
162	CONTWOYTO	-110.66	65.59		Y					Y				Y	
284	CORO	-69.86	11.56	Y				Y				Y			
137	CREE	-106.64	57.47		Y					Y		Y			
251	CROSS	-97.58	54.71		Y				Y				Y		
351	DAUPHIN	-99.77	51.27	Y				Y				Y			
244	DEAD	35.49	31.52	Y				Y				Y			
326	DESCHAMBAULT	-103.45	54.78			Y		Y				Y			
281	DORE	-107.28	54.76			Y		Y				Y			
49	DUBAWNT	-101.44	63.13		Y			Y				Y			
128	EAU CLAIRE	-74.40	56.15		Y			Y				Y			
297	EBI	82.92	44.86		Y			Y				Y			
305	EBRIE	-4.26	5.30		Y				Y				Y		
69	EDWARD	29.61	-0.39	Y				Y				Y			
390	EGRIDIR	30.85	38.07	Y				Y				Y			
254	ENNADAI	-101.31	60.96		Y					Y				Y	
723	ENRIQUILLO	-71.58	18.49	Y				Y				Y			
12	ERIE	-81.16	42.25	Y				Y				Y			
149	ESKIMO	-132.76	69.10		Y					Y				Y	
270	EVANS	-77.02	50.97		Y					Y				Y	
1029	EVORON	136.51	51.48		Y			Y						Y	
156	EYASI	35.04	-3.58		Y			Y					Y		
304	FAGNANO	-68.03	-54.55		Y			Y				Y			
315	FERGUSON	-105.27	69.41		Y			Y				Y			
404	FROBISHER	-108.22	56.37		Y						Y		Y		
227	GARRY	-99.40	65.95		Y					Y				Y	
327	GENEVA	6.25	46.37	Y				Y				Y			
172	GODS	-94.21	54.62		Y			Y				Y			
363	GRANVILLE	-100.21	56.40		Y				Y					Y	
252	GRAS	-110.38	64.54		Y					Y				Y	
9	GREAT BEAR	-121.30	65.91			Y				Y		Y			
11	GREAT SLAVE	-114.37	62.09			Y		Y				Y			
253	GUILLAUME-DELISLE	-76.28	56.33		Y					Y		Y			
294	HAR	93.21	48.05	Y				Y				Y			
142	HAR US	92.30	48.06	Y				Y				Y			
302	HAR-HU	97.59	38.31	Y				Y				Y			
214	HAUKIVESI	28.52	62.10		Y				Y					Y	
339	HAZEN	-70.94	81.80				Y				Y				Y
288	HIGHROCK	-100.44	55.83				Y				Y				Y
189	HOTTAH	-118.44	64.95		Y					Y				Y	
59	HOVSGOL	100.48	51.02			Y		Y						Y	
75	HULUN	117.38	48.97	Y				Y				Y			
109	HUNGTZE	118.53	33.34	Y				Y				Y			

5	HURON	-82.21	44.78	Y				Y				Y			
121	HYARGAS	93.30	49.13	Y				Y				Y			
62	ILIAMNA	-154.90	59.56	Y				Y				Y			
144	INARI	27.83	69.04		Y					Y				Y	
293	INDIAN RIVER	-80.64	28.24		Y					Y		Y			
174	ISLAND	-94.70	53.85		Y				Y					Y	
25	ISSYKKUL	77.25	42.46			Y		Y				Y			
1441	ISTADA	67.92	32.48			Y			Y				Y		
245	IZABAL	-89.11	15.57			Y		Y				Y			
141	KAGHASUK	-164.22	60.79		Y			Y				Y			
246	KAMINAK	-94.90	62.20		Y				Y					Y	
320	KAMINURIAK	-95.79	62.96		Y					Y				Y	
264	KAMILUKUAK	-101.73	62.28		Y					Y				Y	
287	KAOYU	119.31	32.87	Y				Y				Y			
197	KARA-BOGAZ-GOL	53.54	41.23	Y				Y				Y			
124	KASBA	-102.27	60.34		Y			Y				Y			
346	KEITELE	25.99	62.89		Y				Y					Y	
45	KHANKA	132.42	44.94	Y				Y				Y			
218	KHANTAYSKOE	91.18	68.36		Y					Y				Y	
67	KIVU	29.23	-2.04			Y		Y				Y			
41	KOKO	100.18	36.89	Y				Y				Y			
344	KRASNOE	174.44	64.53		Y			Y				Y			
262	KULUNDINSKOE	79.58	52.98	Y				Y				Y			
325	KWANIA	32.65	1.72		Y					Y		Y			
382	KYARING	88.32	31.13			Y		Y				Y			
99	KYOGA	33.01	1.50			Y		Y				Y			
331	LABAZ	99.57	72.27		Y			Y					Y		
16	LADOGA	31.39	60.84	Y				Y				Y			
147	LESSER SLAVE	-115.49	55.43	Y				Y				Y			
140	LIMFJORDEN	9.17	56.78	Y				Y				Y			
209	LLANQUIHUE	-72.79	-41.14	Y				Y				Y			
357	LOWER SEAL	-73.42	56.49				Y				Y				Y
175	LUANG	100.38	7.46		Y			Y				Y			
184	MACKAY	-111.30	63.96		Y					Y				Y	
101	MADRE	-97.66	24.64	Y				Y				Y			
163	MALAREN	16.19	59.44		Y					Y				Y	
350	MALHEUR	-118.83	43.34		Y					Y			Y		
176	MANAGUA	-86.35	12.32	Y				Y				Y			
231	MANGUEIRA	-52.84	-33.16	Y				Y				Y			
37	MANITOBA	-98.80	50.99	Y				Y				Y			
368	MANOUANE	-70.99	50.76		Y				Y					Y	
250	MANYCH-GUDILO	42.98	46.26	Y				Y				Y			
100	MARTRE	-117.91	63.33	Y				Y				Y			
6	MICHIGAN	-87.09	43.86	Y				Y				Y			
366	MILLE LACS	-93.65	46.24	Y				Y				Y			
224	MINTO	-74.71	57.34				Y				Y				Y
46	MIRIM	-53.25	-32.89	Y				Y				Y			
76	MISTASSINI	-73.81	50.82		Y					Y		Y			
883	MONO	-118.96	38.01			Y		Y						Y	
286	MURRAY	141.53	-6.95		Y				Y				Y		
36	MWERU	28.74	-9.01	Y				Y				Y			
343	NAHUEL HUAPI	-71.52	-40.92	Y				Y				Y			

377	NAKNEK	-155.67	58.64		Y					Y		Y			
91	NAM	90.66	30.71	Y				Y				Y			
322	NATRON	36.02	-2.34		Y					Y				Y	
338	NERPICH'YE	162.77	56.39		Y			Y				Y			
32	NETILLING	-70.28	66.42		Y					Y				Y	
300	NGORING	97.71	34.93	Y				Y				Y			
21	NICARAGUA	-85.36	11.57	Y				Y				Y			
38	NIPIGON	-88.55	49.80		Y			Y				Y			
198	NIPISSING	-79.92	46.24	Y				Y				Y			
211	NONACHO	-108.92	61.82		Y				Y					Y	
303	NORTH MOOSE	-100.16	54.05			Y		Y				Y			
83	NUELTIN	-99.40	60.25		Y					Y				Y	
10	NYASA	34.59	-11.96	Y				Y				Y			
114	OKEECIIOBEE	-80.86	26.95	Y				Y				Y			
336	OLING	97.27	34.92	Y				Y				Y			
207	OMULAKH	145.59	72.29		Y				Y			Y			
18	ONEGA	35.35	61.90	Y				Y				Y			
15	ONTARIO	-77.77	43.85	Y				Y				Y			
187	ORIVESI	29.59	62.35		Y			Y						Y	
157	PAIJANNE	25.49	61.71		Y					Y		Y			
697	PANGONG	78.61	33.82		Y				Y					Y	
353	PAYNE	-73.82	59.40		Y				Y					Y	
50	PEIPUS	27.59	58.41	Y				Y				Y			
349	PERLAS	-83.67	12.54			Y		Y				Y			
222	PETER POND	-108.55	55.84			Y		Y				Y			
195	PIELINEN	29.71	63.16		Y					Y				Y	
213	PLAYGREEN	-97.75	54.07		Y			Y				Y			
232	POINT	-113.84	65.31		Y				Y				Y		
649	POMO	90.40	28.55		Y					Y				Y	
133	POOPO	-67.06	-18.81		Y				Y			Y			
395	PRINCESS MARY	-97.66	63.93		Y					Y				Y	
164	PURUVESI	29.02	61.77		Y				Y					Y	
273	PYA	30.98	66.07		Y					Y				Y	
240	PYASINO	87.78	69.77		Y			Y				Y			
1240	PYHAJARVI	22.28	61.00		Y			Y				Y			
411	PYRAMID	-119.55	40.03	Y				Y				Y			
130	RAINY	-92.97	48.61		Y					Y				Y	
358	RAZELM	28.97	44.83	Y				Y				Y			
151	RED	-95.08	48.04	Y				Y				Y			
28	REINDEER	-102.27	57.19		Y			Y				Y			
321	ROGOAGUADO	-65.73	-12.91		Y					Y		Y			
127	RONGE	-104.83	55.11		Y			Y				Y			
22	RUDOLF	36.08	3.53	Y				Y				Y			
146	SAINT CLAIR	-82.73	42.50	Y				Y				Y			
158	SAINT JEAN	-72.02	48.66			Y		Y				Y			
285	SAINT JOSEPH	-90.81	51.04		Y					Y				Y	
282	SAKAMI	-76.75	53.22		Y					Y				Y	
194	SALTON	-115.83	33.30	Y				Y				Y			
167	SAN MARTIN	-72.84	-48.75		Y			Y				Y			
356	SANDY	-93.03	53.00		Y					Y				Y	
241	SARYKAMYSHSKOYE	57.61	41.88	Y				Y				Y			
247	SASYKKOL	80.91	46.58			Y		Y				Y			

313	SCOTT	-106.07	60.02		Y				Y				Y		
228	SEG	33.76	63.32		Y			Y				Y			
170	SELAWIK	-160.73	66.51			Y				Y		Y			
271	SELETYTENIZ	73.18	53.23			Y				Y		Y			
292	SELWYN	-104.68	60.00		Y				Y					Y	
135	SEVAN	45.29	40.39	Y				Y				Y			
579	SHAMO	37.55	5.83			Y				Y				Y	
143	SHERMAN	-97.73	67.79		Y					Y				Y	
236	SIMCOE	-79.42	44.47	Y				Y				Y			
27	SMALLWOOD	-64.31	54.19		Y			Y				Y			
365	SNOWBIRD	-102.94	60.64		Y			Y				Y			
319	SOUTH HENIK	-97.29	61.37		Y					Y				Y	
225	SOUTH MOOSE	-100.04	53.83			Y		Y				Y			
2	SUPERIOR	-88.23	47.72	Y				Y				Y			
85	SYVASH	34.74	45.96			Y		Y				Y			
380	TAHOE	-120.04	39.09	Y				Y				Y			
66	TAI	120.24	31.21	Y				Y				Y			
178	TAKIYUAK	-113.17	66.28		Y					Y				Y	
235	TAMIAHUA	-97.57	21.66	Y				Y				Y			
55	TANA	37.31	11.95	Y				Y				Y			
7	TANGANYIKA	29.46	-6.07	Y				Y				Y			
215	TANGRA	86.59	31.05	Y				Y				Y			
73	TAPAJOS	-55.14	-2.88	Y				Y				Y			
316	TATHLINA	-117.64	60.54	Y				Y				Y			
295	TAUPO	175.90	-38.81	Y				Y				Y			
43	TAYMYR	100.76	74.48		Y				Y				Y		
373	TEBESJUAK	-98.98	63.76		Y					Y				Y	
120	TENGIZ	68.90	50.44	Y				Y				Y			
179	TERINAM	85.61	30.90	Y				Y				Y			
212	TESHEKPUK	-153.60	70.59		Y			Y				Y			
20	TITICACA	-69.30	-15.92	Y				Y				Y			
150	TOBA	98.90	2.61		Y					Y				Y	
186	TOP	32.09	65.62		Y					Y				Y	
332	TOWUTI	121.52	-2.79			Y				Y				Y	
367	TROUT	-121.13	60.58	Y				Y				Y			
269	TULEMALU	-99.48	62.99		Y			Y						Y	
255	TUMBA	17.98	-0.82		Y					Y		Y			
425	UBINSKOE	80.05	55.47	Y				Y				Y			
239	ULUNGUR	87.30	47.22	Y				Y				Y			
314	UPEMBA	26.40	-8.65	Y				Y				Y			
53	UVS	92.81	50.33	Y				Y				Y			
51	VAN	42.98	38.66	Y				Y				Y			
29	VANERN	13.22	58.88	Y				Y				Y			
95	VATTERN	14.57	58.33	Y				Y				Y			
1820	VESIJARVI	25.39	61.09		Y				Y					Y	
3	VICTORIA	33.23	-1.30	Y				Y				Y			
171	VIEDMA	-72.56	-49.59	Y				Y				Y			
136	VYG	34.84	63.54		Y			Y				Y			
1128	WALKER	-118.71	38.70			Y		Y				Y			
876	WEISHAN	117.24	34.61	Y				Y				Y			
169	WHOLDAIA	-104.15	60.69		Y				Y				Y		
340	WINNEBAGO	-88.42	44.02	Y				Y				Y			
13	WINNIPEG	-97.25	52.12	Y				Y				Y			

31	WINNIPEGOSIS	-100.05	52.37	Y				Y				Y			
68	WOLLASTON	-103.33	58.30		Y			Y				Y			
44	WOODS	-94.91	49.38	Y				Y				Y			
134	XINGU	-52.20	-2.16	Y				Y				Y			
261	YAMDROK	90.76	28.97		Y				Y				Y		
126	YATHKYED	-98.07	62.69		Y					Y		Y			
105	ZILING	88.95	31.77	Y				Y				Y			

Table 6. Breakdown of sources of data for the prior LSWT field (§4)

13.2 Sources of data for prior LSWT field for v3 dataset

ID	Name	Lon.	Lat.	ATSR-2				AATSR			
				T	C	M	F	T	C	M	F
166	ABAYA	37.83	6.30		Y				Y		
527	ABE	41.79	11.17		Y				Y		
152	ABERDEEN	-98.59	64.55		Y				Y		
200	ABITIBI	-79.59	48.76		Y				Y		
829	ABIYATA	38.76	7.61		Y				Y		
418	ABY	-3.23	5.23		Y				Y		
630	ACHIT	90.54	49.50		Y				Y		
770	ADJUNTAS	-98.78	23.96		Y					Y	
1584	AFRERA YE'CH'EW	40.92	13.29		Y				Y		
1092	AGATA	92.84	67.23		Y						Y
693	AGGIKANI	-100.27	62.52		Y				Y		
1137	AIAPUA	-62.13	-4.46		Y				Y		
2079	AKHTANIZOVSKIY	37.19	45.29		Y				Y		
1969	AKKOL'	63.77	48.86		Y				Y		
1096	AKSAYQUIN	79.85	35.21		Y						Y
552	AKSEHIR	31.42	38.52		Y				Y		
58	ALAKOL	81.75	46.11		Y				Y		
957	ALAOTRA	48.51	-17.49		Y				Y		
432	ALBANIEL	-73.07	51.00		Y				Y		
30	ALBERT	30.91	1.67		Y					Y	
210	ALEXANDRINA	139.09	-35.52		Y			Y			
1748	ALMANOR	-121.19	40.26		Y				Y		
1434	ALVARA OBREGON	-109.80	27.97		Y				Y		
56	AMADJUAK	-71.13	64.99		Y				Y		
1026	AMERICAN FALLS RESERVOIR	-112.75	42.92		Y				Y		
566	AMISK	-102.25	54.58		Y					Y	
354	ANG-LA JEN	83.09	31.53		Y				Y		
444	ANG-TZU	87.14	31.01		Y				Y		
867	ANGAJURJUALUK	-78.97	71.13		Y				Y		
324	ANGIKUNI	-100.04	62.27				Y				Y
234	ANGOSTURA	-92.56	16.12		Y				Y		
511	AQQIKKOL	88.42	37.06		Y				Y		
4	ARAL	60.08	45.13		Y			Y			
1273	ARAPA	-69.98	-15.19		Y						Y
946	ARARUAMA	-42.22	-22.89		Y				Y		
1958	ARGAZINSKOYE	60.40	55.40		Y				Y		
117	ARGENTINO	-73.03	-50.33		Y					Y	
98	ARGYLE	128.77	-16.43		Y			Y			
3048	ARHYMOT LAKE	-160.36	61.63		Y				Y		
1044	ARKATAG	89.42	36.34		Y						Y

1122	AROPUK LAKE	-163.80	61.09		Y				Y		
334	ARTILLERY	-107.82	63.17		Y				Y		
1806	ARU	82.37	34.01				Y				Y
345	ASHUANIPI	-66.14	52.69		Y				Y		
1042	ASNEN	14.72	56.70		Y				Y		
279	ASSAD	38.10	36.07		Y			Y			
23	ATHABASCA	-109.96	59.10		Y			Y			
1053	ATHAPAPUSKOW	-101.62	54.53		Y					Y	
419	ATIKONAK	-64.62	52.73		Y				Y		
1479	ATITLA	-91.20	14.67		Y				Y		
311	ATLIN	-133.75	59.57		Y				Y		
491	AUBRY	-126.46	67.42		Y				Y		
2124	AWASA	38.44	7.06				Y				Y
312	AYAKKUM	89.35	37.55		Y				Y		
1625	AYAN	93.94	69.14				Y				Y
226	AYLMER	-108.46	64.15		Y				Y		
384	BABINE	-126.18	54.88		Y				Y		
173	BAHR AL MILH	43.66	32.78		Y			Y			
1740	BAIA GRANDE	-60.24	-15.52		Y				Y		
8	BAIKAL	108.14	53.63		Y			Y			
1445	BAIRAB	83.12	35.04		Y						Y
97	BAKER	-95.28	64.13		Y				Y		
310	BALATON	17.83	46.88		Y					Y	
1277	BALDOCK	-97.89	56.56		Y				Y		
17	BALKHASH	73.95	45.91		Y					Y	
1736	BANGDAG	81.56	34.95		Y						Y
1804	BANGKOG	89.52	31.74		Y						Y
536	BANGONG	79.71	33.61		Y						Y
81	BANGWEULU	29.76	-11.19		Y			Y			
1248	BARINGO	36.08	0.63		Y				Y		
372	BARKAL	92.26	22.75		Y				Y		
2238	BARKOL	92.80	43.66				Y				Y
1364	BARLOW	-103.05	61.95		Y				Y		
360	BARRA BONITA	-48.69	-23.34		Y				Y		
1102	BARRINGTON	-100.17	56.96		Y						Y
229	BARUN-TOREY	115.81	50.07		Y				Y		
621	BASKATONG	-75.75	46.83		Y				Y		
1516	BAUNT	112.98	55.21		Y				Y		
205	BAY	121.26	14.36		Y				Y		
1152	BEAR	-96.07	55.12		Y				Y		
677	BEAR LAKE	-111.33	42.01		Y					Y	
622	BEAS	76.07	32.00		Y				Y		
925	BEAVER HILL	-94.92	54.24		Y				Y		
1222	BEAVERHILL	-112.54	53.46		Y				Y		
145	BECHAROF	-156.40	57.85		Y			Y			
1417	BEI HULSAN	95.91	36.88		Y				Y		
635	BELOT	-126.26	66.88		Y				Y		
160	BELOYE	37.64	60.18		Y			Y			
1216	BERRE	5.11	43.49		Y			Y			
1164	BEVERLY	-100.52	64.61		Y						Y
267	BEYSEHIR	31.52	37.78		Y			Y			
706	BEYSUGSKTY	38.42	46.15		Y					Y	
805	BICHE	-112.07	54.86		Y				Y		

155	BIENVILLE	-72.98	55.05		Y				Y		
711	BIG SAND	-99.76	57.71				Y				Y
280	BIG TROUT	-90.02	53.77		Y					Y	
1576	BIRCH	-121.61	64.62		Y				Y		
458	BISTCHO	-118.83	59.74		Y				Y		
268	BIWA	136.08	35.25		Y			Y			
2201	BIYLIKOL	70.70	43.04		Y				Y		
333	BLACK	-105.73	59.05		Y					Y	
849	BLACKWATER	-123.12	63.99		Y				Y		
1195	BLANC	-69.04	-54.07		Y				Y		
1113	BLANCA	-71.21	-52.41				Y				Y
763	BLOEMHOFDAM	25.67	-27.69		Y				Y		
106	BLOMMESTEINMEER	-55.07	4.72		Y					Y	
417	BLUENOSE	-119.69	68.51		Y			Y			
64	BOENG TONLE CHHMA	104.15	12.81		Y				Y		
400	BOIS	-125.15	66.82		Y			Y			
1787	BOL'SHO YERAVNOYE	111.49	52.62		Y				Y		
944	BOL'SHOYE MORSKOYE	158.77	70.05		Y				Y		
1028	BOLMEN	13.67	56.92		Y				Y		
502	BOLON'	136.39	49.80		Y				Y		
1596	BOLSENA	11.93	42.60		Y					Y	
1011	BOLSHOY UVAT	70.47	57.54		Y				Y		
1336	BONG	91.15	31.22		Y						Y
645	BOON TSAGAAN	99.09	45.58		Y			Y			
181	BOSTEN	87.07	41.98		Y				Y		
39	BRATSKOYE	103.07	54.85		Y				Y		
768	BROCHET	-101.68	58.64		Y				Y		
1940	BROWN	-90.66	66.71				Y				Y
94	BUENOS AIRES	-72.50	-46.66		Y			Y			
299	BUFFALO	-115.49	60.22		Y				Y		
77	BUHAYRAT ATH THARTHAR	43.17	34.11		Y			Y			
2083	BUL'SHOYE TOKO	130.89	56.05		Y				Y		
1629	BULMER	-120.77	62.80		Y				Y		
3607	BUNG BORAPHET	100.26	15.69		Y						Y
881	BURDUR	30.21	37.73		Y					Y	
2978	BURT LAKE	-84.67	45.47		Y				Y		
795	BURTON	-78.30	54.76		Y				Y		
762	BUSTAKH	141.96	72.53		Y				Y		
291	BUYR	117.69	47.81		Y			Y			
42	CABORA BASSA	31.63	-15.73		Y				Y		
1361	CAIMANE	-106.11	22.99		Y				Y		
1583	CALAFQUEM	-72.15	-39.53		Y				Y		
748	CALCASIEU LAKE	-93.34	29.96		Y					Y	
1370	CALLING	-113.31	55.24		Y				Y		
2202	CAM	83.54	32.11		Y						Y
1375	CANDLE	-105.29	53.82		Y					Y	
168	CANIAPISCAU	-69.84	54.29		Y				Y		
910	CANOE	-108.23	55.18		Y			Y			
1193	CANYON FERRY LAKE	-111.56	46.50		Y				Y		
257	CARATASCA	-83.85	15.35		Y					Y	
443	CARDIEL	-71.26	-48.90		Y					Y	
154	CARONI	-62.83	7.20		Y				Y		
1761	CASCADE RESERVOIR	-116.10	44.63		Y				Y		

1	CASPIAN	50.36	41.85		Y			Y			
1081	CASTIGNON	-68.57	56.32		Y				Y		
2484	CATEMACO	-95.04	18.40		Y				Y		
265	CAXUANA	-51.50	-2.04		Y				Y		
57	CEDAR	-100.14	53.33		Y			Y			
379	CERROS COLORADOS	-68.73	-38.58		Y			Y			
2116	CH'A-ERH-KU-T'E	88.24	31.81				Y				Y
755	CHA-PU-YEH CH'A-K'A	84.03	31.37		Y						Y
14	CHAD	14.19	13.45		Y				Y		
1054	CHAMBRI	143.10	-4.26		Y						Y
579	CHAMO	37.55	5.83		Y				Y		
165	CHAMPLAIN	-73.27	44.45		Y				Y		
1503	CHANG	112.38	30.44		Y				Y		
2156	CHANG DANG	119.55	31.61		Y			Y			
92	CHANY	77.39	54.83		Y				Y		
233	CHAO	117.57	31.57		Y					Y	
153	CHAPALA	-103.05	20.21		Y			Y			
296	CHARDARINSKOYE	68.17	41.15		Y			Y			
1213	CHATYR-KEL'	75.28	40.64		Y						Y
1619	CHEM	79.79	34.15		Y						Y
950	CHERTOVO	80.42	64.13		Y				Y		
844	CHIBOUGAMAU	-74.24	49.85		Y				Y		
2317	CHIEMSEE	12.44	47.88		Y				Y		
204	CHILKA	85.38	19.69		Y			Y			
256	CHILWA	35.71	-15.32		Y				Y		
84	CHIQUITA	-62.61	-30.74		Y			Y			
119	CHISHI	29.72	-8.71		Y			Y			
1943	CHIUTA	35.85	-14.78		Y				Y		
220	CHOCON	-69.01	-39.46		Y			Y			
1567	CHOKE CANYON RESERVOIR	-98.38	28.49		Y						Y
483	CHUKCHAGIRSKOYE	136.58	52.00		Y				Y		
1551	CHUKOCH'YE	160.28	69.45		Y						Y
323	CHURCHILL	-108.29	55.96		Y			Y			
1518	CILDIR	43.23	41.03		Y				Y		
125	CLAIRE	-112.08	58.59		Y			Y			
1188	CLEAR	-122.77	39.02		Y					Y	
2253	CLEAR LAKE RESERVOIR	-121.15	41.86		Y				Y		
646	CLEARWATER	-101.05	54.06		Y			Y			
275	CLINTON COLDEN	-107.45	63.94				Y				Y
277	COARI	-63.37	-4.25		Y				Y		
588	COCHRANE	-71.95	-47.32		Y				Y		
1016	COIPASA	-68.14	-19.22				Y				Y
508	COLD	-110.04	54.53		Y			Y			
219	COLHUE HUAPI	-68.76	-45.47		Y				Y		
426	COLVILLE	-125.99	67.19		Y			Y			
352	CONSTANCE	9.28	47.65		Y				Y		
162	CONTWOYTO	-110.66	65.59		Y				Y		
800	CORANGAMITE	143.38	-38.20		Y				Y		
545	CORMORANT	-100.90	54.22		Y			Y			
1057	CORRIB	-9.17	53.42		Y				Y		
2157	CORTE	-92.13	18.59		Y				Y		
467	COUTURE	-75.38	60.03		Y						Y
3493	CRATER LAKE	-122.11	42.94		Y				Y		

1547	CREAN	-106.17	54.09		Y				Y		
137	CREE	-106.64	57.47		Y				Y		
1353	CROOKED	-98.30	72.60		Y						Y
251	CROSS	-97.58	54.71		Y						Y
590	CUITZEO	-101.18	19.95		Y						Y
754	CUMBERLAND	-102.33	54.04		Y					Y	
1269	CURTIS	-89.21	66.69				Y				Y
629	DABSAN	95.15	36.96				Y				Y
623	DAGUAN	116.38	30.04		Y				Y		
543	DAGZE	88.00	31.70		Y				Y		
827	DALAI	116.62	43.30		Y				Y		
428	DALL LAKE	-163.89	60.30		Y				Y		
1902	DANAU MANINDJAU	100.19	-0.33		Y						Y
1257	DANAU PANIAI	136.33	-3.89		Y				Y		
487	DANAU POSO	120.62	-1.92		Y				Y		
1433	DANAU RANAU	103.94	-4.89		Y						Y
1377	DANAU ROMBERBAI	137.92	-1.87		Y						Y
351	DAUPHIN	-99.77	51.27		Y			Y			
1640	DAVY	-108.26	58.87		Y				Y		
2547	DAYAN	88.85	48.34		Y				Y		
244	DEAD	35.49	31.52		Y			Y			
785	DEBO	-4.16	15.30				Y				Y
1369	DEEP ROSE	-98.68	65.72				Y				Y
326	DESCHAMBAULT	-103.45	54.78		Y					Y	
1199	DEVILS LAKE	-98.97	48.02		Y				Y		
627	DIAN CHI	102.69	24.85		Y				Y		
1278	DJENPANG	116.22	-0.45				Y				Y
509	DNESTROVSKYI	30.31	46.24		Y					Y	
725	DOGAI CORING	89.02	34.57		Y						Y
1891	DOGAICORING QUANG	89.25	35.27		Y						Y
1382	DOGEN	91.16	31.70		Y				Y		
2080	DONG	84.73	32.17				Y				Y
819	DONGGI CONA	98.54	35.30		Y						Y
1658	DONGPING	116.18	36.01		Y				Y		
620	DONGTING	112.92	29.32		Y				Y		
281	DORE	-107.28	54.76		Y			Y			
924	DORGE	92.10	35.21		Y						Y
549	DORGON	93.42	47.73		Y			Y			
489	DORSOIDONG	89.81	33.38		Y				Y		
1656	DOS OUADROS	-50.09	-29.70		Y				Y		
49	DUBAWNT	-101.44	63.13		Y					Y	
1076	DUKAN	44.90	36.11		Y					Y	
580	EAGLE	-93.30	49.69		Y				Y		
2032	EAGLE LAKE	-120.74	40.64		Y				Y		
128	EAU CLAIRE	-74.40	56.15		Y				Y		
2285	EBEYTY	71.73	54.65		Y				Y		
297	EBI	82.92	44.86		Y				Y		
305	EBRIE	-4.26	5.30		Y				Y		
69	EDWARD	29.61	-0.39		Y					Y	
1676	EGG	-105.56	55.06		Y				Y		
390	EGRIDIR	30.85	38.07		Y			Y			
1083	EL'TON	46.67	49.15		Y				Y		
1602	ELOYGYTGYN	172.08	67.50		Y			Y			

254	ENNADAI	-101.31	60.96		Y				Y		
723	ENRIQUILLO	-71.58	18.49		Y					Y	
1975	EPECUEN	-62.87	-37.14		Y				Y		
1840	ERCEK	43.59	38.67		Y				Y		
767	ERH	100.18	25.78		Y				Y		
424	ERICHSEN	-80.41	70.61				Y				Y
12	ERIE	-81.16	42.25		Y			Y			
1526	ERNE	-7.69	54.42		Y						Y
149	ESKIMO	-132.76	69.10		Y					Y	
270	EVANS	-77.02	50.97		Y				Y		
1029	EVORON	136.51	51.48		Y				Y		
156	EYASI	35.04	-3.58		Y				Y		
430	FABER	-117.25	63.95		Y				Y		
304	FAGNANO	-68.03	-54.55		Y				Y		
567	FALCON RESERVOIR	-99.26	26.76		Y				Y		
786	FARIBAULT	-71.92	59.06				Y				Y
801	FEIA	-41.32	-22.02		Y				Y		
897	FEMUNDEN	11.85	62.17				Y				Y
315	FERGUSON	-105.27	69.41		Y				Y		
616	FINCH'A'	37.14	9.47				Y				Y
1357	FITRI	17.45	12.90		Y				Y		
1617	FLASJON	15.85	64.13				Y				Y
375	FLATHEAD LAKE	-114.18	47.89		Y				Y		
1027	FLETCHER	-108.72	63.60		Y						Y
615	FORD	-97.36	63.40		Y				Y		
201	FORT PECK LAKE	-107.29	47.68		Y				Y		
1358	FUTOU	114.20	30.04		Y				Y		
892	FUXIAN	102.89	24.49		Y				Y		
2559	GAIBA	-57.73	-17.75		Y				Y		
347	GANDHI	75.60	24.43		Y				Y		
287	GAOYOU	119.31	32.87		Y					Y	
505	GARDA	10.70	45.67		Y					Y	
227	GARRY	-99.40	65.95		Y				Y		
1557	GAS HURE	90.79	38.12				Y				Y
656	GAUER	-97.84	57.02		Y				Y		
990	GE	119.81	31.60		Y					Y	
1355	GENERAL VINTTER	-71.53	-43.93		Y				Y		
327	GENEVA	6.25	46.37		Y				Y		
687	GEORGE	30.17	0.00		Y				Y		
1831	GLAFSFJ	12.70	59.52		Y				Y		
2358	GLAN	15.98	58.64		Y				Y		
1275	GLUBOKOYE	90.10	69.27				Y				Y
172	GODS	-94.21	54.62		Y					Y	
570	GOELAND	-76.85	49.86		Y				Y		
968	GOLODNAYA GUBA	52.66	67.85		Y				Y		
1424	GOOSE	-101.54	54.44		Y					Y	
464	GOOSE LAKE	-120.41	41.92		Y					Y	
678	GORDON	146.15	-42.72		Y				Y		
1103	GORDON	-113.22	63.08				Y				Y
193	GORKOVSKOYE	43.13	57.11		Y				Y		
442	GOVIND BALLABAH PANT	82.84	24.07		Y			Y			
718	GOZHA	81.08	35.03		Y						Y
399	GRAND	-57.35	49.01		Y				Y		

979	GRAND	-66.02	46.03		Y				Y		
987	GRAND	-60.50	53.68		Y				Y		
1129	GRAND LAKE	-92.75	29.90		Y					Y	
54	GRANDE	-76.73	53.86		Y				Y		
63	GRANDE	-74.87	53.70		Y				Y		
161	GRANDE	-57.86	-30.83		Y				Y		
760	GRANDIN	-118.98	63.99		Y				Y		
363	GRANVILLE	-100.21	56.40		Y				Y		
252	GRAS	-110.38	64.54		Y				Y		
2067	GRASSET	-78.16	49.95		Y				Y		
1170	GREAT	146.75	-41.89		Y				Y		
9	GREAT BEAR	-121.30	65.91		Y					Y	
817	GREAT BITTER	32.44	30.29		Y			Y			
1756	GREAT SACANDAGA LAKE	-74.10	43.20		Y				Y		
26	GREAT SALT LAKE	-112.50	41.20		Y			Y			
11	GREAT SLAVE	-114.37	62.09		Y					Y	
2898	GRENADA LAKE	-89.72	33.86		Y				Y		
2517	GUANTING SHUIKU	115.69	40.33		Y				Y		
1007	GUARICO	-67.37	9.05		Y				Y		
975	GUIERS	-15.84	16.18		Y				Y		
253	GUILLAUME-DELISLE	-76.28	56.33		Y				Y		
1184	GUSINOYE	106.39	51.20		Y				Y		
336	GYARING	97.27	34.92		Y					Y	
1807	GYEZE CAKA	80.90	33.95		Y						Y
738	HABBANIYAH	43.45	33.29		Y					Y	
389	HALL	-82.09	68.74		Y				Y		
408	HAMMAR	47.04	30.76		Y						Y
221	HAMUN-E SABERI	61.28	31.37		Y				Y		
596	HAN SHUI	111.20	32.66		Y				Y		
1276	HANSINE	-85.66	65.60		Y						Y
294	HAR	93.21	48.05		Y					Y	
2270	HAR	95.16	48.46		Y						Y
142	HAR US	92.30	48.06		Y					Y	
302	HAR-HU	97.59	38.31		Y			Y			
1265	HARNEY LAKE	-119.13	43.25		Y				Y		
1380	HATCHETT	-103.70	58.63		Y				Y		
214	HAUKIVESI	28.52	62.10		Y				Y		
339	HAZEN	-70.94	81.80		Y			Y			
834	HEDESUNDEFJ	17.14	60.33				Y				Y
460	HENDRIK VERWOERD	25.92	-30.58		Y						Y
643	HICKS	-99.94	61.38		Y				Y		
288	HIGHROCK	-100.44	55.83		Y				Y		
1422	HINDMARSH	141.91	-36.04		Y				Y		
249	HIRAKUD	83.77	21.64		Y				Y		
1110	HIRFANLI	33.69	39.16		Y				Y		
387	HJALMAREN	15.86	59.23		Y				Y		
736	HOH SAI	92.83	35.73		Y						Y
609	HOH XIL	91.12	35.58		Y						Y
637	HONDO	-64.98	-27.53		Y				Y		
964	HONEY LAKE	-120.32	40.27		Y					Y	
708	HONG	113.28	29.85		Y				Y		
758	HORNAVAN	17.59	66.24		Y						Y
1106	HORTON	-122.50	67.48		Y				Y		

189	HOTTAH	-118.44	64.95		Y			Y			
2345	HOUGHTON LAKE	-84.71	44.34		Y				Y		
59	HOVSGOL	100.48	51.02		Y					Y	
913	HSU-JU	86.41	30.27		Y				Y		
1765	HUANG-CH'I	113.29	40.85				Y				Y
75	HULUN	117.38	48.97		Y			Y			
109	HUNGTZE	118.53	33.34		Y			Y			
5	HURON	-82.21	44.78		Y			Y			
121	HYARGAS	93.30	49.13		Y					Y	
2313	IHEMA	30.77	-1.89		Y				Y		
1869	IHOTRY	43.67	-21.94		Y				Y		
89	IJSSELMEER	5.42	52.66		Y					Y	
2627	IK	71.55	56.05		Y				Y		
192	IL'MEN'	31.30	58.30		Y			Y			
391	ILE-A-LA-CROSSE	-107.75	55.56		Y				Y		
1593	ILERGYTGYN	158.97	70.51		Y				Y		
62	ILIAMNA	-154.90	59.56		Y			Y			
177	IMANDRA	33.07	67.72		Y				Y		
852	IMURUK BASIN	-165.63	65.13		Y				Y		
2543	IMURUK LAKE	-163.19	65.60		Y				Y		
144	INARI	27.83	69.04		Y				Y		
1841	INAWASHIRO KO	140.09	37.47		Y				Y		
1555	INDAWNGY	96.34	25.15		Y				Y		
1722	INDER	51.91	48.47		Y				Y		
1444	INGRAY	-116.14	64.24				Y				Y
266	INHERNILLO	-101.72	18.58		Y				Y		
954	INLAND LAKE	-159.84	66.46		Y				Y		
655	IRIKLINSKOYE	58.82	51.95				Y				Y
1701	IRO	19.42	10.10		Y				Y		
174	ISLAND	-94.70	53.85		Y				Y		
25	ISSYKKUL	77.25	42.46		Y				Y		
1441	ISTADA	67.92	32.48				Y				Y
19	ITAPARICA	-42.01	-10.18		Y			Y			
342	ITARARE	-49.62	-23.38		Y				Y		
1209	ITCHEN	-112.64	65.53				Y				Y
245	IZABAL	-89.11	15.57		Y				Y		
634	IZNIK	29.53	40.45		Y			Y			
936	JANIS YARVI	30.90	62.01		Y				Y		
1219	JAYAKWADI	75.21	19.54		Y				Y		
1575	JAYKO	-103.22	69.82		Y						Y
1563	JEKYLL	-93.66	69.76				Y				Y
983	JEN-CH'ING HSIU-PU-TS'O	83.42	31.27		Y				Y		
1174	JILI	87.45	46.92		Y				Y		
421	JOSEPH	-65.30	52.79		Y				Y		
1264	JUNIN	-76.15	-11.02		Y				Y		
1107	JUNSHAN	116.31	28.51		Y				Y		
1157	K'OK'A	39.08	8.38		Y				Y		
1046	KABAMBA	27.04	-7.90		Y				Y		
1774	KABELE	25.97	-8.94		Y				Y		
1801	KABWE	26.02	-9.16		Y				Y		
1149	KACH	69.88	24.03		Y						Y
1705	KAGALURPAK LAKE	-163.98	60.96		Y				Y		
116	KAINJI	4.56	10.43		Y				Y		

79	KAKHOVSKOYE	33.95	47.27		Y					Y	
988	KALLSJON	13.00	63.60		Y				Y		
1462	KALRI	68.06	24.94		Y				Y		
246	KAMINAK	-94.90	62.20		Y				Y		
320	KAMINURIAK	-95.79	62.96		Y				Y		
104	KAMSKOYE	56.26	58.80		Y				Y		
1360	KAMYSHLYBAS	61.78	46.20		Y				Y		
264	KAMILUKUAK	-101.73	62.28		Y				Y		
131	KAPCHAGAYSKOYEVODO.	77.73	43.82		Y				Y		
197	KARA-BOGAZ-GOL	53.54	41.23		Y			Y			
470	KARAKUL	73.49	39.00		Y						Y
1286	KARASOR	75.57	49.87		Y				Y		
35	KARIBA	27.60	-17.23		Y			Y			
124	KASBA	-102.27	60.34		Y					Y	
1204	KASUMIGA-URA	140.37	36.05		Y				Y		
1419	KAYIGYALIK LAKE	-162.48	61.03		Y				Y		
461	KAYRAKKUMSKOYE	70.06	40.32		Y					Y	
945	KAYRAKKUMSKOYE	61.32	37.18		Y			Y			
318	KEBAN BARAJI	39.23	38.87		Y				Y		
1945	KEELEY	-108.13	54.89		Y				Y		
2596	KEGUM KAGATI LAKE	-164.31	60.32		Y						Y
346	KEITELE	25.99	62.89		Y				Y		
465	KELLER	-121.58	63.95		Y				Y		
1183	KEMIJARVI	27.53	66.62		Y				Y		
843	KERET	32.89	65.87		Y				Y		
1071	KESAGAMI	-80.32	50.31		Y				Y		
433	KETA	89.89	68.75		Y				Y		
1598	KGUN LAKE	-163.81	61.56		Y				Y		
45	KHANKA	132.42	44.94		Y			Y			
2226	KHANSKOYE	38.35	46.24		Y					Y	
218	KHANTAYSKOE	91.18	68.36		Y				Y		
112	KHANTAYSKOYE	87.75	67.96		Y				Y		
1023	KIANTA	29.12	65.03		Y						Y
1218	KIKULETWA	37.41	-3.68		Y				Y		
1887	KILIBEK	70.65	53.88		Y				Y		
2271	KINKONY	45.80	-16.16		Y				Y		
674	KISALE	26.49	-8.28		Y				Y		
2148	KISHI'KAROY	71.34	54.03		Y				Y		
733	KISKITTO	-98.23	54.36		Y			Y			
684	KISKITTOGISU	-98.37	54.21		Y					Y	
1703	KISTIGAN	-92.66	54.60		Y				Y		
1733	KITANGIRI	34.30	-4.09		Y				Y		
1132	KIVIJARVI	25.16	63.15		Y				Y		
67	KIVU	29.23	-2.04		Y				Y		
1605	KIYENG-KYUYEL'	109.57	73.02		Y				Y		
436	KIYEVSKOYE	30.48	50.82		Y					Y	
1056	KIZILIASHSKIY	37.05	45.12		Y					Y	
447	KLUANE	-138.76	61.26		Y				Y		
2838	KLUTINA LAKE	-145.98	61.67				Y				Y
927	KNEE	-94.54	55.08		Y				Y		
1108	KOITERE	30.70	62.97		Y				Y		
1215	KOKORA	101.08	72.99		Y				Y		
1803	KOLMAJARVI	25.82	63.27		Y				Y		

928	KONNEVESI	26.54	62.69		Y				Y		
108	KOSSOU	-5.68	7.55				Y				Y
242	KOVDOZERO	31.99	66.68		Y				Y		
1538	KOVITSKOYE	33.41	67.12		Y				Y		
1881	KOZHOZERO	38.17	63.08		Y				Y		
344	KRASNOE	174.44	64.53		Y				Y		
93	KRASNOYARSKOYE	90.94	54.84		Y				Y		
87	KREMENSHUGSKOYE	32.62	49.28		Y			Y			
756	KRONOTSKOYE	160.20	54.81		Y				Y		
434	KUBENSKOYE	39.45	59.64		Y				Y		
1050	KUCHUKSKOYE	79.77	52.70		Y				Y		
1091	KUKAKLEK LAKE	-155.30	59.18		Y				Y		
262	KULUNDINSKOYE	79.58	52.98		Y				Y		
671	KUNGASALAKH	107.23	74.61				Y				Y
1971	KUO-MANG	89.20	31.21		Y						Y
2264	KURIL'SKOYE	157.10	51.46		Y				Y		
1145	KUS	27.96	40.19		Y					Y	
550	KUSHMURUN	64.78	52.72		Y				Y		
33	KUYBYSHEVSKOYE	48.65	54.54		Y					Y	
1327	KUYUMAZARSKOYE	64.83	39.85		Y					Y	
325	KWANIA	32.65	1.72		Y				Y		
382	KYARING	88.32	31.13		Y				Y		
99	KYOGA	33.01	1.50		Y					Y	
676	LA-ANG	81.21	30.72		Y				Y		
331	LABAZ	99.57	72.27		Y				Y		
940	LABERGE	-135.16	61.19		Y						Y
2988	LAC DES ALLEMANDS	-90.57	29.92		Y				Y		
533	LACHA	38.77	61.31		Y					Y	
16	LADOGA	31.39	60.84		Y			Y			
575	LADY MELVILLE	-92.33	69.14		Y				Y		
1827	LAGKOR	84.11	32.03		Y						Y
1154	LAKE ABERT	-120.21	42.64				Y				Y
1493	LAKE APOPKA	-81.62	28.62		Y					Y	
1991	LAKE BEVERLEY	-158.73	59.66		Y				Y		
2403	LAKE BROOKS	-155.93	58.50		Y						Y
554	LAKE CLARK	-154.33	60.23		Y				Y		
929	LAKE GEORGE	-81.61	29.33		Y					Y	
2616	LAKE HARRIS	-81.81	28.76		Y				Y		
1368	LAKE KISSIMMEE	-81.27	27.90		Y				Y		
534	LAKE LIVINGSTON	-95.14	30.80		Y					Y	
1721	LAKE LOUISE	-146.64	62.41		Y				Y		
556	LAKE MARION	-80.47	33.53		Y					Y	
1148	LAKE MATTAMUSKEET	-76.20	35.50		Y					Y	
746	LAKE MAUREPAS	-90.45	30.27		Y			Y			
278	LAKE MEAD	-114.39	36.33		Y			Y			
3051	LAKE MINCHUMINA	-152.24	63.89		Y				Y		
824	LAKE MOULTRIE	-80.07	33.31		Y					Y	
850	LAKE MURRAY	-81.46	34.09		Y				Y		
884	LAKE NERKA	-159.01	59.53		Y				Y		
122	LAKE OAHE	-100.38	45.49		Y						Y
546	LAKE PEND OREILLE	-116.44	48.13		Y				Y		
1714	LAKE POYGAN	-88.87	44.12		Y				Y		
836	LAKE SALVADOR	-90.25	29.76		Y					Y	

3238	LAKE VERRET	-91.14	29.89		Y				Y		
761	LAKE WINNIBIGOSHISH	-94.17	47.45		Y				Y		
584	LAKES NUYAKUK	-158.70	59.97		Y				Y		
110	LAKES SAKAKAWEA	-102.32	47.81		Y				Y		
561	LAMA	90.63	69.50		Y				Y		
1146	LANGANO	38.59	7.60		Y				Y		
524	LANO	124.24	7.89		Y				Y		
1246	LAPPAJARVI	23.67	63.15		Y				Y		
1075	LAST MOUNTAIN	-105.22	51.03		Y				Y		
450	LEECH LAKE	-94.43	47.18		Y				Y		
939	LEKSOZERO	30.97	63.81		Y				Y		
147	LESSER SLAVE	-115.49	55.43		Y			Y			
531	LIANGZI	114.51	30.23		Y				Y		
1957	LIMINGEN	13.57	64.79		Y						Y
1815	LITTLE SACHIGO	-92.11	54.15		Y				Y		
812	LIXI'OIDAIN	90.18	35.75		Y						Y
1295	LLANCANELO	-69.15	-35.62		Y				Y		
209	LLANQUIHUE	-72.79	-41.14		Y					Y	
908	LOCHE	-109.48	56.46		Y				Y		
376	LOKAN TERKOJARVI	27.77	67.97		Y				Y		
539	LONGGAN	116.14	29.97		Y					Y	
861	LOVOZERO	35.22	67.90		Y				Y		
159	LOW	-76.27	52.51		Y				Y		
1010	LOWER UGASHIK LAKE	-156.88	57.49		Y				Y		
175	LUANG	100.38	7.46		Y				Y		
592	LUMAJANGDONG	81.64	34.01		Y						Y
1871	LUNG MU	80.44	34.62		Y						Y
1430	LUOMA	118.21	34.06		Y					Y	
1350	LURAN	-93.01	64.86				Y				Y
574	M'BAKAOU	12.81	6.41				Y				Y
439	MA-P'ANG YUNG-TS'O	81.49	30.67		Y				Y		
184	MACKAY	-111.30	63.96		Y				Y		
998	MACNAUGHTON	-98.41	67.30		Y				Y		
1019	MAHONY	-125.36	65.50		Y				Y		
90	MAI-NDOMBE	18.32	-2.14		Y				Y		
1307	MAINIT	125.52	9.44		Y				Y		
163	MALAREN	16.19	59.44		Y				Y		
1735	MALARTIC	-78.11	48.34		Y				Y		
10	MALAWI	34.59	-11.96		Y			Y			
350	MALHEUR	-118.83	43.34		Y				Y		
413	MALLERY	-98.36	63.97		Y				Y		
586	MALOMBE	35.26	-14.64		Y			Y			
960	MALYYE CHANY	77.96	54.57		Y				Y		
176	MANAGUA	-86.35	12.32		Y			Y			
664	MANAS	85.94	45.81		Y						Y
1853	MANDIORA	-57.56	-18.13		Y				Y		
231	MANGUEIRA	-52.84	-33.16		Y			Y			
82	MANICOUAGAN	-69.13	51.35		Y				Y		
37	MANITOBA	-98.80	50.99		Y			Y			
1818	MANITOU	-81.99	45.78		Y				Y		
368	MANOUANE	-70.99	50.76		Y				Y		
397	MANYARA	35.81	-3.58		Y				Y		
250	MANYCH-GUDILO	42.98	46.26		Y				Y		

1089	MARJORIE	-99.36	64.15				Y				Y
403	MARKAKOL'	85.77	48.75		Y				Y		
100	MARTRE	-117.91	63.33		Y					Y	
1243	MARY	-103.56	62.38				Y				Y
493	MATAGAMI	-77.50	50.07		Y				Y		
1501	MATATILA	78.32	25.05		Y				Y		
540	MAUNOIR	-124.88	67.46		Y			Y			
396	MCALPINE LANE	-102.64	66.52		Y				Y		
573	MEEPLAEG	-56.62	48.26		Y				Y		
2468	MELKOYE	70.20	69.70		Y				Y		
1354	MEMAR	82.33	34.20		Y						Y
1255	MEYATO	70.64	70.15				Y				Y
518	MHISA	10.99	60.82		Y				Y		
6	MICHIGAN	-87.09	43.86		Y			Y			
520	MIGRIGGYANGZHAM	90.32	33.48		Y				Y		
452	MIGUEL ALEMAN	-96.51	18.26		Y				Y		
366	MILLE LACS	-93.65	46.24		Y			Y			
420	MILLS	-118.15	61.43		Y				Y		
2168	MILLWOOD LAKE	-93.96	33.77		Y				Y		
328	MINGECHAURSKOYE	46.79	40.93		Y					Y	
822	MINGO	-72.14	64.59		Y				Y		
1412	MINIJARVI	29.30	62.73		Y				Y		
705	MININDEE	142.33	-32.41		Y				Y		
46	MIRIM	-53.25	-32.89		Y			Y			
76	MISTASSINI	-73.81	50.82		Y				Y		
1618	MIYUN SHUIKU	116.94	40.51		Y				Y		
1970	MO-K'O-YU	89.01	31.06				Y				Y
673	MOGOTOYEYO	149.15	72.03		Y				Y		
894	MOLOCHNOYE	35.34	46.54		Y					Y	
454	MOLSON	-96.82	54.22		Y					Y	
883	MONO	-118.96	38.01		Y					Y	
2099	MONTE	-62.47	-36.99		Y				Y		
405	MONTREAL	-105.69	54.32		Y			Y			
617	MOOSEHEAD LAKE	-69.71	45.67		Y				Y		
1302	MORARI	78.32	32.89		Y						Y
640	MOSQUITO	-103.33	62.59		Y				Y		
1283	MU-TS'O-PING-NI	86.25	30.63		Y						Y
2211	MUNDUYSKOYE	88.44	66.57		Y				Y		
1649	MURITZ	12.68	53.42		Y				Y		
448	MUSTERS	-69.23	-45.41		Y					Y	
36	MWERU	28.74	-9.01		Y			Y			
1960	MYAKSHINGA	93.53	67.00				Y				Y
1079	NA	91.48	32.02		Y				Y		
1281	NADUDOTURKU	84.11	72.84		Y				Y		
343	NAHUEL HUAPI	-71.52	-40.92		Y				Y		
1659	NAIVASHA	36.36	-0.77		Y				Y		
377	NAKNEK	-155.67	58.64		Y				Y		
2252	NAKTEN	14.65	62.83				Y				Y
91	NAM	90.66	30.71		Y					Y	
1261	NAMAYCUSH	-108.40	70.81				Y				Y
989	NAMRU	90.84	32.08		Y				Y		
1421	NANYI	118.89	31.11		Y				Y		
1726	NARRAN	147.31	-29.90		Y				Y		

369	NASIJARVI	23.97	61.88		Y				Y		
48	NASSER	32.58	22.86		Y			Y			
322	NATRON	36.02	-2.34		Y				Y		
481	NEAGH	-6.42	54.62		Y				Y		
1569	NEDZHELI	125.19	63.61		Y				Y		
1114	NEERGAURE	-79.91	70.22		Y						Y
1121	NEGRA	-53.65	-34.05		Y			Y			
132	NEGRO	-55.93	-32.70		Y			Y			
503	NEJANILINI	-97.87	59.61		Y				Y		
338	NERPICH'YE	162.77	56.39		Y					Y	
792	NERPICH'YE	160.18	69.29		Y			Y			
32	NETILLING	-70.28	66.42		Y				Y		
469	NETSILIK	-93.04	69.25		Y				Y		
893	NEUCHATEL	6.84	46.90		Y				Y		
1115	NEUSIEDL	16.78	47.80		Y				Y		
921	NEYATO	70.38	70.06		Y				Y		
1176	NEYTO	70.91	70.04		Y				Y		
681	NGOIN	88.74	31.52		Y				Y		
300	NGORING	97.71	34.93		Y					Y	
21	NICARAGUA	-85.36	11.57		Y			Y			
1582	NIGHTHAWK	-80.98	48.44		Y				Y		
1061	NILAKKA	26.46	63.12		Y				Y		
1762	NINA BANG	-79.38	70.87		Y				Y		
38	NIPIGON	-88.55	49.80		Y			Y			
198	NIPISSING	-79.92	46.24		Y					Y	
833	NOI	105.39	15.01		Y				Y		
1287	NOKOUE	2.46	6.43		Y				Y		
211	NONACHO	-108.92	61.82		Y				Y		
1403	NONVIANUK LAKE	-155.35	59.00		Y				Y		
2336	NORRA DELLEN	16.71	61.87		Y				Y		
516	NORTH CARIBOU	-90.74	52.79		Y						Y
709	NORTH HENIK	-97.71	61.73		Y				Y		
303	NORTH MOOSE	-100.16	54.05		Y			Y			
1832	NORTH WABASCA	-113.91	56.04		Y				Y		
1185	NOSE	-108.91	65.42				Y				Y
190	NOVOSIBIRSKOYE	82.03	54.37		Y				Y		
682	NOWLEYE	-101.06	62.34		Y				Y		
83	NUELTIN	-99.40	60.25		Y				Y		
3308	NUIGALAK LAKE	-164.65	61.52		Y				Y		
2669	NUNAVAKANUK LAKE	-164.66	62.05				Y				Y
1365	NUNAVAKPAK LAKE	-162.63	60.80		Y				Y		
2309	NUNAVAUGALUK LAKE	-158.91	59.24		Y				Y		
707	NZILO	25.72	-10.66		Y				Y		
526	OHRID	20.73	41.04		Y			Y			
114	OKEECHOBEE	-80.86	26.95		Y			Y			
969	ONDOZERO	33.37	63.78		Y				Y		
18	ONEGA	35.35	61.90		Y			Y			
905	ONEIDA LAKE	-75.93	43.20				Y				Y
422	ONKIVESI	27.77	62.64		Y				Y		
15	ONTARIO	-77.77	43.85		Y					Y	
1868	ONTOJARVI	29.18	64.12		Y				Y		
1344	OOLAGAHL LAKE	-95.61	36.55		Y				Y		
374	OOTSA	-125.76	53.62		Y				Y		

608	OREL'	139.78	53.45		Y				Y		
187	ORIVESI	29.59	62.35		Y					Y	
773	OROG	91.01	50.15		Y				Y		
1431	OROG	100.72	45.05				Y				Y
290	OSSOKAMANUAN	-64.93	53.43		Y				Y		
1379	OTELNUC	-68.19	56.15		Y						Y
202	OULUJARVI	27.70	64.35		Y				Y		
248	OUTARDES QUATRE	-69.15	50.16		Y				Y		
529	OXFORD	-95.44	54.85		Y				Y		
1187	OZHOGINO	146.64	69.25		Y				Y		
1323	P'A-LUNG	83.58	30.87		Y				Y		
685	P'EI-K'U T'SO	85.58	28.90		Y				Y		
1432	P'ENG-TS'O	90.97	31.52		Y				Y		
1066	PA-MU-TS'O	90.58	31.25		Y				Y		
258	PADUSKOYE MORE	30.86	68.38		Y				Y		
157	PAIJANNE	25.49	61.71		Y				Y		
1874	PAL'YEOZERO	33.77	62.59		Y				Y		
1214	PANGNIKTO	-92.97	69.52				Y				Y
1477	PARENT	-77.11	48.60		Y				Y		
2907	PARINACOCHA	-73.70	-15.30		Y						Y
782	PASFIELD	-105.31	58.37		Y				Y		
699	PAVYLON	151.99	68.39		Y				Y		
353	PAYNE	-73.82	59.40		Y				Y		
50	PEIPUS	27.59	58.41		Y			Y			
435	PEKUL'NEYSKOYE	177.10	62.70		Y				Y		
1511	PELEGRINI	-68.01	-38.70		Y				Y		
1221	PELICAN	-100.34	52.46		Y					Y	
845	PELLY	-101.11	65.85		Y						Y
717	PERIBONCA	-71.27	50.14		Y				Y		
1867	PERIPTAVETO	79.01	71.36		Y						Y
349	PERLAS	-83.67	12.54		Y					Y	
986	PERVOYE	71.57	67.94		Y				Y		
2319	PESCHANOYE	53.06	68.64		Y				Y		
1670	PETENWELL LAKE	-89.92	44.17		Y				Y		
222	PETER POND	-108.55	55.84		Y			Y			
813	PETIT MANICOUAGAN	-67.78	51.85		Y				Y		
2799	PHELPS LAKE	-76.47	35.77		Y				Y		
195	PIELINEN	29.71	63.16		Y				Y		
1910	PIGEON	-114.07	53.02		Y				Y		
1647	PILTANLOR	73.37	61.71		Y				Y		
474	PINEHOUSE	-106.47	55.55		Y				Y		
223	PIPMUACAN	-70.12	49.62		Y				Y		
1497	PISO	-11.26	6.74		Y				Y		
735	PITZ	-96.59	63.96		Y				Y		
213	PLAYGREEN	-97.75	54.07		Y					Y	
517	PLETIPI	-70.21	51.70		Y				Y		
810	PLONGE	-107.34	55.12		Y			Y			
1270	PO	116.44	30.15		Y				Y		
1616	POELELA	35.02	-24.52		Y				Y		
232	POINT	-113.84	65.31				Y				Y
649	POMO	90.40	28.55		Y				Y		
499	POOL MALEBO	15.52	-4.22				Y				Y
133	POOPO	-67.06	-18.81		Y				Y		

495	PORTNYAGINO	106.95	74.14		Y				Y		
911	PORTTIPAHTA	26.67	68.07		Y						Y
2812	POTHOLES RESERVOIR	-119.31	47.02				Y				Y
78	POYANG	116.06	29.25		Y				Y		
1749	POZUELOS	-66.00	-22.34		Y						Y
690	PRESPA	21.02	40.89		Y			Y			
409	PRIMROSE	-109.79	54.89		Y			Y			
395	PRINCESS MARY	-97.66	63.93		Y				Y		
2012	PUEBLO VIEJO	-97.89	22.14		Y				Y		
934	PUKAKI	170.15	-43.97		Y				Y		
463	PULICAT	80.18	13.56		Y					Y	
164	PURUVESI	29.02	61.77		Y				Y		
530	PUULAVESI	26.66	61.84		Y				Y		
1207	PUYEHUE	-72.47	-40.68		Y				Y		
273	PYAOZERO	30.98	66.07		Y				Y		
240	PYASINO	87.78	69.77		Y				Y		
1240	PYHAJARVI	22.28	61.00		Y					Y	
1491	PYHAJARVI	25.89	63.61		Y				Y		
411	PYRAMID	-119.55	40.03		Y			Y			
806	QARUN	30.61	29.47		Y			Y			
41	QINGHAI	100.18	36.89		Y			Y			
1031	QUAGAN	124.26	45.25		Y				Y		
1413	QUARTZ	-80.66	70.93		Y						Y
1140	QUUNNGUQ	-112.60	69.92				Y				Y
130	RAINY	-92.97	48.61		Y				Y		
937	RANA PRATAP	75.60	24.82		Y				Y		
416	RANCO	-72.48	-40.23		Y					Y	
1095	RANDIJAUR	19.06	66.80		Y				Y		
358	RAZELM	28.97	44.83		Y			Y			
151	RED	-95.08	48.04		Y			Y			
728	RED DEER	-101.36	52.95		Y			Y			
797	RED SUCKER	-93.67	54.14		Y				Y		
1694	REE	-7.99	53.56		Y						Y
977	REED	-100.45	54.64		Y					Y	
28	REINDEER	-102.27	57.19		Y					Y	
129	REPRESSA DE JUPIA	-50.58	-19.83		Y				Y		
613	RETENUE DE LA LUFIRA	27.02	-10.90		Y				Y		
657	RIJKAVESI	29.75	62.87		Y				Y		
1041	RIOU	-106.39	59.12		Y				Y		
931	ROBERT S. KERR RESERVOIR	-94.95	35.38		Y				Y		
848	ROCKINGHORSE	-112.33	65.88				Y				Y
1706	ROCKY	-101.48	54.12		Y				Y		
127	RONGE	-104.83	55.11		Y			Y			
1467	ROSS R. BARNETT RESERVOIR	-90.01	32.47		Y				Y		
1116	ROSSIGNOL	-65.08	44.20		Y				Y		
1013	ROSSVATNET	14.11	65.79		Y				Y		
1893	ROXEN	15.64	58.49		Y				Y		
86	RUKWA	32.16	-7.84		Y			Y			
831	RUPANCO	-72.44	-40.83		Y				Y		
1771	RWERU	30.32	-2.39		Y				Y		
47	RYBINKSKOYE	38.13	58.49		Y			Y			
804	SACHIGO	-92.07	53.80		Y				Y		

2017	SAGARYCH'YE	146.54	70.98		Y				Y		
407	SAI LI-MU	81.18	44.61		Y				Y		
111	SAIMMAA	28.20	61.39		Y				Y		
146	SAINT CLAIR	-82.73	42.50		Y			Y			
158	SAINT JEAN	-72.02	48.66		Y				Y		
285	SAINT JOSEPH	-90.81	51.04		Y				Y		
794	SAITLAN	78.56	54.98		Y				Y		
282	SAKAMI	-76.75	53.22		Y				Y		
196	SALADA	-115.54	32.19		Y				Y		
329	SALINES GRANDES	-64.82	-29.85		Y				Y		
851	SALTAIM	71.93	56.12		Y				Y		
194	SALTON	-115.83	33.30		Y			Y			
362	SAM RAYBURN RESERVOIR	-94.36	31.26		Y					Y	
167	SAN MARTIN	-72.84	-48.75		Y				Y		
356	SANDY	-93.03	53.00		Y				Y		
982	SANGIYN DALAY	99.10	49.22		Y				Y		
2073	SARMIENTO	-72.67	-51.04				Y				Y
241	SARYKAMYSHSKOYE	57.61	41.88		Y			Y			
247	SASYKKOL	80.91	46.58		Y				Y		
1627	SAUMATRE	-71.96	18.57		Y				Y		
138	SAYANO-SHUSHENSKOYE	92.41	52.26		Y				Y		
438	SCHULTZ	-97.44	64.74		Y				Y		
313	SCOTT	-106.07	60.02		Y				Y		
488	SCUTARI	19.28	42.19		Y			Y			
1498	SEBAGO LAKE	-70.55	43.85		Y				Y		
228	SEGOZERO	33.76	63.32		Y			Y			
170	SELAWIK	-160.73	66.51		Y					Y	
271	SELETYTENIZ	73.18	53.23		Y				Y		
1086	SELINGUE	-8.17	11.50				Y				Y
292	SELWYN	-104.68	60.00		Y				Y		
1904	SEMAJANG	116.47	-0.23		Y				Y		
1133	SEN-KYUYEL	155.27	68.55		Y				Y		
2163	SERGAZERO	36.75	66.77		Y				Y		
107	SEUL	-92.05	50.40		Y				Y		
135	SEVAN	45.29	40.39		Y			Y			
978	SHAGANY	29.97	45.80		Y					Y	
604	SHALA	38.51	7.46		Y					Y	
907	SHALKAR	51.67	50.57		Y					Y	
143	SHERMAN	-97.73	67.79		Y			Y			
791	SHIJIU	118.87	31.46		Y					Y	
1340	SHURYSHKARSKIY	65.14	65.99		Y				Y		
1037	SID	-104.09	62.27		Y				Y		
654	SILJAN	14.80	60.86		Y				Y		
555	SIMARD	-78.92	47.57		Y				Y		
236	SIMCOE	-79.42	44.47		Y			Y			
301	SIPIWESK	-97.81	54.99		Y				Y		
611	SIRIKIT	100.50	17.95		Y				Y		
667	SITIDGI	-132.67	68.54		Y				Y		
1423	SKAGERN	14.25	58.99		Y				Y		
1745	SKILAK LAKE	-150.40	60.44		Y				Y		
27	SMALLWOOD	-64.31	54.19		Y					Y	
672	SMOOTHSTONE	-106.82	54.65		Y			Y			
1505	SNIARDWY	21.75	53.76		Y				Y		

365	SNOWBIRD	-102.94	60.64		Y				Y		
1711	SOBACH'YE	91.52	69.06		Y						Y
410	SOLENOYE	35.24	45.44		Y					Y	
1381	SOLUNTAKH	143.24	71.71		Y				Y		
688	SONG-KEL	75.17	41.84		Y				Y		
319	SOUTH HENIK	-97.29	61.37		Y				Y		
225	SOUTH MOOSE	-100.04	53.83		Y			Y			
72	SOUTHERN INDIAN	-98.61	57.14		Y				Y		
581	SPLIT	-96.25	56.18		Y				Y		
472	SREDNEYE KUYTO	31.59	65.02		Y				Y		
702	ST. FRANCIS	-74.48	45.13		Y				Y		
618	ST. LUCIA	32.47	-28.11		Y				Y		
538	ST. MARTIN	-98.51	51.65		Y				Y		
423	ST. PETER	-72.90	46.15		Y				Y		
2335	ST. THERESE	-121.96	64.36		Y				Y		
1178	STARUMAN	16.69	65.26		Y				Y		
337	STEPHENS	-95.07	56.42		Y				Y		
877	STEVENSON	-95.90	53.90		Y				Y		
811	STORA LULLEVATEN	19.12	67.28		Y						Y
393	STORSJON	14.41	63.09		Y				Y		
1259	STROBEL	-71.23	-48.37		Y				Y		
501	STUART	-124.58	54.55		Y				Y		
1684	SUHAI	93.88	38.86		Y						Y
1509	SUMMER LAKE	-120.73	42.83		Y				Y		
2	SUPERIOR	-88.23	47.72		Y			Y			
721	SURREY	-107.16	69.67		Y				Y		
715	SUVASVESI	28.33	62.62		Y				Y		
624	SWAN	-100.74	52.49		Y					Y	
1997	SYRKOVOYE	64.98	60.65		Y				Y		
85	SYVASH	34.74	45.96		Y					Y	
383	T'A-JO	84.12	31.13		Y				Y		
744	TA-TSE	87.43	31.88		Y				Y		
818	TAAL	121.01	13.99		Y				Y		
619	TADOUIE	-98.33	58.59		Y				Y		
1200	TAHIRYUAK	-112.18	70.95				Y				Y
380	TAHOE	-120.04	39.09		Y			Y			
1158	TAHOE	-108.92	70.03				Y				Y
66	TAI	120.24	31.21		Y					Y	
1205	TAI	112.66	40.55		Y				Y		
2203	TAJO-TZO	84.05	30.41				Y				Y
178	TAKIYUAK	-113.17	66.28		Y				Y		
2159	TAKSLESLUK LAKE	-162.87	61.07		Y						Y
1003	TALBOT	-99.90	54.01		Y			Y			
2190	TAMES	-98.08	22.22		Y				Y		
235	TAMIAHUA	-97.57	21.66		Y			Y			
55	TANA	37.31	11.95		Y			Y			
7	TANGANYIKA	29.46	-6.07		Y			Y			
215	TANGRA	86.59	31.05		Y					Y	
73	TAPAJOS	-55.14	-2.88		Y					Y	
316	TATHLINA	-117.64	60.54		Y				Y		
1004	TATINNAI	-97.70	60.91		Y				Y		
295	TAUPO	175.90	-38.81		Y						Y
43	TAYMYR	100.76	74.48		Y				Y		

514	TAZIN	-109.20	59.81		Y				Y		
1239	TAZLINA LAKE	-146.51	61.88		Y						Y
532	TE ANAU	167.67	-45.18		Y				Y		
373	TEBESJUAK	-98.98	63.76		Y				Y		
1241	TEFE	-64.75	-3.45		Y				Y		
371	TEHEK	-95.62	64.92		Y				Y		
1002	TEKAPO	170.53	-43.75		Y						Y
920	TELMEN	97.33	48.83		Y				Y		
1675	TEMCHI	95.00	66.79				Y				Y
120	TENGIZ	68.90	50.44		Y					Y	
179	TERINAM	85.61	30.90		Y			Y			
212	TESHEKPUK	-153.60	70.59		Y				Y		
490	TESLIN	-132.39	59.97				Y				Y
2655	TETLIN LAKE	-142.77	63.10		Y				Y		
2186	THINGVALLAVAIN	-21.13	64.19		Y						Y
1196	TIBERIAS	35.59	32.80		Y			Y			
825	TIKSHE	31.86	66.28		Y				Y		
633	TIMISKAMING	-79.44	47.20		Y				Y		
20	TITICACA	-69.30	-15.92		Y			Y			
150	TOBA	98.90	2.61		Y				Y		
713	TOBIN	-103.49	53.57		Y					Y	
729	TOKTOGUL'SKOYE	72.91	41.76		Y				Y		
243	TOLEDO BEND RESERVOIR	-93.81	31.55		Y					Y	
1741	TONSKOYE	98.98	72.21		Y				Y		
186	TOPOZERO	32.09	65.62		Y				Y		
1235	TORMEMTOR	79.37	61.22		Y				Y		
594	TORNETRASK	19.34	68.34		Y				Y		
962	TORO	-72.71	-51.22		Y				Y		
1916	TORROJEN	13.00	63.88		Y				Y		
1130	TOSON	96.94	37.13		Y				Y		
332	TOWUTI	121.52	-2.79		Y				Y		
1529	TRASIMENO	12.10	43.14		Y					Y	
367	TROUT	-121.13	60.58		Y				Y		
486	TROUT	-93.28	51.20		Y				Y		
601	TSHCHIKSKOYE	39.34	45.04		Y					Y	
71	TSIMLYANSKOYE	42.98	48.05		Y					Y	
52	TUCURUI	-49.49	-4.57		Y					Y	
1789	TUDAKOL’	64.18	39.12		Y				Y		
269	TULEMALU	-99.48	62.99		Y				Y		
255	TUMBA	17.98	-0.82		Y				Y		
528	TUNGABHADRA	76.13	15.20		Y				Y		
22	TURKANA	36.08	3.53		Y			Y			
771	TURNOR	-108.65	56.56		Y				Y		
2019	TURSUNTSKIY TUMAN	63.96	60.56		Y				Y		
632	TUSTUMENA LAKE	-150.90	60.17		Y				Y		
185	TUZ	33.36	38.86		Y					Y	
1392	TYRIFJORDEN	10.17	60.02		Y				Y		
425	UBINSKOYE	80.05	55.47		Y				Y		
603	UBOLRATNA	102.60	16.69		Y				Y		
710	UDDJAUR	17.82	65.98		Y				Y		
500	UDYL'	139.77	52.07		Y				Y		
1059	UKAL	73.79	21.35		Y				Y		
985	ULAKH ULYUNG	151.34	68.23		Y				Y		

1236	ULUBAT	28.59	40.17		Y				Y		
239	ULUNGUR	87.30	47.22		Y					Y	
548	UMBOZERO	34.40	67.71		Y				Y		
1984	UNDEN	14.46	58.77		Y				Y		
314	UPEMBA	26.40	-8.65		Y				Y		
559	UPPER KLAMATH LAKE	-121.89	42.42		Y				Y		
882	UPPER UGASHIK LAKE	-156.70	57.67		Y				Y		
34	URMIA	45.49	37.64		Y			Y			
102	UST-ILIMSKOYE	102.32	57.15		Y				Y		
523	UTAH LAKE	-111.80	40.20		Y				Y		
669	UTIKUMA	-115.39	55.86		Y				Y		
2955	UVIL'DY	60.50	55.54		Y				Y		
53	UVS	92.81	50.33		Y					Y	
1609	UYALY	81.27	46.43		Y				Y		
562	VAALDAM	28.32	-27.01				Y				Y
1550	VACCARES	4.58	43.52		Y					Y	
515	VALENCIA	-67.74	10.18		Y					Y	
1941	VALLI DI COMACCHIO	12.16	44.60		Y					Y	
51	VAN	42.98	38.66		Y			Y			
1201	VANAJANSELKA	24.09	61.18		Y				Y		
29	VANERN	13.22	58.88		Y			Y			
2060	VASTENJAURE	16.63	67.48		Y						Y
95	VATTERN	14.57	58.33		Y			Y			
1820	VESIJARVI	25.39	61.09		Y				Y		
3	VICTORIA	33.23	-1.30		Y			Y			
1537	VICTORIA	141.30	-34.02		Y				Y		
171	VIEDMA	-72.56	-49.59		Y					Y	
1109	VILLARRICA	-72.09	-39.26		Y					Y	
80	VILYUYSKOYE	111.16	62.73		Y					Y	
1718	VIRIHAURE	16.55	67.37		Y				Y		
901	VIRMASVESI	26.87	62.83		Y				Y		
2054	VISOHISARVI	26.70	61.18		Y				Y		
776	VIVI	93.81	66.76				Y				Y
522	VODLOZERO	36.92	62.32		Y				Y		
61	VOLGOGRADSKOYE	45.85	50.35		Y				Y		
24	VOLTA	0.11	7.63		Y				Y		
679	VORTIS-JARV	26.04	58.22		Y					Y	
237	VOTKINSKOYE	55.01	57.22		Y				Y		
427	VOZHE	39.10	60.57		Y					Y	
1126	VTOROYE	71.15	68.03		Y				Y		
1717	VYALOZERO	35.19	66.83		Y						Y
136	VYGOZERO	34.84	63.54		Y					Y	
1169	WABIGOON	-92.54	49.65		Y				Y		
1128	WALKER	-118.71	38.70		Y					Y	
1249	WALKER	-96.94	54.70		Y				Y		
765	WALMSLEY	-108.61	63.42				Y				Y
1359	WANAPITEI	-80.74	46.73		Y				Y		
779	WAPAWEKKA	-104.66	54.90		Y					Y	
1425	WASEKAMIO	-108.76	56.74		Y				Y		
757	WASHBURN	-107.49	70.07		Y						Y
789	WASKAIOWAKA	-96.44	56.56		Y				Y		
904	WASWANIPI	-76.50	49.60		Y				Y		
837	WATERHEN	-99.57	52.09		Y					Y	

1590	WATTERSON	-99.38	61.21		Y				Y		
1112	WEAGAMOW	-91.37	52.88		Y				Y		
876	WEISHAN	117.24	34.61		Y					Y	
1062	WEKUSKO	-99.82	54.76		Y					Y	
1266	WELLINGTON	147.32	-38.10		Y				Y		
449	WHARTON	-99.74	64.00				Y				Y
512	WHITE FISH	-106.74	62.67		Y				Y		
872	WHITE LAKE	-92.50	29.74		Y					Y	
2169	WHITEFISH LAKE	-160.01	61.37		Y				Y		
973	WHITEHILLS	-95.98	64.51		Y				Y		
169	WHOLDAIA	-104.15	60.69		Y				Y		
1623	WILLIAM	-99.38	53.89		Y				Y		
103	WILLISTON	-123.91	55.95		Y				Y		
1220	WILLOW	-119.07	62.17		Y				Y		
1489	WINEFRED	-110.53	55.51		Y				Y		
340	WINNEBAGO	-88.42	44.02		Y			Y			
13	WINNIPEG	-97.25	52.12		Y			Y			
31	WINNIPEGOSIS	-100.05	52.37		Y			Y			
68	WOLLASTON	-103.33	58.30		Y					Y	
44	WOODS	-94.91	49.38		Y			Y			
790	WU-LIANG-SU	108.83	40.93		Y				Y		
1653	XIAOXIHAIZ SHUIKU	78.73	39.72		Y						Y
639	XIJIR ULAN	90.26	35.22		Y						Y
134	XINGU	-52.20	-2.16		Y				Y		
1790	YAGGAIN CANCO	89.81	33.00		Y						Y
840	YALPUG	28.63	45.48		Y				Y		
714	YAM	33.17	61.95		Y				Y		
519	YAMBA	-111.25	64.96				Y				Y
1123	YAMBUTO	79.42	71.19		Y				Y		
1739	YAMBUTO	69.13	69.50		Y				Y		
261	YAMDROK	90.76	28.97		Y						Y
1597	YANGCHENG	120.79	31.43		Y				Y		
2395	YARDI	40.50	10.21		Y				Y		
126	YATHKYED	-98.07	62.69		Y				Y		
572	YELLOWSTONE LAKE	-110.39	44.43		Y				Y		
778	YESSEY	102.40	68.43		Y				Y		
751	YLI -KITKA	28.64	66.13		Y				Y		
2018	YUELIANG PAO	123.87	45.70		Y				Y		
731	ZAPATOSA	-73.83	9.14		Y				Y		
40	ZAYSAN	83.44	48.70		Y				Y		
662	ZETA	-106.64	71.05				Y				Y
88	ZEYSKOYE	127.80	54.26		Y				Y		
880	ZHALAULY	74.18	52.89		Y				Y		
1979	ZHANGDU	114.73	30.66		Y				Y		
105	ZILING	88.95	31.77		Y					Y	
917	ZIMBAMBO	26.88	-8.11		Y				Y		
445	ZIWAY	38.84	7.98		Y				Y		
732	ZONAG	91.94	35.55		Y				Y		
113	ZZZZ	48.36	52.74		Y				Y		
238	ZZZZ	-49.05	-18.39		Y				Y		
306	ZZZZ	13.97	8.88		Y				Y		
309	ZZZZ	-113.52	41.11				Y				Y
330	ZZZZ	99.04	14.75		Y				Y		

341	ZZZZ	-47.77	-18.42		Y				Y		
361	ZZZZ	34.17	48.77		Y				Y		
385	ZZZZ	-94.14	16.14		Y			Y			
398	ZZZZ	133.51	-17.79		Y						Y
406	ZZZZ	-134.19	59.98		Y				Y		
414	ZZZZ	-74.40	10.86		Y					Y	
415	ZZZZ	102.66	18.61		Y				Y		
431	ZZZZ	-172.85	66.94		Y				Y		
437	ZZZZ	-118.44	52.15		Y				Y		
455	ZZZZ	32.22	14.73		Y				Y		
456	ZZZZ	90.34	34.79		Y						Y
459	ZZZZ	-176.01	67.69		Y				Y		
462	ZZZZ	25.95	-15.67		Y				Y		
466	ZZZZ	118.98	29.59		Y				Y		
471	ZZZZ	31.22	49.98		Y				Y		
476	ZZZZ	-55.38	-2.24		Y				Y		
482	ZZZZ	-99.49	56.36				Y				Y
484	ZZZZ	42.03	34.38		Y					Y	
485	ZZZZ	3.66	6.52		Y				Y		
494	ZZZZ	-50.09	-19.96		Y				Y		
513	ZZZZ	-58.25	-2.92		Y				Y		
521	ZZZZ	-94.73	72.77				Y				Y
535	ZZZZ	-107.55	24.51		Y			Y			
551	ZZZZ	-178.26	68.50		Y				Y		
558	ZZZZ	-106.00	50.08		Y				Y		
564	ZZZZ	58.49	43.44		Y						Y
568	ZZZZ	-105.64	61.44				Y				Y
569	ZZZZ	-117.71	60.93		Y				Y		
577	ZZZZ	-73.05	70.39				Y				Y
583	ZZZZ	-73.45	70.61				Y				Y
607	ZZZZ	-89.21	52.94		Y				Y		
612	ZZZZ	140.25	51.64		Y				Y		
614	ZZZZ	114.54	23.91		Y				Y		
631	ZZZZ	-101.35	55.18		Y				Y		
648	ZZZZ	-65.96	-13.02		Y					Y	
660	ZZZZ	-55.23	-25.22		Y				Y		
665	ZZZZ	-75.32	64.98		Y				Y		
670	ZZZZ	178.37	63.52		Y				Y		
675	ZZZZ	-79.39	56.16				Y				Y
683	ZZZZ	-54.99	-1.99		Y				Y		
689	ZZZZ	-159.93	70.41		Y						Y
692	ZZZZ	-50.74	-1.87		Y				Y		
701	ZZZZ	3.95	6.51				Y				Y
704	ZZZZ	-64.28	55.47		Y				Y		
727	ZZZZ	38.38	37.60		Y			Y			
730	ZZZZ	-104.35	51.88		Y			Y			
750	ZZZZ	96.96	19.99		Y				Y		
752	ZZZZ	-101.88	55.72		Y				Y		
753	ZZZZ	-107.07	55.87		Y				Y		
759	ZZZZ	0.90	5.92		Y				Y		
769	ZZZZ	-88.16	50.76		Y				Y		
777	ZZZZ	-97.42	66.48		Y				Y		
781	ZZZZ	-111.05	64.16		Y				Y		

783	ZZZZ	89.22	69.35		Y				Y		
796	ZZZZ	99.87	74.09		Y				Y		
799	ZZZZ	47.83	31.17		Y				Y		
802	ZZZZ	-12.62	16.15		Y				Y		
828	ZZZZ	-109.71	65.06				Y				Y
838	ZZZZ	31.88	64.48		Y				Y		
856	ZZZZ	-64.25	53.64		Y				Y		
868	ZZZZ	-109.54	64.38				Y				Y
870	ZZZZ	48.20	49.04		Y				Y		
879	ZZZZ	74.35	44.85		Y						Y
887	ZZZZ	-102.35	61.70		Y				Y		
888	ZZZZ	27.37	63.03		Y				Y		
902	ZZZZ	72.95	53.84		Y				Y		
915	ZZZZ	-60.79	-3.33		Y				Y		
919	ZZZZ	30.68	65.06		Y				Y		
922	ZZZZ	-110.70	69.07				Y				Y
923	ZZZZ	35.36	68.46		Y						Y
930	ZZZZ	-110.06	61.14				Y				Y
933	ZZZZ	172.51	-43.79		Y				Y		
935	ZZZZ	-176.55	67.98		Y				Y		
949	ZZZZ	-102.01	54.17		Y				Y		
953	ZZZZ	-56.63	-2.26		Y				Y		
961	ZZZZ	18.21	65.74		Y				Y		
970	ZZZZ	117.07	30.83				Y				Y
976	ZZZZ	-118.32	63.09		Y						Y
981	ZZZZ	-117.49	64.17		Y						Y
992	ZZZZ	34.14	62.38		Y				Y		
994	ZZZZ	-102.00	56.28		Y				Y		
995	ZZZZ	-48.80	-28.37		Y				Y		
1000	ZZZZ	-72.26	54.32		Y						Y
1009	ZZZZ	-85.20	52.31		Y				Y		
1035	ZZZZ	73.77	53.43		Y				Y		
1058	ZZZZ	-111.46	58.62		Y				Y		
1060	ZZZZ	-74.55	10.82		Y				Y		
1063	ZZZZ	117.93	49.07		Y				Y		
1067	ZZZZ	-97.32	60.40		Y						Y
1069	ZZZZ	-106.37	63.31		Y						Y
1087	ZZZZ	143.23	46.77		Y				Y		
1093	ZZZZ	-104.86	60.27		Y				Y		
1097	ZZZZ	-68.76	-35.05				Y				Y
1099	ZZZZ	-50.06	65.13		Y				Y		
1111	ZZZZ	-67.10	-18.11				Y				Y
1139	ZZZZ	85.23	66.83		Y				Y		
1156	ZZZZ	-104.37	58.14		Y				Y		
1160	ZZZZ	-92.57	54.39		Y				Y		
1189	ZZZZ	-55.99	48.06		Y				Y		
1190	ZZZZ	-54.31	-2.29		Y					Y	
1192	ZZZZ	89.97	32.46		Y						Y
1202	ZZZZ	-97.69	66.31		Y				Y		
1203	ZZZZ	45.22	39.20				Y				Y
1206	ZZZZ	116.87	34.97		Y				Y		
1208	ZZZZ	140.04	53.43		Y				Y		
1225	ZZZZ	-104.59	69.78				Y				Y

1237	ZZZZ	-93.49	53.15		Y				Y		
1250	ZZZZ	38.51	59.65		Y				Y		
1258	ZZZZ	-63.26	55.89		Y				Y		
1262	ZZZZ	-97.71	65.62				Y				Y
1263	ZZZZ	-103.38	66.44		Y						Y
1268	ZZZZ	-83.37	14.82		Y				Y		
1274	ZZZZ	-91.22	65.89		Y				Y		
1279	ZZZZ	-106.86	64.33				Y				Y
1282	ZZZZ	-56.00	-1.81		Y				Y		
1291	ZZZZ	-116.71	68.26		Y				Y		
1293	ZZZZ	45.02	34.20		Y				Y		
1294	ZZZZ	93.44	48.90		Y					Y	
1297	ZZZZ	-175.16	67.40		Y				Y		
1306	ZZZZ	84.78	30.22		Y						Y
1318	ZZZZ	-75.44	69.56				Y				Y
1319	ZZZZ	34.90	61.11		Y				Y		
1326	ZZZZ	-96.91	62.91				Y				Y
1333	ZZZZ	-97.07	58.11		Y				Y		
1338	ZZZZ	-100.02	63.29				Y				Y
1362	ZZZZ	78.02	53.33		Y				Y		
1363	ZZZZ	-102.26	62.30		Y						Y
1366	ZZZZ	-100.05	65.51				Y				Y
1385	ZZZZ	63.66	49.01		Y				Y		
1393	ZZZZ	-167.06	65.92		Y				Y		
1398	ZZZZ	99.63	74.38		Y				Y		
1409	ZZZZ	142.53	-32.27		Y				Y		
1435	ZZZZ	-107.74	56.89		Y				Y		
1437	ZZZZ	-83.93	15.28		Y					Y	
1440	ZZZZ	17.66	67.67		Y				Y		
1453	ZZZZ	-99.61	65.26				Y				Y
1458	ZZZZ	137.34	50.28		Y				Y		
1463	ZZZZ	-102.27	65.10		Y				Y		
1472	ZZZZ	179.00	69.30		Y				Y		
1475	ZZZZ	-83.32	14.33		Y				Y		
1481	ZZZZ	-120.00	64.03		Y						Y
1482	ZZZZ	46.67	30.71		Y				Y		
1484	ZZZZ	-111.20	69.21				Y				Y
1495	ZZZZ	-60.28	-3.48		Y						Y
1504	ZZZZ	115.33	29.29		Y				Y		
1510	ZZZZ	-104.04	51.91		Y				Y		
1515	ZZZZ	-95.43	65.17				Y				Y
1523	ZZZZ	-126.27	65.41				Y				Y
1524	ZZZZ	-110.45	56.51		Y			Y			
1525	ZZZZ	-109.40	69.73				Y				Y
1528	ZZZZ	-154.40	57.11				Y				Y
1534	ZZZZ	84.97	31.22		Y						Y
1535	ZZZZ	-55.51	-2.15		Y				Y		
1539	ZZZZ	-105.68	69.26		Y				Y		
1540	ZZZZ	-127.06	67.55		Y				Y		
1552	ZZZZ	-93.03	54.15		Y				Y		
1560	ZZZZ	-59.70	-3.15		Y				Y		
1566	ZZZZ	-84.58	15.81		Y				Y		
1571	ZZZZ	26.60	63.29		Y				Y		

1572	ZZZZ	-104.39	62.80		Y				Y		
1573	ZZZZ	155.08	68.38		Y				Y		
1578	ZZZZ	-96.27	65.22				Y				Y
1594	ZZZZ	-102.78	54.36		Y					Y	
1607	ZZZZ	-68.06	66.28				Y				Y
1608	ZZZZ	38.19	45.82		Y				Y		
1613	ZZZZ	154.93	68.18		Y				Y		
1615	ZZZZ	30.54	63.57		Y				Y		
1621	ZZZZ	-117.00	67.38				Y				Y
1632	ZZZZ	28.15	59.28		Y				Y		
1637	ZZZZ	151.75	68.56				Y				Y
1652	ZZZZ	85.72	29.85		Y						Y
1654	ZZZZ	-97.54	62.16				Y				Y
1664	ZZZZ	-102.99	65.02				Y				Y
1666	ZZZZ	-131.79	67.69		Y			Y			
1683	ZZZZ	-71.96	65.53		Y						Y
1685	ZZZZ	-92.92	69.94				Y				Y
1698	ZZZZ	-113.24	67.28				Y				Y
1712	ZZZZ	-98.54	59.21		Y						Y
1713	ZZZZ	-91.94	52.96		Y				Y		
1727	ZZZZ	-69.10	54.52		Y						Y
1728	ZZZZ	-106.40	70.29				Y				Y
1730	ZZZZ	89.68	30.94		Y						Y
1734	ZZZZ	147.16	71.01		Y				Y		
1737	ZZZZ	-101.90	58.39				Y				Y
1750	ZZZZ	-172.44	65.23		Y				Y		
1752	ZZZZ	-55.63	-2.11		Y				Y		
1759	ZZZZ	-111.74	68.88		Y						Y
1769	ZZZZ	-164.99	66.46		Y				Y		
1784	ZZZZ	-103.84	56.53				Y				Y
1785	ZZZZ	93.92	37.49				Y				Y
1788	ZZZZ	27.90	64.20		Y				Y		
1793	ZZZZ	60.89	50.75		Y				Y		
1795	ZZZZ	-92.43	67.82				Y				Y
1802	ZZZZ	-60.47	-31.37		Y				Y		
1812	ZZZZ	90.63	35.93		Y						Y
1826	ZZZZ	-68.79	66.68		Y						Y
1835	ZZZZ	93.38	37.71				Y				Y
1845	ZZZZ	-98.00	60.82		Y						Y
1847	ZZZZ	-94.01	71.57		Y				Y		
1848	ZZZZ	-73.24	68.53		Y						Y
1850	ZZZZ	-106.35	61.82				Y				Y
1864	ZZZZ	-95.72	62.08				Y				Y
1872	ZZZZ	-66.97	-14.01		Y				Y		
1876	ZZZZ	90.06	33.41		Y						Y
1879	ZZZZ	92.06	73.87				Y				Y
1883	ZZZZ	-93.95	66.50		Y				Y		
1897	ZZZZ	-97.73	62.00		Y				Y		
1907	ZZZZ	66.18	65.76		Y						Y
1908	ZZZZ	-107.39	54.46		Y				Y		
1917	ZZZZ	89.43	35.80		Y						Y
1927	ZZZZ	80.06	71.02		Y				Y		
1928	ZZZZ	82.72	35.56		Y						Y

1933	ZZZZ	-117.18	64.50		Y						Y
1951	ZZZZ	-65.79	-13.15		Y				Y		
1954	ZZZZ	-57.78	-17.52		Y				Y		
1955	ZZZZ	-62.68	-3.67				Y				Y
1965	ZZZZ	37.96	68.11		Y						Y
1966	ZZZZ	-103.88	62.19		Y				Y		
1967	ZZZZ	85.75	34.39		Y						Y
1985	ZZZZ	83.68	67.07				Y				Y
1989	ZZZZ	-98.49	51.05		Y				Y		
1993	ZZZZ	119.45	36.43		Y				Y		
2000	ZZZZ	-74.06	53.39		Y				Y		
2009	ZZZZ	-108.51	69.29		Y				Y		
2013	ZZZZ	27.21	66.09		Y						Y
2015	ZZZZ	-50.37	-29.93		Y				Y		
2021	ZZZZ	-96.66	54.49		Y				Y		
2022	ZZZZ	-104.67	63.17		Y				Y		
2026	ZZZZ	105.72	74.49		Y				Y		
2027	ZZZZ	40.72	57.92		Y				Y		
2048	ZZZZ	88.58	33.85		Y						Y
2055	ZZZZ	-110.52	68.91		Y						Y
2057	ZZZZ	77.41	53.27		Y				Y		
2058	ZZZZ	-103.19	66.76				Y				Y
2064	ZZZZ	-99.51	52.82		Y				Y		
2071	ZZZZ	-9.35	53.62		Y				Y		
2076	ZZZZ	-95.30	63.51				Y				Y
2077	ZZZZ	176.03	69.81		Y				Y		
2084	ZZZZ	83.59	67.18		Y				Y		
2085	ZZZZ	116.35	28.75		Y				Y		
2087	ZZZZ	-125.84	66.31		Y				Y		
2092	ZZZZ	-53.90	-34.33		Y				Y		
2097	ZZZZ	-93.53	50.75		Y				Y		
2102	ZZZZ	-100.63	54.03		Y				Y		
2104	ZZZZ	112.49	29.21		Y				Y		
2107	ZZZZ	138.39	70.84		Y				Y		
2109	ZZZZ	-127.40	66.17		Y						Y
2111	ZZZZ	-74.06	9.15		Y				Y		
2112	ZZZZ	-54.70	-2.20		Y				Y		
2113	ZZZZ	64.54	54.13		Y						Y
2117	ZZZZ	-116.57	62.07		Y				Y		
2119	ZZZZ	-76.16	50.91		Y				Y		
2120	ZZZZ	-105.18	69.75		Y						Y
2127	ZZZZ	124.13	46.61		Y				Y		
2129	ZZZZ	28.43	45.43		Y				Y		
2130	ZZZZ	-126.09	68.64		Y				Y		
2132	ZZZZ	-90.15	41.99		Y				Y		
2138	ZZZZ	91.19	33.89		Y						Y
2142	ZZZZ	-71.95	65.70		Y				Y		
2145	ZZZZ	-174.66	64.83		Y				Y		
2150	ZZZZ	72.09	53.89		Y				Y		
2158	ZZZZ	32.95	63.47		Y						Y
2162	ZZZZ	-114.01	52.54		Y				Y		
2167	ZZZZ	26.88	56.77		Y				Y		
2172	ZZZZ	-67.72	56.26		Y						Y

2179	ZZZZ	-94.16	55.04		Y				Y		
2184	ZZZZ	-96.47	66.46				Y				Y
2185	ZZZZ	90.16	54.67		Y				Y		
2192	ZZZZ	-112.92	52.48		Y				Y		
2199	ZZZZ	-50.75	66.72				Y				Y
2228	ZZZZ	-72.47	-52.04		Y				Y		
2232	ZZZZ	146.09	-36.45				Y				Y
2239	ZZZZ	78.49	54.55		Y				Y		
2243	ZZZZ	-55.81	-1.90		Y				Y		
2245	ZZZZ	-100.74	49.66		Y				Y		
2246	ZZZZ	163.78	59.99		Y						Y
2247	ZZZZ	67.40	66.77		Y						Y
2249	ZZZZ	-106.42	72.07				Y				Y
2257	ZZZZ	78.88	70.93		Y						Y
2259	ZZZZ	-111.70	58.77		Y				Y		
2262	ZZZZ	-136.96	60.45		Y						Y
2263	ZZZZ	-108.33	55.55		Y				Y		
2273	ZZZZ	152.30	68.58		Y				Y		
2276	ZZZZ	-121.13	59.08		Y				Y		
2280	ZZZZ	-56.79	-28.07		Y				Y		
2292	ZZZZ	29.72	65.94		Y						Y
2297	ZZZZ	-91.54	52.58		Y				Y		
2303	ZZZZ	-107.16	59.17		Y				Y		
2304	ZZZZ	84.64	35.42		Y						Y
2305	ZZZZ	83.11	35.29		Y						Y
2310	ZZZZ	-66.60	57.48		Y						Y
2314	ZZZZ	115.58	49.52		Y				Y		
2315	ZZZZ	117.38	38.74		Y				Y		
2316	ZZZZ	114.23	33.02		Y				Y		
2323	ZZZZ	-114.66	56.63		Y				Y		
2325	ZZZZ	-109.08	65.04		Y				Y		
2326	ZZZZ	-115.38	53.65		Y				Y		
2329	ZZZZ	179.07	62.48		Y				Y		
2330	ZZZZ	-99.68	54.47		Y				Y		
2331	ZZZZ	66.90	58.92		Y				Y		
2346	ZZZZ	-73.15	69.64				Y				Y
2348	ZZZZ	-107.22	66.27				Y				Y
2351	ZZZZ	-114.67	60.23				Y				Y
2357	ZZZZ	107.75	74.45		Y				Y		
2360	ZZZZ	34.12	67.03		Y						Y
2361	ZZZZ	87.00	33.86				Y				Y
2364	ZZZZ	-2.75	31.57		Y						Y
2365	ZZZZ	47.63	31.60		Y				Y		
2367	ZZZZ	-96.42	56.26				Y				Y
2368	ZZZZ	-104.11	54.43		Y				Y		
2369	ZZZZ	-93.43	30.00		Y				Y		
2371	ZZZZ	-144.32	60.30				Y				Y
2376	ZZZZ	146.66	71.15		Y				Y		
2384	ZZZZ	-107.86	71.44		Y						Y
2386	ZZZZ	81.89	34.73		Y						Y
2388	ZZZZ	46.91	48.21		Y						Y
2397	ZZZZ	-49.55	62.52				Y				Y
2408	ZZZZ	33.51	45.21		Y				Y		

2415	ZZZZ	91.86	35.32		Y						Y
2418	ZZZZ	-108.61	53.61		Y				Y		
2419	ZZZZ	-166.09	65.24		Y						Y
2420	ZZZZ	-108.46	54.48		Y				Y		
2421	ZZZZ	-99.41	52.42		Y				Y		
2425	ZZZZ	26.77	54.86		Y				Y		
2427	ZZZZ	-3.70	16.27				Y				Y
2428	ZZZZ	34.30	64.11		Y				Y		
2435	ZZZZ	79.09	64.50		Y						Y
2436	ZZZZ	-105.97	54.48		Y				Y		
2447	ZZZZ	-115.41	58.96		Y				Y		
2448	ZZZZ	-107.53	71.05				Y				Y
2450	ZZZZ	-95.26	60.60		Y				Y		
2458	ZZZZ	32.99	61.78		Y				Y		
2464	ZZZZ	37.32	60.88		Y				Y		
2466	ZZZZ	-106.41	59.71		Y				Y		
2470	ZZZZ	-111.08	58.39		Y				Y		
2473	ZZZZ	16.75	60.57		Y				Y		
2475	ZZZZ	88.78	36.01				Y				Y
2477	ZZZZ	-139.82	62.35		Y				Y		
2483	ZZZZ	100.16	75.12		Y				Y		
2485	ZZZZ	-125.95	67.39		Y				Y		
2486	ZZZZ	-97.43	27.85		Y			Y			
2493	ZZZZ	35.18	63.96		Y				Y		
2495	ZZZZ	-118.92	63.20		Y						Y
2497	ZZZZ	65.71	59.70		Y				Y		
2503	ZZZZ	25.93	61.21		Y				Y		
2507	ZZZZ	68.39	50.14		Y				Y		
2511	ZZZZ	89.72	33.63		Y						Y
2513	ZZZZ	-96.83	57.84		Y				Y		
2518	ZZZZ	-72.33	-51.90		Y				Y		
2525	ZZZZ	97.58	79.42				Y				Y
2526	ZZZZ	24.21	69.66		Y				Y		
2528	ZZZZ	160.18	69.39		Y				Y		
2532	ZZZZ	8.22	56.37				Y				Y
2535	ZZZZ	124.24	67.79		Y						Y
2540	ZZZZ	-22.11	80.17				Y				Y
2541	ZZZZ	-131.66	60.65		Y						Y
2544	ZZZZ	-104.97	52.50		Y				Y		
2550	ZZZZ	-74.71	9.72		Y				Y		
2554	ZZZZ	17.41	54.71		Y				Y		
2557	ZZZZ	-103.90	69.67		Y				Y		
2558	ZZZZ	137.60	34.75		Y				Y		
2560	ZZZZ	-107.55	53.42		Y				Y		
2569	ZZZZ	88.17	31.99		Y						Y
2570	ZZZZ	-72.98	64.88		Y				Y		
2574	ZZZZ	100.21	72.31		Y				Y		
2594	ZZZZ	-108.40	53.07		Y				Y		
2595	ZZZZ	-106.25	53.96		Y				Y		
2601	ZZZZ	-99.15	72.07		Y				Y		
2602	ZZZZ	149.67	68.31		Y				Y		
2605	ZZZZ	-111.91	61.58				Y				Y
2611	ZZZZ	91.47	31.30		Y						Y

2613	ZZZZ	87.25	34.57				Y				Y
2623	ZZZZ	-98.48	63.15		Y				Y		
2631	ZZZZ	-114.89	71.44				Y				Y
2639	ZZZZ	87.67	70.20		Y				Y		
2641	ZZZZ	-84.13	15.62		Y				Y		
2649	ZZZZ	115.68	29.78		Y				Y		
2656	ZZZZ	-122.23	62.94		Y				Y		
2663	ZZZZ	96.55	49.15				Y				Y
2665	ZZZZ	-65.82	52.61		Y						Y
2672	ZZZZ	-93.28	69.63				Y				Y
2673	ZZZZ	-95.68	49.24		Y				Y		
2676	ZZZZ	-110.18	69.58				Y				Y
2677	ZZZZ	88.73	71.90				Y				Y
2678	ZZZZ	29.45	61.53				Y				Y
2682	ZZZZ	91.85	49.10		Y				Y		
2684	ZZZZ	119.96	-4.11		Y				Y		
2685	ZZZZ	-113.95	62.86				Y				Y
2693	ZZZZ	-89.05	13.67		Y				Y		
2695	ZZZZ	155.89	67.86		Y				Y		
2696	ZZZZ	78.61	52.87		Y				Y		
2697	ZZZZ	-87.93	66.51				Y				Y
2701	ZZZZ	87.49	40.56				Y				Y
2709	ZZZZ	-108.51	55.10		Y				Y		
2714	ZZZZ	-87.73	70.83				Y				Y
2719	ZZZZ	17.49	67.99				Y				Y
2720	ZZZZ	85.81	33.67				Y				Y
2724	ZZZZ	-78.63	22.22		Y				Y		
2725	ZZZZ	140.53	51.86		Y				Y		
2728	ZZZZ	-18.89	64.27		Y						Y
2731	ZZZZ	-110.69	54.15		Y				Y		
2735	ZZZZ	-116.39	64.53				Y				Y
2750	ZZZZ	145.40	69.15		Y				Y		
2752	ZZZZ	-70.07	56.47				Y				Y
2762	ZZZZ	-60.87	-32.08		Y				Y		
2763	ZZZZ	151.62	70.84		Y						Y
2775	ZZZZ	33.13	63.19		Y				Y		
2779	ZZZZ	-74.36	8.72				Y				Y
2786	ZZZZ	91.36	35.70				Y				Y
2789	ZZZZ	-118.12	73.07				Y				Y
2794	ZZZZ	69.23	50.02				Y				Y
2796	ZZZZ	33.23	64.34		Y				Y		
2797	ZZZZ	-95.33	63.77		Y				Y		
2798	ZZZZ	15.66	60.53		Y				Y		
2803	ZZZZ	28.99	45.50		Y				Y		
2806	ZZZZ	-113.00	64.86				Y				Y
2809	ZZZZ	-126.61	68.12		Y				Y		
2816	ZZZZ	33.13	68.26				Y				Y
2819	ZZZZ	92.21	34.81		Y						Y
2822	ZZZZ	-63.88	55.56				Y				Y
2823	ZZZZ	-117.65	64.82				Y				Y
2828	ZZZZ	-52.45	67.61		Y						Y
2839	ZZZZ	119.40	32.62		Y				Y		
2840	ZZZZ	68.69	50.13		Y				Y		

2851	ZZZZ	-69.44	64.14		Y				Y		
2857	ZZZZ	-113.97	71.46				Y				Y
2865	ZZZZ	-103.28	62.28				Y				Y
2872	ZZZZ	-118.69	73.05				Y				Y
2877	ZZZZ	86.75	35.13		Y						Y
2880	ZZZZ	50.18	67.25		Y						Y
2881	ZZZZ	91.57	34.34				Y				Y
2883	ZZZZ	-102.70	67.41		Y				Y		
2914	ZZZZ	-84.81	15.87		Y				Y		
2923	ZZZZ	67.65	26.42		Y				Y		
2925	ZZZZ	24.78	63.53		Y				Y		
2926	ZZZZ	112.25	54.83		Y				Y		
2927	ZZZZ	15.74	41.88		Y				Y		
2937	ZZZZ	-94.15	69.78				Y				Y
2940	ZZZZ	66.34	59.63		Y				Y		
2944	ZZZZ	-107.15	52.68		Y				Y		
2946	ZZZZ	91.51	31.47		Y				Y		
2960	ZZZZ	-132.93	67.98		Y				Y		
2961	ZZZZ	37.50	45.28		Y				Y		
2962	ZZZZ	178.95	63.32		Y						Y
2970	ZZZZ	-111.94	50.44				Y				Y
2972	ZZZZ	-80.01	72.22				Y				Y
2974	ZZZZ	-101.04	53.64		Y				Y		
2976	ZZZZ	176.74	62.56		Y				Y		
2984	ZZZZ	152.13	68.68		Y				Y		
2985	ZZZZ	31.26	56.24		Y				Y		
2986	ZZZZ	-88.86	66.77				Y				Y
2996	ZZZZ	54.14	37.33		Y						Y
2999	ZZZZ	71.42	63.54		Y				Y		
3002	ZZZZ	-133.66	68.95		Y				Y		
3007	ZZZZ	-75.07	8.36		Y				Y		
3020	ZZZZ	96.91	37.28		Y						Y
3022	ZZZZ	30.98	66.51		Y						Y
3025	ZZZZ	-1.10	45.14				Y				Y
3031	ZZZZ	38.20	66.42		Y				Y		
3034	ZZZZ	-107.90	69.62				Y				Y
3040	ZZZZ	-99.37	52.87		Y				Y		
3044	ZZZZ	86.72	32.96		Y						Y
3045	ZZZZ	87.37	35.97		Y						Y
3049	ZZZZ	-97.38	66.89				Y				Y
3053	ZZZZ	-71.14	-16.37				Y				Y
3054	ZZZZ	156.08	69.46		Y						Y
3055	ZZZZ	73.09	61.99		Y				Y		
3078	ZZZZ	88.70	32.98		Y						Y
3079	ZZZZ	-110.03	56.32		Y				Y		
3091	ZZZZ	154.89	68.51		Y				Y		
3095	ZZZZ	149.42	71.98		Y						Y
3096	ZZZZ	-97.98	72.18				Y				Y
3097	ZZZZ	34.45	57.57		Y				Y		
3102	ZZZZ	67.92	60.74		Y				Y		
3105	ZZZZ	-107.31	70.95				Y				Y
3108	ZZZZ	146.92	71.08		Y						Y
3111	ZZZZ	81.94	34.44				Y				Y

3128	ZZZZ	-108.72	71.56		Y				Y		
3129	ZZZZ	-128.43	66.89		Y				Y		
3132	ZZZZ	-74.71	9.62		Y						Y
3133	ZZZZ	-123.98	66.66		Y				Y		
3135	ZZZZ	-98.55	55.55		Y				Y		
3139	ZZZZ	72.43	68.71		Y						Y
3150	ZZZZ	-69.39	-53.96		Y				Y		
3156	ZZZZ	86.66	35.73		Y						Y
3166	ZZZZ	-116.23	64.42		Y				Y		
3168	ZZZZ	-115.53	71.69				Y				Y
3171	ZZZZ	-166.48	68.39		Y				Y		
3173	ZZZZ	151.86	67.86		Y						Y
3180	ZZZZ	-132.05	69.10		Y				Y		
3181	ZZZZ	-93.22	55.55		Y				Y		
3188	ZZZZ	-114.40	53.70		Y				Y		
3189	ZZZZ	139.98	-37.42		Y						Y
3191	ZZZZ	140.89	40.46		Y				Y		
3196	ZZZZ	-1.14	44.48		Y				Y		
3200	ZZZZ	65.57	38.37		Y				Y		
3201	ZZZZ	88.36	35.41		Y						Y
3202	ZZZZ	-91.60	52.48		Y						Y
3203	ZZZZ	124.09	46.79		Y				Y		
3208	ZZZZ	48.87	38.93		Y				Y		
3210	ZZZZ	88.92	72.97		Y				Y		
3211	ZZZZ	-50.61	70.11				Y				Y
3213	ZZZZ	97.64	73.67		Y				Y		
3218	ZZZZ	-61.48	-33.71		Y				Y		
3219	ZZZZ	-50.27	65.58				Y				Y
3231	ZZZZ	-110.34	53.91		Y				Y		
3233	ZZZZ	-115.88	65.05		Y				Y		
3243	ZZZZ	-106.46	54.08		Y				Y		
3244	ZZZZ	61.56	50.97		Y				Y		
3257	ZZZZ	38.11	61.72		Y				Y		
3258	ZZZZ	69.07	42.74		Y				Y		
3259	ZZZZ	-120.74	68.72		Y				Y		
3260	ZZZZ	-49.97	66.25				Y				Y
3268	ZZZZ	-3.82	15.31		Y				Y		
3269	ZZZZ	56.22	74.16				Y				Y
3272	ZZZZ	16.59	66.96				Y				Y
3275	ZZZZ	-108.51	71.19				Y				Y
3276	ZZZZ	111.64	52.66		Y				Y		
3278	ZZZZ	-75.28	60.34				Y				Y
3281	ZZZZ	14.56	61.08		Y				Y		
3283	ZZZZ	-52.07	-31.61		Y			Y			
3292	ZZZZ	79.03	64.14		Y						Y
3295	ZZZZ	72.23	69.25		Y						Y
3307	ZZZZ	12.23	42.12		Y				Y		
3312	ZZZZ	137.76	71.04		Y				Y		
3334	ZZZZ	24.38	66.60		Y						Y
3343	ZZZZ	88.19	32.90				Y				Y
3347	ZZZZ	61.58	54.58		Y				Y		
3350	ZZZZ	14.65	53.47		Y						Y
3365	ZZZZ	112.87	52.21		Y				Y		

3368	ZZZZ	155.69	69.43		Y				Y		
3369	ZZZZ	88.39	72.71		Y				Y		
3372	ZZZZ	158.65	69.93		Y						Y
3373	ZZZZ	42.42	11.65		Y				Y		
3375	ZZZZ	75.92	70.73		Y				Y		
3379	ZZZZ	27.43	56.33		Y				Y		
3391	ZZZZ	-128.93	66.99		Y				Y		
3392	ZZZZ	-91.69	52.95		Y				Y		
3394	ZZZZ	86.74	31.56				Y				Y
3397	ZZZZ	-77.90	48.13		Y				Y		
3398	ZZZZ	154.54	67.71		Y				Y		
3400	ZZZZ	-92.23	54.52		Y				Y		
3403	ZZZZ	-97.70	69.46				Y				Y
3415	ZZZZ	-117.12	63.76		Y				Y		
3421	ZZZZ	65.59	52.60		Y				Y		
3427	ZZZZ	64.39	65.68		Y				Y		
3430	ZZZZ	-85.03	49.43		Y				Y		
3431	ZZZZ	-117.40	70.72				Y				Y
3441	ZZZZ	-117.95	62.62				Y				Y
3443	ZZZZ	70.52	69.86		Y				Y		
3446	ZZZZ	-129.98	69.58		Y				Y		
3448	ZZZZ	-110.78	69.42				Y				Y
3453	ZZZZ	161.82	56.14		Y				Y		
3471	ZZZZ	-60.73	-29.63		Y				Y		
3476	ZZZZ	125.82	43.88		Y				Y		
3478	ZZZZ	147.17	-42.11				Y				Y
3480	ZZZZ	-97.20	56.10		Y				Y		
3483	ZZZZ	59.01	68.74		Y				Y		
3491	ZZZZ	-161.77	60.49		Y				Y		
3494	ZZZZ	-105.40	70.20				Y				Y
3500	ZZZZ	77.77	52.31		Y				Y		
3508	ZZZZ	179.76	69.03				Y				Y
3510	ZZZZ	-108.59	70.45				Y				Y
3523	ZZZZ	-85.60	51.47		Y				Y		
3524	ZZZZ	-163.59	67.15		Y				Y		
3529	ZZZZ	-125.36	65.22		Y				Y		
3531	ZZZZ	26.53	61.00		Y				Y		
3534	ZZZZ	86.49	33.95		Y						Y
3536	ZZZZ	70.94	69.75		Y				Y		
3539	ZZZZ	87.84	32.79				Y				Y
3544	ZZZZ	-106.81	71.22				Y				Y
3548	ZZZZ	-92.73	66.12				Y				Y
3557	ZZZZ	-163.96	60.12		Y						Y
3562	ZZZZ	174.80	61.94		Y				Y		
3568	ZZZZ	-117.78	65.06		Y				Y		
3570	ZZZZ	-95.39	54.56		Y				Y		
3575	ZZZZ	47.43	30.78		Y						Y
3587	ZZZZ	-117.72	56.24		Y				Y		
3589	ZZZZ	-119.38	62.32				Y				Y
3604	ZZZZ	-105.26	52.61				Y				Y
3605	ZZZZ	70.15	69.16		Y						Y
3614	ZZZZ	-100.67	27.49		Y				Y		

Table 7. Breakdown of sources of data for the prior LSWT field (§4) for ARC-Lake v3.0 data products. Where the lake name is given as ZZZZ, no name is available in the GLWD database.